miRNA-154 mediates the transdifferentiation of alveolar type II to alveolar type I cells in the mouse model of Bronchopulmonary Dysplasia

Inauguraldissertation
zur Erlangung des Grades eines Doktors der Medizin
des Fachbereichs Medizin
der Justus-Liebig-Universität Gießen

vorgelegt von Rako, Zvonimir Andelko
aus Bielefeld

Gießen 2019

Aus der Medizinischen Klinik und Poliklinik II,

unter der Leitung von Prof. Dr. Werner Seeger,

des Fachbereichs Medizin der Justus-Liebig-Universität Gießen

1. Gutachter: Prof. Dr. Saverio Bellusci

2. Gutachter: PD Dr. Rajkumar Savai

Tag der Disputation: 02.04.2020

Erklärung zur Dissertation

„Hiermit erkläre ich, dass ich die vorliegende Arbeit selbständig und ohne unzulässige Hilfe oder Benutzung anderer als der angegebenen Hilfsmittel angefertigt habe. Alle Textstellen, die wörtlich oder sinngemäß aus veröffentlichten oder nichtveröffentlichten Schriften entnommen sind, und alle Angaben, die auf mündlichen Auskünften beruhen, sind als solche kenntlich gemacht. Bei den von mir durchgeführten und in der Dissertation erwähnten Untersuchungen habe ich die Grundsätze guter wissenschaftlicher Praxis, wie sie in der „Satzung der Justus-Liebig-Universität Gießen zur Sicherung guter wissenschaftlicher Praxis“ niedergelegt sind, eingehalten sowie ethische, datenschutzrechtliche und tierschutzrechtliche Grundsätze befolgt. Ich versichere, dass Dritte von mir weder unmittelbar noch mittelbar geldwerte Leistungen für Arbeiten erhalten haben, die im Zusammenhang mit dem Inhalt der vorgelegten Dissertation stehen, oder habe diese nachstehend spezifiziert. Die vorgelegte Arbeit wurde weder im Inland noch im Ausland in gleicher oder ähnlicher Form einer anderen Prüfungsbehörde zum Zweck einer Promotion oder eines anderen Prüfungsverfahrens vorgelegt. Alles aus anderen Quellen und von anderen Personen übernommene Material, das in der Arbeit verwendet wurde oder auf das direkt Bezug genommen wird, wurde als solches kenntlich gemacht. Insbesondere wurden alle Personen genannt, die direkt und indirekt an der Entstehung der vorliegenden Arbeit beteiligt waren. Mit der Überprüfung meiner Arbeit durch eine Plagiatserkennungssoftware bzw. ein internetbasiertes Softwareprogramm erkläre ich mich einverstanden.“

_____ _____

Ort, Datum Unterschrift

List of Contents

List of Figures

List of Tables

Abbreviations

ACE	Angiotensin-converting enzyme
Acta2/α-SMA	*Alpha-Actin-2/alpha smooth muscle actin*
Adrp	*Adipose differentiation-related protein*
AECI/AECII	Alveolar type I/II (cells)
Ago	Argonaute
Akt	Proteinkinase B
ALSG	Aplasia of lacrimal and salivary glands
AML	Acute myeloid leukaemia
aMYF	Alveolar myofibroblasts
Apln	*Apelin*
Aqp5	*Aquaporin-5*
BPD	Bronchopulmonary Dysplasia
Bmp	*Bone morphogenetic protein*
BSA	Bovine Serum albumin
CAD	Coronary Artery Disease
Cav1	*Caveolin-1*
CC10	*ClubCell-Specific 10 kD*
CCSP	*Clara Cell Secretory Protein*
cDNA	*Complementary Desoxyribonucleic Acid*
CF	Cystic Fibrosis
CO_2	carbon dioxide
COPD	Chronic Obstructive Pulmonary Disease
DAPI	4',6-diamidino-2-phenylindole
DEPC	Diethyl pyrocarbonate
DGCR8	DiGeorge syndrome critical region gene 8
DNA	Desoxyribonucleic Acid
dNTP	*2'-desoxyribonucleosid-5'-triphosphate*
dsRNA	*Double-stranded ribonucleic acid*
ECM	Extra-cellular matrix
EDTA	Ethylenediaminetetraacetic acid
Erk	Extracellular signal-regulated kinase
EtOH	Ethanol
Etv4/5	*ETS Variant 4/5*

EX	Embryonic day X (e.g. E18.5 = 18th day of embryonic development)
Fgf9	*Fibroblast growth factor 9*
Fgf10	*Fibroblast growth factor 10*
Fgfr3/4	*Fibroblast growth factor receptor 3/4*
FISH	Fluorescence In-situ-hybridization
FRS2α/β	Fibroblast growth factor receptor substrate 2α/β
GDF	Growth Differentiation Factor
Gprin3	*G protein-regulated inducer of neurite outgrowth 3*
H^+	Proton
H_2CO_3	Carbonic acid
H_2O	Water
HCl	Hydrochloric Acid
HCO_3^-	Bicarbonate
H&E	Hematoxylin & Eosin
Hopx	*Homeodomain-only protein*
HYX	Hyperoxia
IHC	Immunohistochemistry
IL-1β	Interleukin-1β
IPF	Idiopathic pulmonary fibrosis
JNK	Jun N-terminal kinase
LADD	Lacrimo-auriculo-dento-digital syndrome
LIF	Lipofibroblasts
MAPK	Mitogen-activated protein kinase
miRISC	*miRNA*-induced silencing complex
miRNA/micro-RNA	*micro-ribonucleic acid*
MLI	Mean Linear Intercept
mRNA	*Messenger ribonucleic acid*
NaCl	Sodium Chloride
Nkx2.1	*NK2 Homebox 1*
NOX	Normoxia
NSCLC	Non-Small Cell Lung Cancer
O_2	Oxygen
p15	CDKN2B

PACT	PKR activator
PAH	Pulmonary Arterial Hypertension
Pai-1	Plasminogen activator inhibitor-1
PBS	Phospho-buffered saline
Pdgfa	Platelet-derived growth factor subunit A
Pdgfrα	Platelet-derived growth factor receptor A
PFA	Paraformaldehyde
PI3K	Phosphoinositide 3-kinase
PLCγ	Phosphoinositide phospholipase C
pre-miRNA	*Precursor micro-ribonucleic acid*
pri-miRNA	*Primary micro-ribonucleic acid*
PX	Postnatal day X (e.g. P5 = 5th day after birth)
Ran-GTP	Ras related nuclear protein- Guanosine-5'-triphosphate
Ras-Raf-MAPK	Ras GTPase-rapid accelerated fibrosarcoma-mitogen activated protein kinase
RAAS	Renin-angiotensin-aldosterone-system
RNA	*Ribonucleic acid*
RNase	Ribonuclease
ROS	Reactive Oxygen Species
RPM	Rounds per Minute
RT-qPCR	Reverse Transcription quantitative polymerase chain reaction
rtTA	*Reversed tetracycline-controlled transactivator*
SCD	Sickle Cell Disease (SCD)
Scgb1a1	*Secretoglobulin family 1A member 1*
SCLC	Small Cell Lung Cancer
Sftpc/Spc	*Surfactant Protein C*
SH2	Src homology 2
Shh	*Sonic hedgehog*
siRNA	*Small interfering ribonucleic acid*
Sox2	(sex determining region Y)-box 2
Spry2	*Sprouty protein 2*
STAT	Signal Transducer and Activator of Transcription
Taq polymerase	DNA polymerase isolated from Thermus Aquaticus
Tet(O)	*Tet(O) operator*

Tgf-β	Transforming growth factor β
TNF-α	Tumor necrosis factor α
TRBP	Transactivating response RNA-binding protein
Ttf-1	Thyroid transcription factor 1
UTR	Untranslated region
WNT/β-Catenin	Wingless-related integration site / β-Catenin

Marginal Note:
Molecular factors in small letters refer to mice (e.g. Fgfr2b), whereas written in big letters refer to humans (e.g. FGFR2b). When referred to nucleic acids (such as *miRNAs*, *mRNAs* and others) the letters are *italic* (e.g. *Fgf10*). When referred to proteins, the letters are regular (e.g. Fgf10).

	Mouse	Human
Protein	Fgf10	FGF10
Nucleic acids	*Fgf10*	*FGF10*

Table 1: Nomenclature of proteins and genes
Molecular factors in small and regular letters refer to murine proteins (e.g. Fgf10), whereas written in big and regular letters refer to human proteins (e.g. FGF10). When referred to nucleic acids (such as *mRNAs*, *DNA* and others) the letters are small and *italic* when referred to murine nucleic acids (e.g. *Fgf10*), when referred to human nucleic acids the letters are big and *italic* (e.g. *FGF10*). For *miRNA* nomenclature see section **1.1.4**.

When speaking of "*miR-154*" it is referred to both *isomiRNAs*, namely *miR-154-3p* and *miR-154-5p*.

1. Introduction

1.1 *microRNAs* – modulators of translational expression

1.1.1 Discovery of *microRNA* function

In 1993, Lee and colleagues and Wightman and colleagues described a "novel kind of antisense translational control mechanism" (Lee et al., 1993; Wightman et al., 1993). *Lin-4* is a gene known to affect the transition between larval stages L1 and L2 during development in Caenorhabditae by decreasing the level of the Lin-14p protein. The gene encodes two *RNA* transcripts, which are not translated into proteins. These two *RNA* transcripts are 22 (*lin-4S*) and 61 (*lin-4L*) nucleotides in length. It was hypothesized that the short *lin-4S* is the functional product as it is more abundant in the cell. Complementary sequences between *lin-4* and multiple sites situated in the *3'-UTR* of *lin-14* (the *mRNA* of Lin-14p) were found, indicating that *lin-4* exerts its function by binding directly with the *lin-14 3'-UTR* through a "direct *RNA-RNA* interaction". This was underlined by the fact that *lin-4* was not able to down-regulate Lin-14p when the sequence of the *lin-14 3'-UTR* was modified. As the *mRNA* levels of *lin-14* were not decreased during development, it is obvious that the down-regulation of Lin-14p occurs on a post-transcriptional level. Comparing C. elegans to other nematode species (C. briggsae, C. remanei and C. vulgaris) it appeared that different *lin-4* clones can function in C. elegans, indicating that the sequences of the respective clones are conserved between the species.

In 2000, Reinhart and coworkers described another 21-nucleotide long *RNA* "*let-7*", which affected its target *lin-41* in a similar manner mediating transition from larval stages to adult stages in Caenorhabditae (Reinhart et al., 2000). In the same year *let-7* was described in other species including humans (Pasquinelli et al., 2000). In 2001, these short RNA transcripts were referred to as "*micro-RNAs*" for the first time (Lagos-Quintana et al., 2001; Lau et al., 2001; Lee and Ambros, 2001).

Today these characteristics previously described are known to be applicable for many other *microRNAs* (*miRNAs*). *Lin-4S* corresponds to the mature *miRNA* form and as *lin-4L* shares the same 5' sequence as *lin-4S*, it can be obviously regarded as the *pre-miRNA* precursor (Bartel, 2004).

1.1.2 *miRNA* biogenesis

miRNA biogenesis starts with the transcription of the *primary miRNA (pri-miRNA)* by RNA polymerase II (see Figure 1). The *pri-miRNA* is a few hundreds to a few thousand nucleotides long, 5' capped, 3' polyadenylated and contains a hairpin secondary structure (Sessa and Hata, 2013). It is also reported that in some cases *pri-miRNAs* can be transcribed by RNA polymerase III (Borchert et al., 2006). In the nucleus the *pri-miRNA* is cleaved by the RNase III enzyme Drosha and its cofactor DGCR8 (DiGeorge syndrome critical region gene 8) near the hairpin base liberating the *precursor miRNA (pre-miRNA)* of about 70-90 nucleotides in length (Berezikov et al., 2007; Tomari and Zamore, 2005). Interestingly, *miRNAs* can be transcribed as a single *pre-miRNA* having its own individual promoter or in a polycistronic manner resulting in the transcription of various *pre*-miRNAs (Seitz et al., 2004). Next, the *pre-miRNA* is exported to the cytoplasm by Exportin-5 and Ran-GTP (Bartel, 2004), where it is further processed by the type III RNase Dicer and its cofactors TRBP (transactivating response RNA-binding protein) and PACT (Sessa and Hata, 2013). Dicer cleaves the *pre*-miRNA on the loop side of the hairpin structure (Berezikov et al., 2007). The result is an about 22 nucleotides long double-stranded *miRNA/miRNA** duplex. Interestingly, alternative pathways of *miRNA* biogenesis can bypass cleavage by Drosha. So called mirtrons form alternative precursors for *miRNA* biogenesis, entering the pathway downstream of Drosha (Berezikov et al., 2007). After the separation of the two strands, one of the strands (guide strand; mature *miRNA*) is shipped into the miRISC (*miRNA*-induced silencing complex), a multi-protein complex containing Argonaute (Ago) proteins. The other strand (passenger strand; *miRNA**) is degraded. First it was believed that the guide strand is the functional one, whereas the passenger strand is the one being merely degraded. But it is also described that both strands can have biological functions (Packer et al., 2008). The thermodynamic stability of the ends of the *miRNA/miRNA** duplex is determining which strand is chosen to be integrated into the miRISC (Krol et al., 2010; Ro et al., 2007). The retained strand is the one with the less stable 5'-end (Krol et al., 2010). But as both strands can be functional and loaded into the miRISC, the *miRNA* strand selection might underlie more sophisticated mechanisms (Ro et al., 2007). Finally the miRISC guides the mature *miRNA* to the respective target *mRNAs* and the *miRNA* can function as a post-transcriptional repressor by binding the 3'-UTR.

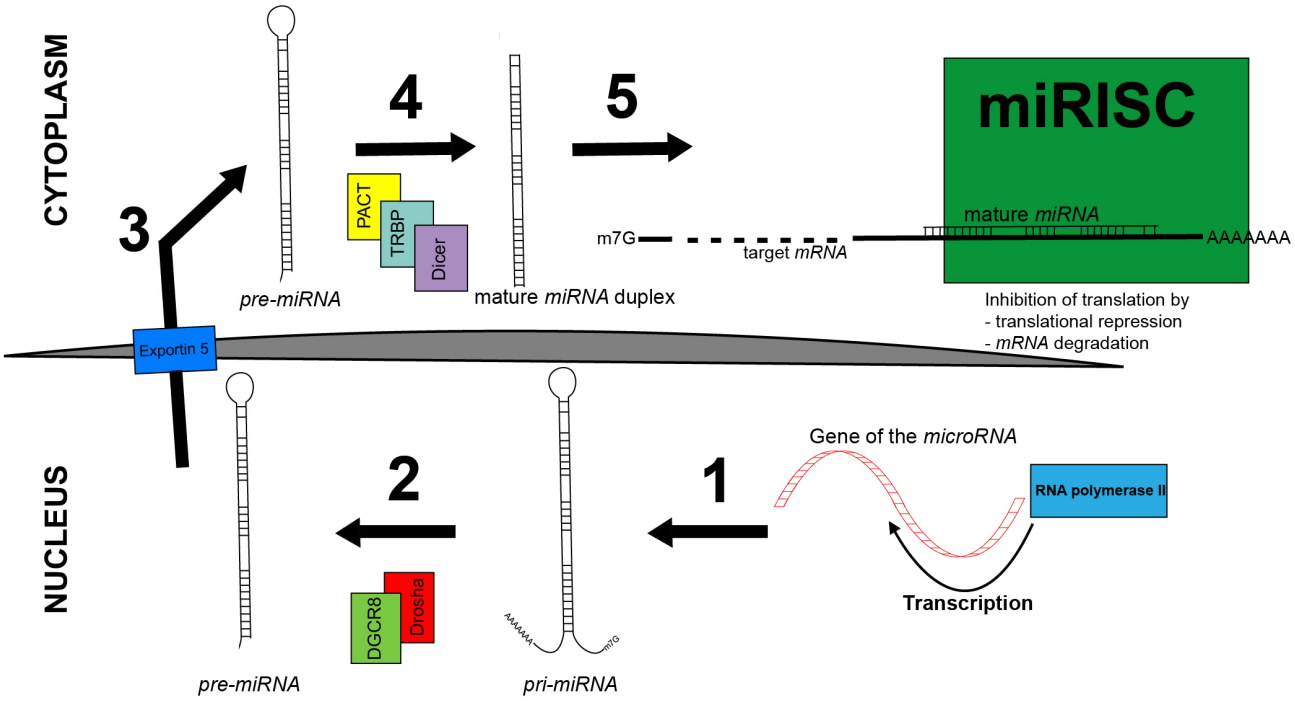

Figure 1: *miRNA* biogenesis (adapted from Sessa and Hata, 2013): Simplified schematic of miRNA biogenesis. After transcription by RNA polymerase II (**1**) the *primary miRNA* (*pri-miRNA*) is cleaved by type III RNase Drosha with its cofactors, such as DGCR8 (**2**), and the resulting *precursor miRNA* (*pre-miRNA*) is exported to the cytoplasm (**3**), where the *pre-miRNA* is further cleaved to the mature double stranded *miRNA*/*miRNA* complex by RNase type III Dicer with its cofactors TRBP and PACT (**4**). One of the strands is loaded into the miRISC (**5**), which guides the functioning mature *miRNA* to its target, whereas the other strand is cleaved. For Abbreviations see sections 1.1.2 and Abbreviations.

Regulation of the transcription of miRNAs is similar to that of protein-coding genes, for example by feedback loops (Krol et al., 2010). As post-transcriptional repressors *miRNAs* are able to influence their own synthesis by affecting the levels of proteins, which are involved in *miRNA* biogenesis and its regulation.

1.1.3 *miRNA* characteristics

Mature *miRNAs* are about 22 nucleotides long, single-stranded *RNAs*, exerting their function by post-transcriptionally regulating gene expression by targeting *mRNAs*, leading to translational repression or *mRNA* degradation. In some

cases it is reported that *miRNAs* can also act as translational activators (Bartel, 2004; Krol et al., 2010; Rebane et al., 2014; Sessa and Hata, 2013).

miRNAs are usually located in non-coding "intergenic regions" or in introns (Benetatos et al., 2013; Sessa and Hata, 2013). In some cases *miRNAs* are organized in clusters with simultaneous expression of the cluster members (Benetatos et al., 2013).

The sequences of many known *miRNAs* and the *3'-UTR* of their target *mRNAs* are highly conserved between species (Bartel, 2004; Friedman et al., 2009; Pasquinelli et al., 2000; Sessa and Hata, 2013). For example humans and mice share exactly the same sequence for *miR-154-3p* and *miR-154-5p* (http://www.mirbase.org/) (*hsa-miR-154-3p* = *mmu-miR-154-3p* = 5'-AAU CAU ACA CGG UUG ACC UAU U-3'; *hsa-miR-154-5p* = *mmu-miR-154-5p* = 5'- UAG GUU AUC CGU GUU GCC UUC G). Furthermore *miRNA* expression levels are different between tissues, developmental stages and diseases (Bartel, 2004; Krol et al., 2010; Sessa and Hata, 2013). Therefore cell-type-specific *miRNA* expression profiles might be used for characterization of different cells in a given organism at a given developmental stage, as well as in pathological cells in the future (Bartel, 2004). *miRNA* expression profiles are also conserved between species ((Sessa and Hata, 2013); here comparing *miRNA* expression between the human and murine species regarding lung development) indicating evolutionary conserved functions of different *miRNAs*.

It is assumed that *miRNAs* regulate over 60% of all human protein-coding genes and influence almost every cellular process such as development, proliferation, differentiation, cell apoptosis and endocytosis and hereby receptor internalization (Cao et al., 2016; Chen and Shen, 2013; Fiore et al., 2009; Friedman et al., 2009; Gioia et al., 2014; Krol et al., 2010; Lee et al., 1993; Pasquinelli et al., 2000; Reinhart et al., 2000; Sessa and Hata, 2013; Zhang et al., 2011).

miRNAs regulate *mRNA* expression levels by targeting the *mRNAs 3'-UTR* with their seed region (Krol et al., 2010). The seed region is located on the 5' end of the *miRNA* and usually comprises the *miRNA* nucleotides 2 to 8 (Krol et al., 2010). Base-pairing between the *miRNA* and the target *mRNA* leads to change in protein expression by *mRNA* degradation, translational repression or even translational

induction (see above), whereby it is believed that perfect complementarity rather leads to *mRNA* decay, whereas imperfect complementarity preferably leads to repression of *mRNA* translation (Seitz et al., 2004). The complexity of *miRNA* interaction is obvious if one considers that a given *miRNA* species can have many different target *mRNAs* and that likewise a given *mRNA* species can be affected by various *miRNAs* (Bartel, 2004; Krol et al., 2010). Moreover it is easily imaginable that *miRNAs* rather slightly modify protein levels allowing exact fine-tuning of cellular protein expression than completely repress target *mRNA* expression (Bartel, 2004; Chen and Shen, 2013; Fiore et al., 2009; Friedman et al., 2009).

1.1.4 *miRNA* nomenclature

In 2003, Ambros and colleagues stated criteria to be fulfilled to accept novel *miRNAs* on the basis of expression/gene sequence and biogenesis (Ambros et al., 2003). Throughout the years newly discovered *miRNA*-like sequences deriving from non-canonical biogenesis pathways and technological improvements led to revisions of these criteria and discussions postulating a change from a biogenesis to a functional approach (Desvignes et al., 2015). In order to ensure a correct and exact designation of the various *miRNAs* (*microRNAs*), a nomenclature for *miRNAs* was created based on numerical labels. *miRNAs* and *siRNAs* share many similarities such as biochemical structure and function (Ambros et al., 2003; Bartel, 2004). Still they can be distinguished by some characteristics such as the genomic location of origin, the structure of the respective precursor (hairpin-forming *RNA* vs. *dsRNA*), the number of functional mature products delivered from one precursor, the highly conserved evolution of *miRNAs* in contrast to *siRNAs* and the targets that they silence ("auto-silencing" vs. "hetero-silencing") (Ambros et al., 2003; Bartel, 2004).

Depending on the similarity of sequence compared with previously described *miRNAs* a newly discovered *miRNA* receives the next higher number (Ambros et al., 2003; Griffiths-Jones, 2004; Griffiths-Jones et al., 2006) (e.g. *miR-154* was discovered before *miR-541*). Orthologs between different species receive the same numerical identity (Ambros et al., 2003; Griffiths-Jones, 2004; Griffiths-Jones et al., 2006). Variation of the capitalization of the prefix "*miR*" describes either the

mature form of the *miRNA* ("*miR-xxx"*) or the precursor ("*mir-xxx"*) (Griffiths-Jones, 2004; Griffiths-Jones et al., 2006). Furthermore, *miRNAs* are given a three-letter prefix to assign them to a certain species. For example murine *miR-17* is denoted as "*mmu-miR-17*" (mmu = Mus musculus), whereas human *miR-17* is denoted as "*hsa-miR-17*" (hsa = Homo sapiens) (Griffiths-Jones et al., 2006; http://www.mirbase.org/). Identical mature *miRNAs* deriving from different "genomic loci in a given organism" are annotated with numerical suffixes such as *hsa-miR-124-1*, *hsa-miR-124-2* and *hsa-miR-124-3* (Ambros et al., 2003; Griffiths-Jones, 2004; Griffiths-Jones et al., 2006; http://www.mirbase.org/). Paralogous mature *miRNAs* differing in one or two bases in their sequence are annotated with an additional letter suffix such as *pma-mir-152a* and *pma-mir-152b* (pma = lamprey) (Ambros et al., 2003; Griffiths-Jones, 2004; Griffiths-Jones et al., 2006; http://www.mirbase.org/). Often the hairpin structure of a *pre-miRNA* can give rise to two functional mature *miRNAs*, one from the 5'-arm and one from the 3'-arm. There are two possible ways to describe these two *miRNAs* (Griffiths-Jones, 2004):

Initially it was believed that in most of the cases one of the two *miRNAs* is predominantly expressed (guide strand), whereas the other one is barely detectable and probably decayed (passenger strand) (Ro et al., 2007). Thus the less predominant form is annotated with an asterisk (e.g. *miR-154** vs. *miR-154*) (Bartel, 2004).

But it was shown that the predominant of the two *miRNAs* can differ between tissue, species and developmental stage and in some cases both *miRNAs* can be equally expressed (Desvignes et al., 2015; Ro et al., 2007; Williams et al., 2007). Therefore it is preferred to refer to the two mature *miRNAs* in a different manner: The *miRNA* originating from the 5'-arm of the precursor's hairpin is annotated with the suffix "*-5p*", while the *miRNA* originating from the other arm (3') is annotated with "*-3p*" (in our case *miR-154-5p* vs. *miR-154-3p*) (Griffiths-Jones et al., 2006). Both, the "*-5p*" and the "*-3p*" can describe the "predominantly expressed" *miRNA* strand (see Table 2), meaning that for example the suffices "*-3p*" and "*-5p*" can both equal an asterisk (http://www.mirbase.org/).

Asterisk	*-5p/-3p*
hsa-miR-154	*hsa-miR-154-5p*
*hsa-miR-154**	*hsa-miR-154-3p*
hsa-miR-541	*hsa-miR-541-3p*
*hsa-miR-541**	*hsa-miR-541-5p*
mmu-miR-541	*mmu-miR-541-5p*
*mmu-miR-541**	*mmu-miR-541-3p*

Table 2: Comparing different ways of designation of *miRNAs*
Which arm of the *pre-miRNA* is predominantly expressed can differ between *miRNAs* (*miR-154* vs. *miR-541* in human) and between species (*miRNA-541* in human vs. mice).

1.1.5 Involvement of *miRNAs* in diseases

As previously mentioned *miRNAs* are participating in a wide array of biological processes in different types of organisms. It is obvious that dysregulation of expression of these small regulators can affect the balance in signaling pathways leading to pathological conditions. Moreover an altered concentration of *miRNAs* can be found in the blood stream under pathological conditions (Akhavantabasi et al., 2012).

In the recent past the involvement of many different *miRNAs* in various diseases was examined in humans and animal models such as Huntington's Disease (Packer et al., 2008), Schizophrenia (Gardiner et al., 2012), Crohn's Disease (Cheng et al., 2015), Ulcerative Colitis (Polytarchou et al., 2015), Atopic Dermatitis (Rebane et al., 2014), Psoriasis (Xu et al., 2013), Acute Ischemic Stroke (Li et al., 2017b), Rheumatoid Arthritis (Ceribelli et al., 2011), Multiple Sclerosis (Ceribelli et al., 2011), Breast Cancer (Akhavantabasi et al., 2012), Diabetes (Xiang et al., 2015) and Coronary Artery Disease (Wang et al., 2016a). Furthermore *miRNAs* are involved in an enormous number of different tumors (Xin et al., 2014), whereby they either function as tumor suppressors (Liu et al., 2016) or even promote tumorigenesis (Li et al., 2017a). In the latter case the *miRNAs* are sometimes called "*oncomirs*".

On the one hand *miRNAs* might be used as therapeutic targets for new pharmacological approaches and replace current therapies, hopefully leading to a

better outcome for the patients, or on the other hand they might be used as biomarkers for diagnostic purposes and facilitate detection of diseases at earlier stages, hence giving better preconditions for a successful curative therapy. Besides, it has been reported that *miRNAs* might be involved in cellular mechanisms mediating drug resistance (Wei et al., 2017a).

All in all *miRNAs* constitute an intriguing field of research, which will acquire new insights in the understanding of molecular mechanisms. Further studies and experimental approaches have to be performed on this field in order to transfer gathered insights to the human organism to develop new therapeutics.

miRNAs are involved in a great number of biological and pathological events in the lung. The role of many different *miRNAs* has been examined in various pathologies of the lung (Sessa and Hata, 2013). In Non-Small Cell Lung Cancer (NSCLC) *miR-93* was up-regulated in NSCLC cell lines promoting tumorigenesis by activating *PI3K/Akt* Pathway, probably via inhibiting *LKBI*, *PTEN* and *p21* (Li et al., 2017a), whereas *miR-495* was down-regulated in drug-resistant Small Cell Lung Cancer (SCLC) leading to an unleashing of Ekt (BMX) tyrosine kinase which entailed poor prognosis (Wei et al., 2017a). In Chronic Obstructive Pulmonary Disease (COPD) *miR-149-3p* was found to reduce inflammation by directly inhibiting the *TLR4*/*NF-κB* pathway leading to decreased IL-1β and TNF-α levels (Shen et al., 2017). On the contrary, *miR-155* advanced inflammatory processes and secretion of mucus in Asthma by targeting *CTLA-4*, which is a T-cell inhibitor (Zhang et al., 2017). Oglesby and colleagues found elevated *miR-221* expression in human bronchial epithelial cells and a mouse model mimicking Cystic Fibrosis (CF) leading to a decrease of the transcription factor ATF6 by directly targeting it (Oglesby et al., 2015). In Pulmonary Arterial Hypertension (PAH) *miR-135a* was increased and its target *BMPR2* was decreased (Lee and Park, 2017). Mutations of *BMPR2* are known to be causative in PAH. Zhou and coworkers investigated *miR-28-3p* and its capability as a potential diagnostic marker for Pulmonary Embolism (Zhou et al., 2016). Various *miRNAs* such as *hsa-miR-200b, hsa-miR-455* and *hsa-let-7f-1* and their roles in different pathways, which might be involved in pneumonia, were examined (Huang et al., 2017). In the context of Pulmonary Sarcoidosis the *miRNA* expression profiles were investigated in BALF cells and peripheral blood lymphocytes indicating an involvement in pathogenesis (Kiszalkiewicz et al.,

2016). Nardiello and Morty reviewed different studies on the involvement of *miRNAs* in Bronchopulmonary Dysplasia (BPD) (Nardiello and Morty, 2016).

1.1.7 *miR-154* characteristics*

miR-154-3p and *miR-154-5p* (or *miR-154* and *miR-154**) are both part of the human "*DLK1-DIO3* genomic region", which is located on chromosome region *14q32* (murine chromosome *12F2* region) (Benetatos et al., 2013; Dixon-McIver et al., 2008; Seitz et al., 2004; Williams et al., 2007). Beside "paternally expressed imprinted genes *DLK1*, *RTL1*, and *DIO3* and the maternally expressed imprinted genes *MEG3* (*Gtl2*), *MEG8* (*RIAN*), and anti-sense *RTL1* (*asRTL1*)" it contains a *miRNA* cluster with 54 *miRNAs*, thus being one of the largest *miRNA* containing clusters in humans (Benetatos et al., 2013). Seitz and colleagues investigated the expression of the *miRNA* cluster members and found the *miRNAs* to be "only expressed from the maternally inherited chromosome" (Seitz et al., 2004). Furthermore they found that none of the *miRNAs* binds their target *mRNAs* with full complementarity, assuming that they rather act by translational repression of their target *miRNAs* than post-transcriptional decay (Seitz et al., 2004). The expression of the genes on the maternal chromosome *12F* in mice is regulated by so-called "*DMRs*" (differentially methylated region) (Kagami et al., 2010; Lin et al., 2003). Additionally Benetatos and colleagues described the involvement of various members of this cluster in human pathologies (Benetatos et al., 2013).

miR-154-3p and *miR-154-5p* are highly conserved between mice and humans, which can be demonstrated by means of sequence equality (http://www.mirbase.org/) (*hsa-miR-154-3p* = *mmu-miR-154-3p* = 5'-AAU CAU ACA CGG UUG ACC UAU U-3'; *hsa-miR-154-5p* = *mmu-miR-154-5p* = 5'- UAG GUU AUC CGU GUU GCC UUC G). Within the *DLK1-DIO3* genomic region it is located in the maternally expressed imprinted intergenic region *Mirg* (Seitz et al., 2004; Williams et al., 2007). "Imprinting means that these *miRNAs* are only expressed from the maternally inherited chromosome and their expression is regulated by an intergenic germline-derived differentially methylated region" (Williams et al., 2007). Furthermore it was expressed in the pulmonary stroma and epithelium during neonatal stages, but in the "airway and alveolar epithelium" during adult stages (Williams et al., 2007).

Williams and colleagues compared the *miRNA* expression profiles in embryonic and adult lung tissue in human and mice and found similar expression profiles and "differential expression" between the species, indicating evolutionary conservation of *miRNA* function in lung development between the two species (Williams et al., 2007): *miR-154* was more abundant in "neonatal mouse and embryonic human lung" compared to adult lungs. Furthermore *hsa-miR-154** was found to be more abundant in fetal lungs compared to adult lungs. This is also consistent with data previously generated in our lab (*data not shown*): during murine embryonic lung development the level of *miR-154* constantly increases, but decreases towards the postnatal stage.

miR-154 is known to act suppressive in different tumors such as Hepatocellular Carcinoma by targeting *ZEB2* (Pang et al., 2015), Colorectal Cancer by targeting *TLR2* (Xin et al., 2014), Glioblastoma (*WNT5A* is the target of interest) (Zhao et al., 2017a), Prostate Cancer and Breast Cancer by targeting *E2F5* (Xu et al., 2016; Zheng et al., 2017). *miR-154* levels were found to be increased in Medullary Thyroid Carcinoma (Mian et al., 2012).

Bernardo and coworkers examined the role of *miR-154* in a mouse model mimicking increased blood pressure by "transverse aortic constriction" and therefore leading to cardiac hypertrophy and dysfunction and found *miR-154* to be up-regulated not only in the mouse model, but also in human heart tissue with heart failure from hypertrophic cardiomyopathy (Bernardo et al., 2016). It was found that inhibition of *miR-154* is able to attenuate the progress of heart failure by maintaining heart function, cardiac size and weight and reducing fibrosis. They suggest that the effect of *miR-154* on p15 might be one of the underlying mechanisms.

Gururajan and colleagues described the oncogenic effect of *miR-154** in prostate cancer (Gururajan et al., 2014). It promotes epithelial-to-mesenchymal transition (EMT) and therefore benefits bone metastasis by suppressing the tumor suppressor protein STAG2.

miR-154-3p expression was found to be decreased in the "Ductal Carcinoma In Situ of Breast (DCIS)" (Li et al., 2013). To the best of our knowledge its role in DCIS was not further evaluated yet.

Hibino and colleagues examined the role of *miR-451* in "tissue-engineered vascular graft" (TEVG) stenosis in a mouse model (Hibino et al., 2016). Unlike *miR-451*, *miR-154* was found to be up-regulated in grafts with distinct stenosis. Without further elaboration they assumed Tgf-β1 to be associated with *miR-154* up-regulation by referring to Milosevic and coworkers (Milosevic et al., 2012).

In Acute Myeloid Leukaemia (AML) with the translocation t(15;17) 7 *miRNAs* mapped at the human miRNA cluster located on the chromosome 14q32 were found to be up-regulated in AML compared to control bone marrow, with *miR-154* and *miR-154** being among them (Dixon-McIver et al., 2008).

In the context of Coronary Artery Disease (CAD) *miRNA* expression profiles of platelets of CAD patients compared to healthy patients were examined (Chen et al., 2014). Among other differentially expressed *microRNAs miR-154* was found to be down-regulated in CAD platelets indicating a potential involvement of *miR-154* in the pathogenesis of CAD. Further experimental approaches are required to evaluate the role of *miR-154* in CAD.

Jain and colleagues examined the *miRNA* expression profile of platelets of patients suffering from Sickle Cell Disease (SCD) compared to healthy patients (Jain et al., 2013). Of the 40 significantly deregulated *miRNAs* they found 24 being down-regulated, among which 14 belong to the "maternally imprinted chromosome *14q32* region", including *miR-154**.

Milosevic and colleagues examined the involvement of *miR-154* in the fibrotic phenotype of IPF patients' lungs (Milosevic et al., 2012). They described the up-regulation of various members of the *miRNA* cluster, which is mapped on human chromosome *14q32* and part of the imprinted *DLK1-DIO3* domain, including *miR-154*, induced by TGF-β1 stimulation via its downstream effector SMAD3 *in vitro*. *miR-154* induced proliferation and migration in lung fibroblasts partly via repression of p15 (CDKN2B) protein level, a cell cycle inhibitor, and induction of the WNT/β-Catenin pathway. Comparing *miRNA* expression profiles of IPF lungs to fetal lungs they found the same *miRNAs* being increased, supposing that the IPF phenotype might be a "reversal of lung differentiation". The effects were reversible upon *miR-154* inhibition, indicating that they were attributable to *miR-154*.

Xing and coworkers found decreased expression levels of *rno-miR-154-5p* in neonatal lungs of Wistar rats after 14 days of hyperoxic treatment using a BPD model (Xing et al., 2015) alongside with various other dysregulated *miRNAs*. Interestingly, at days 3 and 7 no significant change in *rno-miR-154-5p* was found.

Lin and colleagues described the tumor suppressive effect of *miR-154* on NSCLC in an *in vivo* and *in vitro* approach (Lin et al., 2015). They found *miR-154* expression to be down-regulated in NSCLC. *miR-154* mimic transfection affected "proliferation, apoptosis, cell cycle arrest, migration and invasion, and tumor growth".

*In this section *miRNAs* are referred to in the same manner as in the literature

When referring to both *isomiRNAs*, namely "*miR-154-3p*" and "*miR-154-5p*", both will be denoted together as "*miR-154*" in the subsequent paragraphs.

1.2 The Lung – Parallels and differences between human and murine lung development

1.2.1 Development of the human and murine lung

In order to understand the impact of BPD on the lung, it is meaningful to succinctly visualize the physiological lung development. Chao and colleagues from our laboratory have elucidated the human and murine lung development, dividing it into four phases: the pseudoglandular, the tubular, the saccular, and the alveolar phase (Chao et al., 2015; Chao et al., 2016) (see Figure 2). The following section focuses on postnatal lung development, especially the alveolar phase.

1.2.1.1 Prenatal lung development

The lung is basically composed of two main components: the lung mesenchyme, which originates from the mesoderm and the lung epithelium, which originates from the gut endoderm (Chao et al., 2015). The pseudoglandular phase takes place from gestational weeks 4-17 in humans, and E9.5-E16.5 in mice. Basically it starts with the formation of *Nkx2.1* (*Ttf-1*) positive cells in the ventral area of the anterior foregut compared with *Sox2* expressing cells in the dorsal area

of the anterior foregut. Out of these two compartments the anterior foregut is divided forming the future trachea (ventrally) and esophagus (dorsally), which are further elongating. Moreover this phase is mainly characterized by “branching morphogenesis” leading to further dichotomous subdivision of the airways and airway lengthening into the surrounding mesenchyme of the bronchi (Weinstein et al., 1998).

Several different signaling pathways influence these processes, such as Fgf10, Bmp, Wnt and Shh. Epithelial cells originating from this phase are “basal, neuroendocrine, ciliated, and secretory cells”, while the mesenchyme gives rise to “smooth muscle, lymphatic, endothelial, nerve, and chondrocytic cells” (Chao et al., 2015): most of them are formed from E13.5 until E16.5.

The following canalicular phase takes gestational weeks 17-26 in humans, and E16.5-E17.5 in mice. Further division of the respiratory airways escalates, while the associated mesenchymal layer narrows and capillaries are formed. “Distal lung epithelial progenitors” differentiate and form a “primitive respiratory epithelium”, facilitating gas exchange, which marks this as the “earliest time point” for potential survival after birth: Between E16.5 and E18.5 alveolar type I (AECI: Aqp5+) and surfactant-producing alveolar type II cells (AECII: Sftpc+) emerge at this phase out of “alveolar bipotential progenitor cells”, the mesenchyme gives rise to lipofibroblasts (LIF; Adrp+) in mice (Chao et al., 2016; Desai et al., 2014; Treutlein et al., 2014). When the lung is fully developed, alveolar type I cells with their elongated, squamous shape form the scaffold of the alveoli, the gas exchange unit of the lung, and cover about 96% of the alveolar surface, although they are less abundant than the rather cuboidal alveolar type II cells (Desai et al., 2014; Hou et al., 2015). AECI cells are an important element of the air-blood barrier on the “air side” (with the capillary endothelium as its counterpart on the “blood side”; both are separated by a basal lamina in between), which is why AECI cells take part in the gas exchanging process (Makanya et al., 2013). Surfactant, produced and secreted by the AECII cells, reduces the alveolar surface’s tension and hereby prevents the collapsing of the alveoli (El Agha and Bellusci, 2014). Furthermore, especially within the scope of lung injury, AECII cells have a progenitor function after birth and are able to transdifferentiate into AECI cells (Desai et al., 2014; Hou et al., 2015). AECII cells are located in close proximity to the lipofibroblasts: they

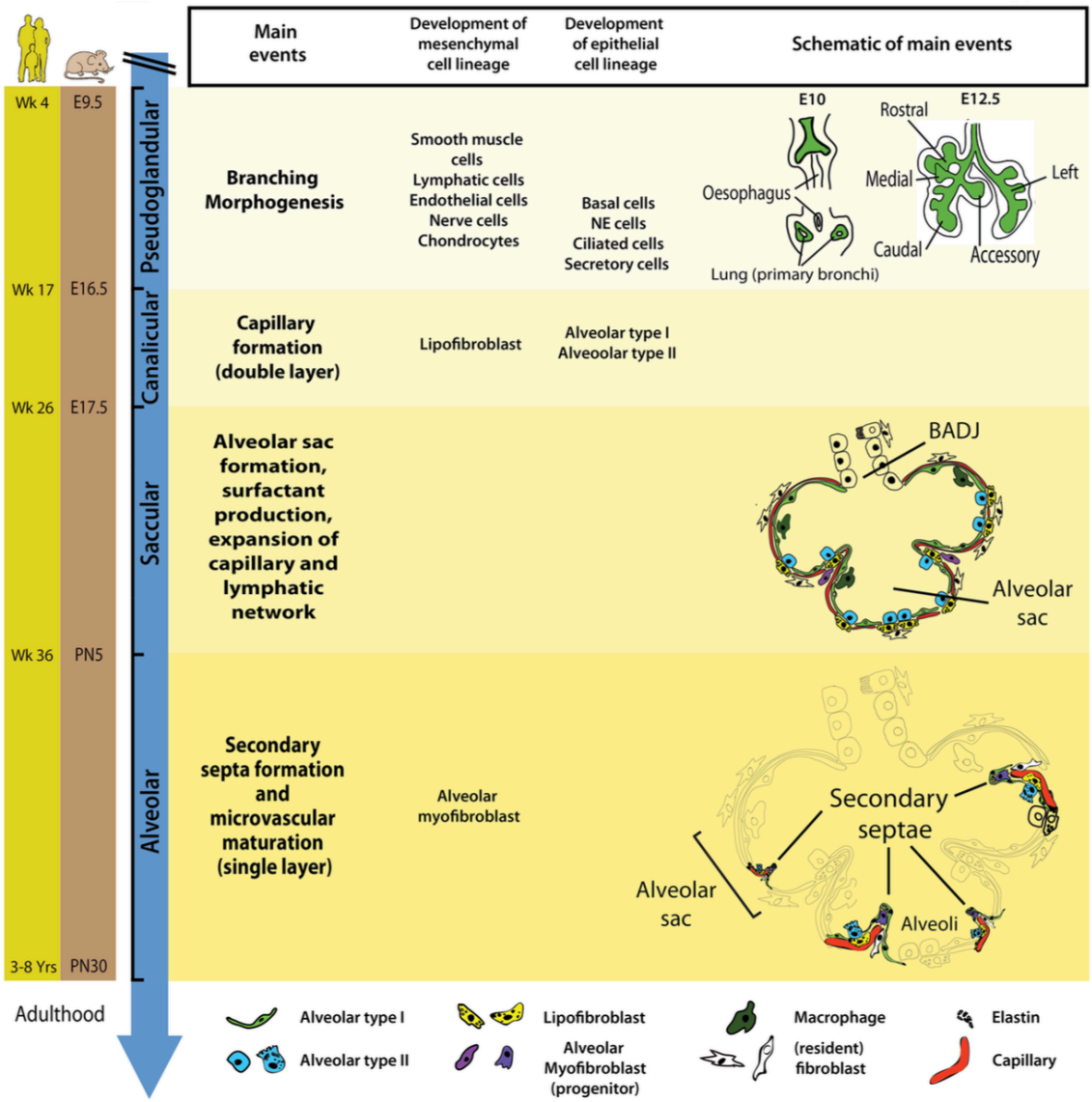

Figure 2: Different stages of murine and human lung development (Chao et al., 2015): Illustration of the different phases of human and murine lung in comparison. On the left side the time intervals for the particular stage (pseudoglandular, canalicular, saccular, alveolar) are depicted in yellow for human and in brown for murine lungs. Furthermore the main events occurring in the particular phases are named with the upcoming cell types, which are typical for each developmental stage and a schematic of the main events. The key for the depicted cell types is found on the bottom. For detailed description see section 1.2.1.

form a functional unit for surfactant production, as the lipofibroblasts supply the AECII cells with lipids. It is discussed whether lipofibroblasts might form a progenitor population for AECII cells (Chao et al., 2016). The patterning of the

lung and formation of proximal and distal structure are complexly orchestrated by different signaling pathways such as Wnt/β-Catenin, Fgf, Bmp4 and N-myc (Shu et al., 2005). The hierarchy of the different emerging cell types and their progenitors is very complex and would go beyond the constraints of this work (El Agha and Bellusci, 2014).

Subsequently, the saccular phase follows, which takes gestational weeks 26-36 in humans and from embryonic day E17.5 until postnatal day P5 in mice (Chao et al., 2015). In this phase alveolar sacs (or "primary septa") are formed, surfactant is produced, small blood and lymphatic vessels spread and in order to "facilitate gas exchange" the mesenchymal layer thins, reducing the distance between the alveolar lumen and the blood. The process of alveolar thinning and alveolar surface expansion includes the spreading and elongating of the AECI cells, leading to optimized conditions for gas exchange and further alveolar maturation (Wang et al., 2016b). All in all the development of the lung epithelium and mesenchyme cannot be described separately as they are closely interwoven one with another: It is far more complex. The mesoderm is the origin of many different evolving cells and signaling molecules affecting the epithelium. Many different signaling pathways are involved in lung development. Discussing every single one of them would definitely go beyond the scope of this work (Chao et al., 2015; De Langhe et al., 2006; El Agha and Bellusci, 2014; Morrisey and Hogan, 2010).

1.2.1.2 Postnatal lung development

Finally, the alveolar phase takes center stage. In humans it starts already before birth from gestational week 36 until roughly the eighth year of age, whereas in mice it occurs after birth from postnatal day P5 until P30. This difference between the two species is the reason why the BPD mouse model is suitable for the simulation of the effect of the application of high oxygen concentrations on prematurely born human babies: although mice are exposed to hyperoxia postnatally, this setting corresponds with developmental stages of preterms (Chao et al., 2016). The alveolar phase is characterized by alveologenesis: Elastin is deposited in the alveolar sacs leading to an emersion of secondary septa at the very same place of elastin deposition. The cells, which are responsible for the secondary septation, are called "alveolar myofibroblasts" (De Langhe et al., 2006). The

secondary septa subdivide the alveolar sacs, resulting in the formation of mature alveoli. The process of alveolarization advances, leading to an increase of alveolar surface and therefore the area for gas exchange increases. The process of alveologenesis mainly takes part in the period of P5-P15 in mice ("first 6 months after birth in humans") (Chao et al., 2015). Afterwards maturation of the alveoli occurs (Kugler et al., 2017). "Microvascular maturation" enables "more efficient gas exchange": The alveolar walls mature by becoming thinner and the two-capillary-layer transforms into a single capillary layer. These processes ease gas exchange by approximating the alveolar and the vascular lumen as the barrier in between decreases in thickness and the capillaries are now surrounded by oxygen within the alveoli from both sides (Burri, 2006; Chao et al., 2015; Perl and Gale, 2009).

Many different signaling ligands and receptors seem to affect secondary septation: absence of Pdgfa leads to lack of Pdgfrα expressing cells, which potentially form a progenitor population for the α-SMA expressing alveolar myofibroblasts (Bostrom et al., 1996; Perl and Gale, 2009; Popova et al., 2014). Kugler and colleagues examined the role of Sonic hedgehog (Shh) signaling in alveolarization and found Shh signaling to be required for proper alveolar myofibroblast differentiation (Kugler et al., 2017). FGF signaling appears to be required for the differentiation of alveolar myofibroblasts. In a murine emphysema model Perl and coworkers showed that the re-alveolarization induced by application of retinoic acid is dependent on FGF signaling (Perl and Gale, 2009). The absence of both Fgfr3 and Fgfr4 can lead to impaired alveologenesis (Weinstein et al., 1998). De Langhe and colleagues showed a disturbed alveolar myofibroblast formation, and hence decreased elastin deposition in a mouse model, which contained a spliced version of Fgfr2 receptor, simulating increased Fgf9 signaling (De Langhe et al., 2006). Disruption of any of the mentioned pathways or cells leads to impairment of either alveolar myofibroblast formation or elastin deposition. For an overview of the processes of lung development depicted here, see Figure 2.

The result of the process of lung development is for both, humans and mice, a lung composed of five lobes. In humans the right thoracic cavity houses three lobes, whereas the left thoracic cavity houses two lobes and it comprises "23 airway generations". In mice the left lung comprises only one lobe, but the right lung consists of four lobes ("cranial, medial, caudal, and accessory lobe") and it forms

"12 airway generations" (Chao et al., 2015). The organ is capable to efficiently supply oxygen to the organism contingent upon a vast alveolar surface area of about 70 m^2, made up of more than 300 million alveoli, a small distance for gas diffusion of about 0.1 µm between the alveolar lumen and the blood flow, a system of conductive airways supplying oxygen to the alveoli and a network of blood vessels and capillaries bringing venous blood to the alveoli and conducting away oxygenated blood (Burri, 2006; Warburton et al., 2000). Furthermore the lung functions as a regulator of the acid-base balance (Hamm et al., 2015): The kidney forms the metabolic component of acid-base regulation, whereas the lung forms the respiratory component. By modulating respiratory rate and tidal volume exhaling CO_2 can be altered, and the balance of the following biochemical equation can be modified, keeping the pH at a steady state, when there are disorders concerning the metabolic component: $CO_2 + H_2O \Leftrightarrow H_2CO_3 \Leftrightarrow H^+ + HCO_3^-$. The lung has also an endocrine function, as cells in the lung can produce ACE (angiotensin-converting enzyme), which is involved in the RAAS (renin-angiotensin-aldosterone-system), regulating blood pressure and electrolyte homeostasis (Coates, 2003).

1.3 BPD – When lung development prematurely stagnates

1.3.1 Bronchopulmonary Dysplasia

Bronchopulmonary dysplasia (BPD) is the most prevalent chronic airway disease of preterm infants, whereby low gestational age and weight at birth embody important factors increasing the probability of occurence (e.g. 20% of the infants born with a gestational weight of under 1500g and a gestational age of under 30 weeks suffer from BPD in the US) (Baraldi and Filippone, 2007; Chao et al., 2015; Nardiello and Morty, 2016; Northway et al., 1967). Between 10,000 and 15,000 preterm infants are affected by BPD each year in the US (Voynow, 2017). As more and more prematurely born infants survive at lower gestational ages due to improved therapy the number of BPD patients increases (Baraldi and Filippone, 2007; Chao et al., 2015; Owen et al., 2017). Despite improved therapies the consequences for the airways remain into adulthood leading to high costs for health care (Baraldi and Filippone, 2007; Chao et al., 2015). BPD might also be associated with other diseases of preterm infants such as premature retinopathy (Baraldi and Filippone, 2007) and pulmonary hypertension (Chao et al., 2015; Silva et al., 2015).

Complex inflammatory processes including the activation of neutrophils and macrophages, inflammatory cytokines and different signaling pathways and the change of ECM composition are induced in the lung perturbing proper lung development (Niedermaier and Hilgendorff, 2015).

Briefly worded, from the pathophysiological point of view BPD disturbs the accurate lung development and the lung stops advancing in development, remaining in a premature condition. BPD interrupts the secondary septa formation during the simultaneously occurring phase of alveolarization, leading to a decreased number and an increased alveolar diameter (Xing et al., 2015). Furthermore thicker alveolar septa remain disrupting the maturation of the pulmonary vasculature (Nardiello and Morty, 2016). All in all this leads to restricted gas exchange due to less surface in the alveoli and increased distance for gas diffusion between the alveolar lumen and the capillary lumen.

The histological description of BPD has changed in the past decades. First described by Northway and coworkers in 1967 (Northway et al., 1967), nowadays named "old" BPD (Baraldi and Filippone, 2007; Chao et al., 2015), it was characterized by inflammatory processes disrupting the architecture of the lung, especially the airways. Over time new treatments of premature infants, such as antenatal steroids and intratracheal application of surfactant, lead to a new histological image of BPD (therefore "new" BPD), which shows hypoalveolarization, disruption of pulmonary vascular structures, interstitial fibrosis and clinically appears less severe (Baraldi and Filippone, 2007; Chao et al., 2015; Voynow, 2017).

The diagnosis of BPD still depends on supplemental oxygen application required during the first 28 days of life and at a post-menstrual age of 36 weeks. New diagnostic criteria and approaches are required in order to better define BPD (Voynow, 2017).

There are different symptoms characterizing BPD such as wheezing, coughing and asthma-like afflictions (Baraldi and Filippone, 2007). Gas exchange impairments due to impaired alveolar ventilation and oxygen and carbon dioxide diffusion lead to hypoxemia and hypercapnia (Niedermaier and Hilgendorff, 2015). Although the symptoms attenuate with age, the lung function parameters in spirometry remain restricted compared to standard values (Baraldi and Filippone, 2007) and symptoms may remain in adulthood (Chao et al., 2015).

Optimal time points and dosage of these therapeutical approaches still have to be evaluated. Although high oxygen concentrations and mechanical ventilation support the oxygen supply to the blood stream in this stressful phase, it is associated with mechanical stress and oxygen toxicity, which, as previously mentioned, is causative for BPD. So far gentle respiratory support with minimal duration and titrated supplemental oxygen concentrations and optimal nutrition represent the methods to prevent or alleviate the occurrence of BPD (Owen et al., 2017). More research is required in this field in order to optimize already existing therapeutical methods or evolve new approaches to on the one hand support the patients' breathing and on the other hand minimize the damage and protect the lungs from evolving BPD (Owen et al., 2017).

The fact that more and more patients with BPD survive due to optimized therapy, but still carry symptoms and have impaired lung function, demands better understanding of the pathological processes underlying this complex disease and development of new and better diagnostic approaches (e.g. *miRNAs* as markers in peripheral blood) in order to distinguish prematurely born infants with and without BPD to enable therapy at an early stage or prevent unnecessary therapy (Chao et al., 2015; Nardiello and Morty, 2016; Silva et al., 2015). Furthermore new therapeutic tools are required to attenuate the symptoms of impaired lung function after surviving BPD to improve the condition of these patients and to lower high costs caused by BPD. The method of application of therapeutics is another interesting factor, as drugs may potentially be administered via trachea (Madurga et al., 2014).

As previously mentioned, *microRNAs* are involved in almost every known molecular process (Krol et al., 2010). Only little is known about their role in late lung development and their involvement in BPD (Nardiello and Morty, 2016). The change of expression levels has been described for several *miRNAs* in BPD, but a causal role in BPD remains to be detected (Nardiello and Morty, 2016; Xing et al., 2015).

1.4 Fgf and Tgf-β signaling – Crucial players in lung development

1.4.1 Fibroblast Growth Factor signaling

Fibroblast Growth Factors (FGFs) are a group of polypeptides of about 200 amino acids, that play a role in several diseases and biological processes in different

types of species (Itoh and Ornitz, 2011). They are involved in organogenesis in embryos by mediating differentiation, migration and proliferation of cells (Chao et al., 2015; Eswarakumar et al., 2005). In adulthood they can function similar to hormones in an "intracrine, paracrine and endocrine" fashion (Eswarakumar et al., 2005; Itoh and Ornitz, 2011). In mammals, there are 22 different FGFs known, but as only either Fgf15 or Fgf19 appear in a certain species (Fgf15 in rodents, Fgf19 in other vertebrates), they are numbered consecutively from Fgf1 to Fgf23 (Fgf15 and Fgf19 seem to be orthologous) (Itoh and Ornitz, 2011; Ornitz and Itoh, 2015). The 22 FGFs can further be divided into 7 subgroups of evolutionary relationships (Itoh and Ornitz, 2011; Ornitz and Itoh, 2015).

The receptors of the FGFs are called Fibroblast Growth Factor Receptors (FGFRs) and embody tyrosine kinase receptors anchored in the cell membrane (Itoh and Ornitz, 2011). These FGFRs consist of an extracellular domain containing three components similar to immunoglobulins (D1-D3) with the cofactor heparin sulfate (proteoglycan) for ligand binding, a transmembrane part anchoring the receptor in the cell surface and an intracellular domain for signal transduction, which basically forms the intracellularly located tyrosine kinase (Eswarakumar et al., 2005; Itoh and Ornitz, 2011; Ornitz and Itoh, 2015). Both, in humans and mice, out of four *FGFR/Fgfr* genes (*FGFR1-4/Fgfr1-4*) 7 different protein products can be formed by alternative splicing of the D3 immunoglobulin-like domain, enabling the FGFRs 1-3 to assume two different forms, such as FGFR2b or FGFR2c (Ornitz and Itoh, 2015). The crucial region for binding specificity of FGFRs is formed by immunoglobulin-like domains D2 and D3 and the connecting area in between the two of them (Ornitz and Itoh, 2015). Therefore it is plausible that alternative splicing of D3 is able to change binding specificity. Binding of a specific FGF to its specific receptor leads to receptor dimerization and autophosphorylation of tyrosine residues, which induces different signaling pathways inside the cell such as Ras-Raf-MAPK, PI3K-Akt, STAT and PLCγ by tyrosine/threonine phosphorylation, creating new binding sides for downstream signaling effectors such as FRS2α, FRS2β or SH2/PLCγ (Eswarakumar et al., 2005) (see Figure 3). Different downstream targets are activated such as Etv4 and Etv5, which are transcription factors that are also involved in an inhibitory feedback loop affecting Fgf signaling (Herriges et al., 2015). Sprouty proteins are also downstream factors, which are

activated upon FGF signaling. They are able to inhibit FGF signaling (Warburton et al., 2000). Furthermore Bmp4 is another downstream factor, which is targeted by Fgf10 and is thereupon able to inhibit further Fgf signaling activity (Chao et al., 2015; Chao et al., 2017).

Various ligands act on the same receptor but still induce different effects. For example, in the isolated lung endoderm both Fgf7 and Fgf10 activate Fgfr2b, but upon Fgf7 activation the effect is rather proliferative and therefore leads to a "cyst-like structure", whereas Fgf10 acts chemotactive and induces branching of the airways (Bellusci et al., 1997; Cardoso et al., 1997; Lebeche et al., 1999). Basically

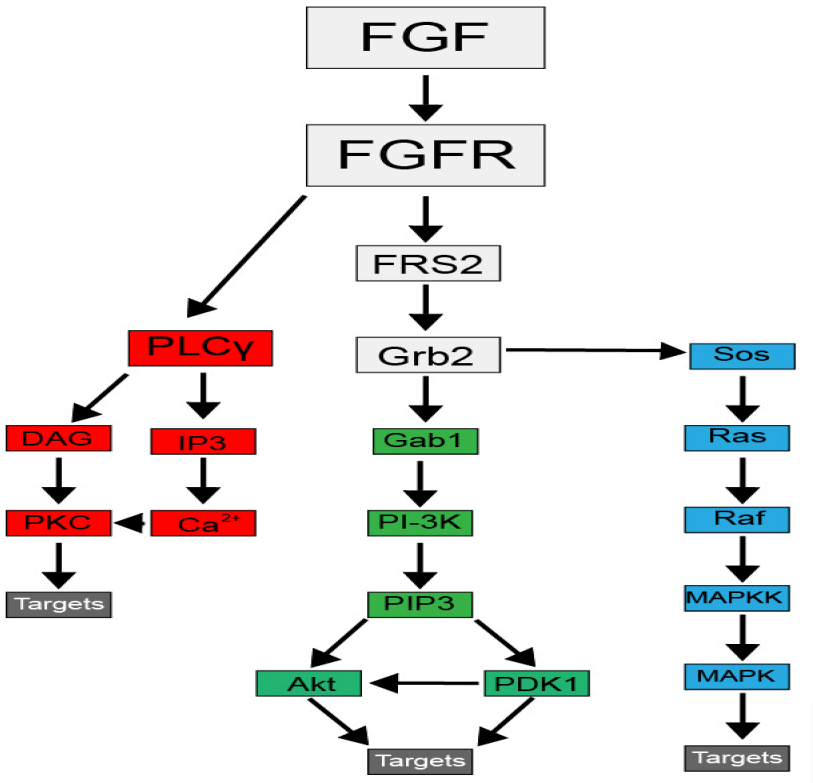

Figure 3: Activated signaling pathways downstream of FGFR (adapted from Eswarakumar et al., 2005): Simplified illustration of how FGF signaling is able to activate different types of downstream effectors. Upon FGFR activation various downstream signaling pathways can be activated depending on ligand and receptor species, such as the PLCγ, PI3K-Akt and Ras-Raf-MAPK signaling cascade to activate downstream targets. Components of the PLCγ pathway are depicted in red, the PI3K-Akt pathway in green and Ras-Raf-MAPK axis in blue. Factors, which are not specifically referred to any of the pathways, are depicted in bright grey. Dark grey boxes denote targets of the signaling axes. For detailed information see section 1.4.1.

this is due to a differential phosphorylation pattern after receptor activation differing between the ligands (El Agha and Bellusci, 2014). Also the same ligand can activate different receptors: For example FGF10 is able to induce receptor activity for both FGFR1b and FGFR2b (Ornitz and Itoh, 2015). It is easily imaginable how many different binding combinations between the various receptors and ligands can induce a vast variety of different cellular processes.

FGF signaling is involved in several processes such as "cell proliferation, differentiation and pattern formation" and it regulates the interaction of lung epithelium and mesenchyme in lung development (Warburton et al., 2000).

An interruption of Fgf signaling can lead to various pathologies. A missense mutation in the *FGF10* gene is accompanied with Aplasia of lacrimal and salivary glands (ALSG) (Entesarian et al., 2007). Rohmann and coworkers found mutations in *FGFR2*, *FGFR3* and *FGF10* genes to be associated with the autosomal-dominant Lacrimo-auriculo-dento-digital syndrome (LADD), which commonly goes along with malformation of ears, teeth, fingers, kidney, respiratory system and genitals, and is accompanied with facial dysmorphism, deafness and aplasia of the lacrimal duct (Rohmann et al., 2006). Overexpression of *Fgf10* in the sclera might be associated with an extreme form of myopia (Hsi et al., 2013).

Fgf10 plays an outstanding role in lung development (Chao et al., 2016). It has been shown most obviously in *Fgf10*-null mice (*Fgf10-/-*). Although the trachea was formed no further lung development occurred beyond this, as not even the right or left primary lung buds were found. Furthermore these mice lacked limb outgrowth, demonstrating the involvement of Fgf10 in limb development, which is in accord with the previously mentioned LADD syndrome (Rohmann et al., 2006; Sekine et al., 1999). Fgf10 is expressed in the submesothelial mesenchyme and acts on the Fgfr2b receptor in the epithelium allowing epithelial-mesenchymal communication. In early lung development it is involved in branching of the airways by a chemotactic effect on the epithelium (Bellusci et al., 1997). Furthermore it maintains the epithelial progenitor cells in their multipotent status (Chao et al., 2017). In the alveolar phase and in adult lungs *Fgf10* is found to be expressed in high levels, suggesting a role in late lung development as well, but not much is known about its exact function at that phase (El Agha and Bellusci, 2014). A reduction of *Fgf10* leads to an impaired formation of lung epithelial cells, including AECII cells, indicating the involvement of *Fgf10* in the development of

alveolar epithelial cells, as well as lung epithelial cells in general. Furthermore, in the same genetic mouse model it has been shown that alveolar myofibroblast formation and subsequently the deposition of Elastin were reduced upon down-regulation of Fgf10 signaling further emphasizing the importance of *Fgf10* in the process of alveolar septation and indicating a potential role for *Fgf10* in postnatal lung development in general (Ramasamy et al., 2007).

Chao and colleagues examined the role of Fgf10 in the BPD mouse model comparing the effect of hyperoxic injury on the lung of *Fgf10*-deficient mice (*Fgf10*+/-) to control mice (*Fgf10*+/+). It was found that although both groups survived under normoxic conditions showing no difference in histological lung structure, *Fgf10*-deficient mice were not able to survive hyperoxic lung injury compared to control mice. All control mice survived, whereas the *Fgf-10*-deficient mice died within a couple of days after birth. Furthermore the differentiation of AECII cells was limited in *Fgf10*+/- mice and the histological examination of the lungs showed more severe hypoalveologenesis in those mice, suggesting that Fgf10 signaling might have a protective ability in hyperoxic lung injury and might alleviate the sequelae of Bronchopulmonary Dysplasia (Chao et al., 2017). Interestingly, FGF10 protein level was found to be decreased in BPD patients' lungs compared to control samples (Benjamin et al., 2007). It is obvious to assume that Fgf10 might play a very important role in both lung development and lung repair after injury.

1.4.2 Tgf-β signaling

The classical model of Tgf-β signaling is that after ligands activate the receptor, Smad proteins move to the nucleus and influence the transcription of target genes (see Figure 4). But other pathways can also be activated, which function without Smad proteins (Derynck and Zhang, 2003).

There are 29 known ligands, which can be separated into four different groups, such as the Tgf-βs (Transforming growth factors), activins/inhibins, BMPs and GDFs, and other ligands, which do not belong into any of these groups (Derynck and Zhang, 2003; Nickel et al., 2017; Shi and Massagué, 2003).

The construction of a Tgf-β receptor is composed of a tetrameric structure, containing two type I and two type II serine/threonine kinase receptors. Both types

consist of around 500 amino acids and can be subdivided into three compartments: the N-terminal compartment for ligand binding, which is located outside the cell, a compartment anchoring the receptor in the cell's membrane and the C-terminal serine/threonine kinase compartment. 7 different type I and 5 different type II receptors are known. Without ligand binding the receptors form homomeric dimers. Interestingly, different types of ligands primarily bind either type I receptors (e.g. BMPs), or type two receptors (Tgf-βs and activin) or both combined. The combination of different type I and type II components on the one hand allows to influence ligand binding specificity and on the other hand influences which signaling pathways and target genes are activated after ligand binding, leading to a great variability of ligand specificity and effects on the cell. This means that a single ligand can have a different effect when binding to receptors that are composed of different type I and type II serine/threonine receptors (Derynck and Zhang, 2003; Shi and Massagué, 2003).

8 Smad proteins are known, which are numbered consecutively from Smad1 to Smad8 (Derynck and Zhang, 2003). The Smad proteins can be divided into 3 groups of Smads: receptor-regulated Smads (Smads 1, 2, 3, 5 and 8; often referred to as "R-Smads"), inhibitory Smads (Smad6 and Smad7) and Smad4, which functions as a co-mediator. Basically Smad proteins are polypeptides consisting of about 500 amino acids, with an N-terminal MH1 unit for DNA-binding (except Smad6 and Smad7) and a C terminal MH2 unit for receptor interaction and complex formation (Derynck and Zhang, 2003; Shi and Massagué, 2003) (see Figure 4). Binding of the dimeric ligand to the receptor complex brings the serine/threonine kinases in close positioning, allowing the type II receptor to phosphorylate the so-called type I receptor-specific GS region, which subsequently activates the signaling cascade by activating R-Smad proteins by C-terminal phosphorylation by the type I receptor. The activated R-Smads and Smad4 form a heteromeric complex and translocate to the cell's nucleus, where they are attached by further cofactors. In the nucleus the activated Smads are dephosphorylated, which dissociates the heteromeric complex and enables the Smads to directly bind DNA in a sequence-specific fashion and hereby affect transcription of target genes.

Some Smads inhibit the signaling cascade in a negative feedback loop. There are different mechanisms of inhibition, such as receptor targeting, leading to the

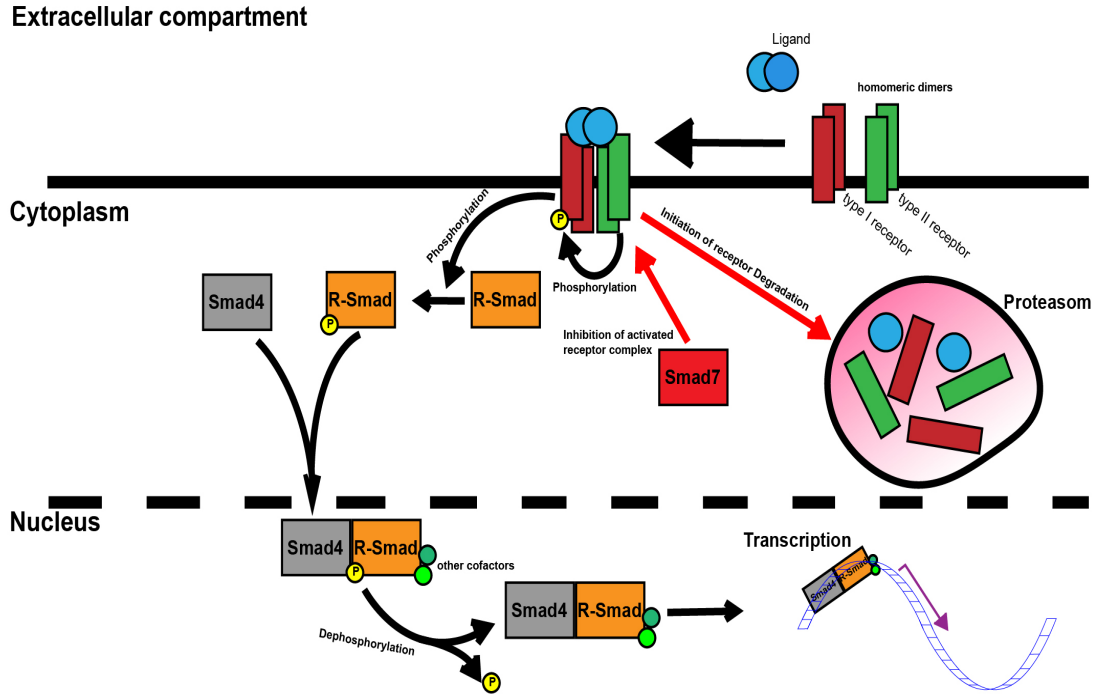

Figure 4: Tgf-β signaling (adapted from Shi and Massagué, 2003): Simplified illustration of Tgf-β receptor activation. Binding of the homodimeric ligand to the heterotetrameric receptor complex leads to the phosphorylation and activation of the type I receptor by the type II receptor and subsequent activation of regulatory Smad proteins (R-Smad) by phosphorylation. R-Smad is complexed by Smad4 and other cofactors when translocating to the nucleus, where genetic expression is activated after the R-Smad is dephosphorylated. The components of the R-Smad complex are then transported to the proteasome complex after it is ubiquitinated and degraded (not depicted). An antagonizing mechanism is inhibition of the activated receptor complex by Smad7, which induces receptor degradation by proteasome complex. Activating processes are depicted with black arrows, inhibitory processes are depicted with red arrows. For further detailed description see section 1.4.2.

receptor's degradation, or competing with R-Smads at different levels of the signaling cascade. Furthermore, dephosphorylation and degradation of Smad proteins ends Smad signaling. The Tgf-β signaling pathway is far more complex than it is depicted here. For example, there are various co-receptors attached to the Tgf-β receptor complex modulating the interaction of the ligand and the receptor (Derynck and Zhang, 2003; Nickel et al., 2017; Shi and Massagué, 2003). Tgf-β

ligands can induce other signaling pathways apart from Smad proteins, such as Erk, JNK, PI3K and MAPK (Derynck and Zhang, 2003).

Tgf-β signaling is involved in many different types of cellular processes in various organisms (Shi and Massagué, 2003). With its growth inhibitory effect Tgf-β signaling functions tumor suppressing on the one hand, but on the other hand, when expressed by tumor cells, can lead to the progression of cancerous processes (Shi and Massagué, 2003). For example in mammary carcinoma, it acts as a tumor suppressor in early stages, but benefits cancer in progressed stages (Zhao et al., 2017b). This phenomenon is referred to as the "TGF-β paradox" (Tian and Schiemann, 2009). It has been shown that members of the Tgf-β superfamily are able to inhibit proliferation and differentiation of the lung epithelium (Warburton et al., 2000). In early murine lung development Tgf-β signaling was shown to disrupt the formation of lung buds by down-regulating Fgf10, which is required for lung bud formation. Still Tgf-β was found to be involved in lung development (Chen et al., 2010). In late lung development it has been shown that *Smad3* deficiency (*Smad3* knockout mice) leads to hypoalveologenesis, indicating that Tgf-β signaling is involved in the process of alveolarization (Chen et al., 2005). Then again excessive Tgf-β signaling appears to interrupt proper alveologenesis, but can be ameliorated by anti-Tgf-β antibodies (Nakanishi et al., 2007). Tgf-β signaling also plays a vital role in the alveolar maturation in late lung development, allowing AECI cells to spread and properly form their flat shape (Wang et al., 2016b). Furthermore, TGF-β1 signaling is known to act pro-fibrotic in pulmonary fibrosis (Milosevic et al., 2012; Wei et al., 2017b). In this context, the expression of PAI-1 was shown to be induced by TGF-β1, with PAI-1 having an effect on ECM remodeling (Milenkovic et al., 2017). The link between Tgf-β1 and Pai-1 is obvious when considering, that it was shown in the murine kidney, that *Pai-1* deficiency leads to a prevention of Tgf-β1 mediated collagen deposition (Krag et al., 2005). Apparently Pai-1 can act as a downstream mediator of Tgf-β signaling. Moreover, the relationship between Tgf-β1, Caspase-1 and Il-1β was examined in the context of bleomycin-induced murine lung fibrosis (Krag et al., 2005). It was found that inhibiting Il-1β leads to a decreased expression of the fibrosis marker Tgf-β1 and Pai-1 and inhibited the formation of a fibrotic phenotype after bleomycin application.

1.4.3 Antagonism of Fgf10 signaling and Tgf-β signaling

In lung development the effects of Fgf10 and Tgf-β can be described as rather opposing: In early lung development Fgf10 signaling is required for lung bud formation (Chen et al., 2010), whereas Tgf-β signaling has to be repressed in order to allow lung bud formation (Chen et al., 2007). Retinoic acid has been shown to be important for the formation of lung buds by directly regulating and balancing Wnt signaling and Tgf-β and therefore indirectly fine-tuning Fgf10 levels. The fact that Tgf-β inhibits Fgf10 signaling underlines this antagonistic relationship (Chen et al., 2010; Chen et al., 2007; Lebeche et al., 1999).

Another example for the antagonistic relationship between Fgf10 and Tgf-β signaling is branching morphogenesis: In the developing lung Fgf10 is a known stimulator for branching morphogenesis (Bellusci et al., 1997), whereas Tgf-β1 has been shown to inhibit branching morphogenesis (Serra et al., 1994).

Similarly, in a BPD mouse model Fgf10 signaling was shown to be protective against hyperoxic injury (Chao et al., 2017), whereas Tgf-β signaling mediates the pro-fibrotic effect of hyperoxia on the lung (Alejandre-Alcazar et al., 2007).

2. Aims of the current study

Using a pull down experiment and an in vivo approach overexpressing *miR-154* colleagues from our laboratory found the transcription products of some genes, which are known as involved in either Fgf signaling or Tgf-β signaling, to be significantly and differentially expressed, and therefore to be potential targets of *miR-154*, such as *Hopx* (*Homeodomain-only protein*), *Cav1* (*Caveolin-1*), *Gprin3* (*G protein-regulated inducer of neurite outgrowth 3*) and *Apln* (*Apelin*) (*data not published, data not shown*). CAV1 has been shown to be down-regulated by TGF-β1 via p38/MAPK inducing proliferation and an anti-apoptotic effect in myofibroblasts (Sanders et al., 2015). In murine small intestine Fgf10 was shown to be capable of down-regulating the expression of the stem cell marker *Hopx* (Al Alam et al., 2015). Furthermore, and most interestingly, *Hopx* expression was shown in the bipotent alveolar epithelial cell progenitor and in AECI cells, but not AECII cells, suggesting *Hopx* as a marker gene for AECI cells (Treutlein et al., 2014). Unpublished data from our team found *Gprin3* to be regulated by Fgf10 during early lung development (Bellusci and Jones, *data not published*). It was shown that APLN indirectly regulates the expression of FGF2 and FGFR1 in PAH via its mediator *microRNAs miR-424* and *miR-503* (Kim et al., 2013).

As previously mentioned, both Fgf signaling and Tgf-β signaling play crucial roles in lung development, although acting in an antagonistic fashion. It is likely, that proper lung development requires a balanced and fine-tuned expression level of both pathways, as disorders of this balance, regardless of which pathway prevails, cause disturbances of lung development leading to pathological lung phenotypes (Alejandre-Alcazar et al., 2007; Bellusci et al., 1997; Chao et al., 2017; Chen et al., 2005; Sekine et al., 1999). It has been previously described that the expression of *miR-154*, as well as other members of the *miRNA* cluster were up-regulated upon TGF-β1 stimulation via SMAD3 in the context of IPF (Milosevic et al., 2012).

In summary, it is assumable, that *miR-154* can influence the balance between Fgf signaling and Tgf-β signaling, when considering the potential involvement by affecting factors related to Fgf and Tgf-β signaling pathways (previously mentioned in this section). As the pathogenesis of BPD seems to be influenced by these signaling pathways (Alejandre-Alcazar et al., 2007; Chao et al., 2017), it is

tempting to imagine, that *miR-154* is of importance in BPD. In the current study we are rather focusing on *miR-154-3p*.

Therefore the aims of this study can be summarized as follows:

1.) To examine the temporo-spatial expression pattern of *miR-154-3p* and *miR-154-5p* in the model of hyperoxic lung injury (BPD mouse model).
2.) To show the impact of airway epithelial-specific *miR-154* overexpression on the lung histology and gene expression compared to wildtype controls and after hyperoxic lung injury compared to normoxic controls.
3.) To describe the potential role of *miR-154* in the BPD mouse model as a potentially protective factor.

3. Material and methods

3.1 Generation of mice

3.1.1 Hyperoxia-induced lung injury (BPD mouse model)

To expose mice to hyperoxia Proox 110 compact oxygen controller (BioSpherix) was used (see Figure 5). Oxygen concentration was adjusted to 85%. The time periods of oxygen exposure are described in the following sections.

For the hyperoxic lung injury experiment wildtype mice were generated on a CD1 background and sacrificed at three different time points (P2, P5 and P8). Mice were either exposed to 85% O_2 (hyperoxia; HYX) or room air (normoxia; NOX; used as controls) from birth (P0) until lung harvest (P2, P5 or P8, respectively). In order to prevent injury from oxygen toxicity the murine mothers were rotated every day between normoxic and hyperoxic conditions. Mice were kept under a 12h/12h light/dark cycle. Colleagues with the required qualification performed euthanasia with a carbon dioxide anesthesia.

Figure 5: Proox 110 compact oxygen controller. Animal cages are placed in the chamber. The chamber has small punctures on the sidewalls allowing gas circulation. Oxygen is admitted into the chamber. The required percentage on O_2 concentration is adjusted on the oxygen controller, which is located centrally on top of the chamber. Further more the valve, which is located right-sided on top of the chamber, is connected to the oxygen gas cylinder (not depicted).

3.1.2 Generation of transgenic mouse line *CCSP-rtTA/CCSP-rtTA;tet(O)miR-154/+* for hyperoxic lung injury experiment and induction of *miR-154* expression

The *tet(O)miR-154* responder line was created by Dr. Gianni Carraro on a C57BL6 background. An integration of a *tet(O)-miR-154-lacZ* cassette was performed in order to produce a transgenic mouse line. *CCSP-rtTA* (Perl et al., 2002; Perl et al., 2009) mice were crossed with *tet(O)miR-154* mice to generate mice over-expressing both *isomiRNAs*, *miR-154-3p* and *miR-154-5p*, under the club cell-specific promotor *CCSP*. In our case *CCSP-rtTA/CCSP-rtTA;tet(O)miR-154/+* double transgenic mice were crossed with *CCSP-rtTA/CCSP-rtTA*;+/+ mice to either generate *CCSP-rtTA/CCSP-rtTA*;*tet(O)miR-154/+* (experimental group) or *CCSP-rtTA/CCSP-rtTA*;+/+ (control group) mice. *CCSP-rtTA/CCSP-rtTA*;+/+ mice were crossed with wildtype mice with an FVB/N background to generate *CCSP-rtTA/+*;+/+ which were added to the control group. Therefore the genotype of control mice is either *CCSP-rtTA/CCSP-rtTA*;+/+ or *CCSP-rtTA/+*;+/+.

In the following sections the experimental group will be referred to as *Tg(Scgb1a1-rtTA)/Tg(Scgb1a1-rtTA);Tg(miR-154)/+* and the control group will be referred to as *Tg(Scgb1a1-rtTA)/Tg(Scgb1a1-rtTA);+/+*.

To activate the inducible gain-of-function system doxycycline food (0.0625% doxycycline, Altromin Spezialfutter GmbH & Co. KG, Lage, Germany) was administered one day before birth (E18) until lung harvest (P16) for all mice. Both experimental mice and control mice were either exposed to hyperoxia (85% O_2; HYX) from birth (P0) until P8 or if not exposed to hyperoxia used as controls (NOX). Therefore we generated 4 sets of mice (WT/NOX; Mut/NOX; WT/HYX; Mut/HYX). Lungs were harvested at P16.

In order to demonstrate that the mouse line is functioning and that both, *miR-154-3p* and *miR-154-5p* are actually overexpressed after doxycycline administration, we have performed an RT-qPCR for both *microRNAs*, which shows a highly significant increase for both *isomiRNAs* (see Figure 6.E+F).

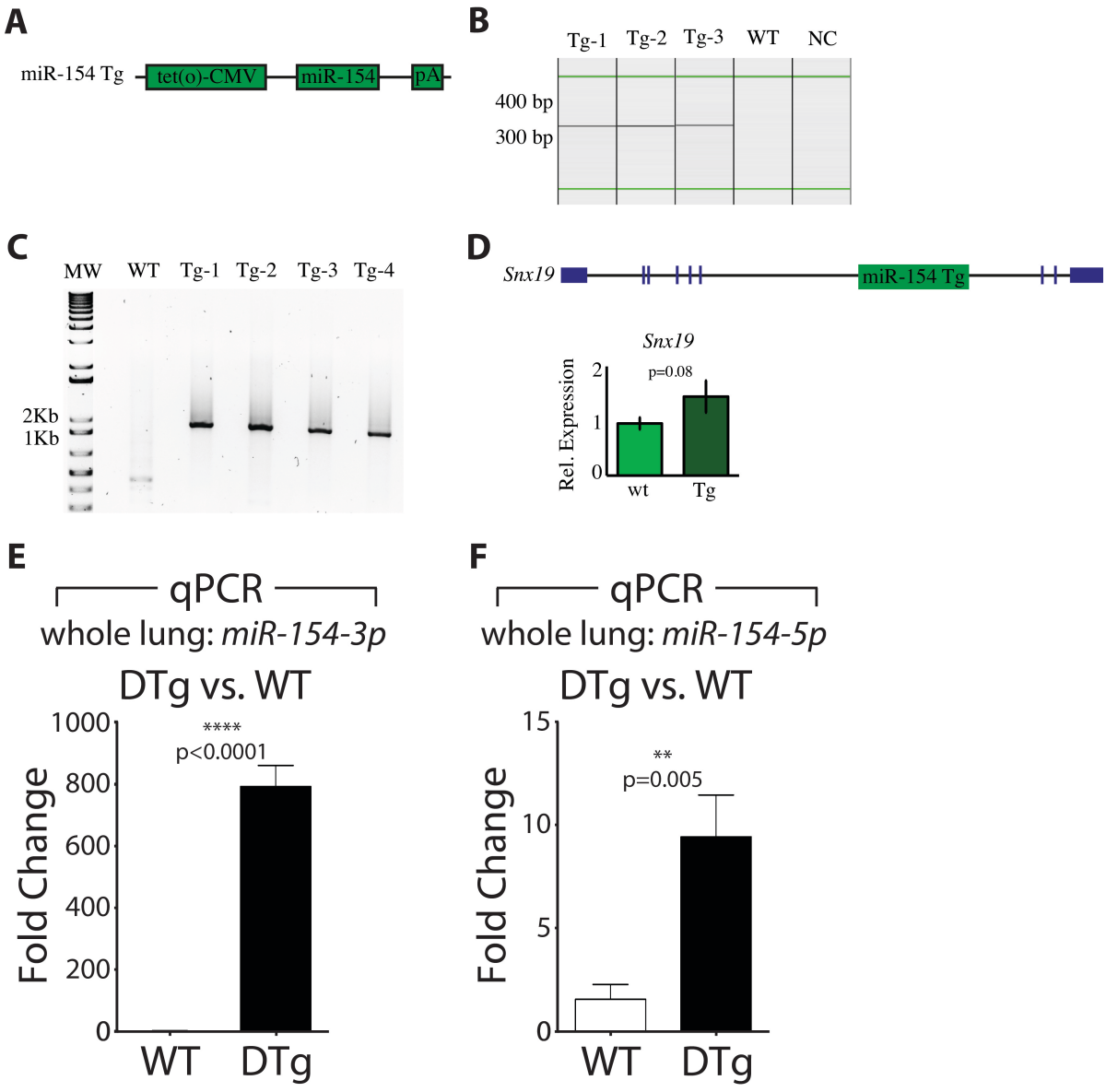

Figure 6: Validation of the transgenic mouse line *CCSP-rtTA/CCSP-rtTA;tet(O)miR-154/+*: A. Scheme of *miR-154* transgene. **B.** Genotyping PCR performed on DNA extracted from *Tg(tet(O)miR-154)* mice. **C.** The integration of the transgene (Tg) was analyzed by restriction digestion and nested PCRs, followed by sequencing. **D.** Scheme of *Snx19* gene and the Tg integration site. Expression of *Snx19* after Tg integration was analyzed by qPCR in embryonic lungs. **E. + F.** Increased expression of *miR-154-3p* (**E**) and *miR-154-5p* (**F**) in double transgenic mice (DTg: *CCSP-rtTA/CCSP-rtTA;tet(O)miR-154/+*) vs. WT (*CCSP-rtTA/CCSP-rtTA;+/+*) after Dox induction from E18-P16. **A.-D.** from Dr. Gianni Carraro.

3.2 Extraction of murine lung specimen

After euthanasia, the thoracic cavity was opened by median sternotomy. Transcardiac perfusion was performed with phospho-buffered saline (PBS) to rinse the lungs from blood. Carotids were lanced to allow the PBS to flow out of the lungs. After clamping the right bronchus, the right lung was taken out by severing the right bronchus distally from the clamp. The caudal lobe was stored in 700 µl of QIAzol® Lysis Reagent (QIAGEN Sciences, 79306, Maryland, USA) at -80°C for RNA Isolation, the remaining lobes were stored at -80°C. After tracheotomy, the left lung was perfused with Paraformaldehyde (PFA 4%, 335.2, Carl Roth GmbH & Co. KG, Karlsruhe, Germany) at a pressure of 20 cm H_2O. The left lung was taken out and stored in PFA 4% at 4°C over night. Finally the tips of the murine tails were stored at -20°C for genotyping. After extraction, the lungs were kept in 4% PFA for 24 h at 4°C. Then the lungs were stored in PBS for 24 h at 4°C. The samples underwent increasing gradients of ethanol and were incubated in Xylol and a Xylol-Paraffin compound (1:1). Finally the samples were stored in Paraffin for 24 h. Next the lungs were poured off into cassettes and cooled down on a cooling plate for 1-2 hours. 5 µm sections were sliced with the Leica RM 2235 microtome.

3.3 Genotyping of the *CCSP-rtTA/CCSP-rtTA*;*tet(O)miR-154/+* mouse line*

After lung harvest the tail tip of each mouse was collected for genotyping. Tail tips were digested with 200 µl of DirectPCR® Lysis Reagent Tail (Peqlab, 31-102-T, Erlangen, Germany) for each sample. After adding 2 µl of Proteinase K-solution (Peqlab, 04-1076, Erlangen, Germany) samples were stored at 56°C over night at 1400 rpm. To stop Proteinase K activity the samples were kept at 85°C for 45 min.

For the detection of the *CCSP-rtTA* transgene capillary electrophoresis and PCR were performed with the QIAxcel DNA Fast Analysis Kit (3000) (Qiagen, 929008, Hilden, Germany). The Mastermix for PCR was composed as follows: 4.4 µl H_20, 0.5 µl of 25 mM $MgCl_2$, 0.1 µl of 25 mM *dNTPs*, 5 µl Qiagen Master Mix, 0.1 µl Taq Polymerase, 0.1 µl of 100 µM of each Primer (see below), 1 µl *DNA* template.

***CCSP* promotor**	5'- act gcc cat tgc cca aac ac -3'
***rtTA* coding sequence**	5'- aaa atc ttg cca gct ttc ccc -3'

Table 3: Primer sequences for PCR for *CCSP-rtTA*

PCR was run with the following protocol:

Temperature (°C)	Time
94	5 min
94	30 sec
58	30 sec
72	30 sec
72	5 min
4	Hold

*30 cycles of steps 2-4 before continuing with step 5

Table 4: PCR protocol for *CCSP-rtTA*

For the detection of the *tet(O)miR-154* transgene the same procedure was performed as above. Composition for PCR: 4.5 µl H_2O, 0.5 µl 25 mM $MgCl_2$, 0.1 µl of 25 mM *dNTPs*, 5 µl Qiagen Master Mix, 0.1 µl of 100 µM of each primer (see below), 1 µl *DNA* template.

***tet(O)miR-154* forward**	5'- gga att cca cca cac tgg c -3'
***tet(O)miR-154* reverse**	5'- agt ggc agc ctc tcg gtc at -3'
Wildtype	5'- tgg ttc tca tgg gag cta aa -3'

Table 5: Primer sequences for PCR for *tet(O)miR-154*

PCR was run with the following protocol:

Temperature (°C)	Time
94	3 min
94	30 sec
60	1 min
72	1 min
72	2 min
4	Hold

*30 cycles of steps 2-4 before continuing with step 5

Table 6: PCR protocol for *tet(O)miR-154*

For *CCSP-rtTA* the expected band for mutant mice appears at 500 bp, for *tet(O)miR-154* at 231 bp.

**CCSP-rtTA/CCSP-rtTA;tet(O)miR-154/+* is also referred to as *Tg(Scgb1a1-rtTA)/Tg(Scgb1a1-rtTA); Tg(miR-154)/+* in the following sections

3.4 Isolation of alveolar type II cells after hyperoxic lung injury and after *miR-154* induction

Mice on a C57BL6 background were either exposed to 85% O_2 or kept in room air (see section 3.1.1). At P3 the mice were sacrificed and the lungs were harvested. In another approach airway-specific *miR-154* expression was induced from P0 until P16 (see section 3.1.2), compared to control mice. Afterwards AECII cells were isolated and kindly provided for us by Elisabeth Kappes and Dr. med. Cho-Ming Chao.

3.5 *RNA* Extraction for Reverse Transcription and quantitative PCR

The procedure is described for whole lung samples. Whenever the treatment of isolated AECII cells differs from the description, it is mentioned in brackets.
RNA was isolated using the miRNeasy Mini Kit (QIAGEN, Hilden, Germany). Tissue was transferred to gentleMACS M Tubes (Miltenyi Biotec, Bergisch Gladbach, Germany), attached to gentleMACS Dissociator (Miltenyi Biotec) and homogenized for 1 min (setting "RNA"). Tubes were centrifuged for 5 min at 2000 RPM. Supernatant was transferred to Eppendorfs and 1/5 total volume of chloroform was added (procedure for isolated Alveolar Type 2 cells starts from this step). After shaking the Eppendorfs for 15 sec, the content was transferred to Heavy phase-lock gel tubes (5 PRIME 2302830). Phase-lock tubes were centrifuged for 15 min at 12,000 RCF at 4°C. Now three phases were formed in the tubes. The upper aqueous layer was added to a new Eppendorf. 1.5 total volume of 100% Ethanol was added. The liquid was transferred to RNeasy Mini Spin Column (from miRNeasy Mini Kit). Tubes were spun down for 15 seconds at 10,000 RPM and the supernatant was discarded. The pellet remaining in the Mini Spin Column was washed by adding 700 µl of RWT Buffer (from the kit, concentrate previously diluted 1:3 with ethanol), centrifuging columns at 10,000 RPM for 15 s and discarding the flow-through (this step was skipped for isolated Alveolar Type 2 cells). 500 µl of RPE Buffer (concentrate previously diluted 1:5 with ethanol) were added and the column was spun down at 10,000 RPM for 15 sec. The same procedure with RPE Buffer was redone but centrifuged at 10,000 RPM for 2 min. After discarding the supernatant the column with the pellet was put into another Eppendorf in which the *RNA* will be collected. RNase free water was added to the column (volume dependent on expected RNA yield). The Eppendorf with the

column was centrifuged for 1 min at 10,000 RPM. Finally the measurement of absorbance spectra was performed with the ND-1000 (Nanodrop, Montchanin, DE) to estimate the yielded concentration of *RNA* and purity of the samples from the absorbance at 260 nm. Samples were stored at -80°C.

3.6 Hematoxylin & Eosin Staining (H&E)

Slides were deparaffinized with Xylol (3 x 10 min) and decreasing concentrations of ethanol (100%, 95%, 70%, 50% and 30%) for 2 min each. After slides were incubated in Hematoxylin solution (Roth, T865.2) for 45 seconds and washed under running tap water for 10 min slides were incubated in Eosin (Richard-Allan Scientific Eosin-Y, 359551, Kalamazoo, MI) for 90 seconds. Before covering the slides with Pertex mounting media slides were dipped shortly in 80% and 100% of ethanol.

3.7 Fluorescence In-Situ-Hybridization (FISH)

DEPC water	2000 ml MiliQ (Rnase free water) + 2 ml DEPC (Sigma)	Stirred and autoclaved
DEPC-PBS water	1800 ml MiliQ (RNase free water) + 200 ml PBS 10x (Life technologies) + 2 ml DEPC	Stirred and autoclaved
Proteinase K buffer	-5 ml 1M Tris-HCl Ph 7.4 (Roth) -2 ml 0.5 M EDTA (Sigma) -0.2 ml 5 M NaCl (Fluka) -900 ml MiliQ (RNase free water) -0.1% DEPC autoclaved (see above)	Autoclaved
4% PFA in PBS	-450 ml sterile H_2O (heated on stir plate to 60°C) -20 g of dry PFA (Roth) -Several drops of 6 M NaOH (Roth) -50 ml PBS	Filtered through Filtropur BT25 (Sarstedt)

Table 7: Solutions for FISH

The required instruments were purged with RNAse ZAP Decontamination (Sigma) and rinsed with DEPC water. 5 µm sections of the left lobe of the murine lung were deparaffinized with Xylen (Carl Roth GmbH + Co. KG, Karlsruhe, Germany) and a decreasing gradient of ethanol (EtOH). After washing the slides with DEPC-PBS, the sections were digested with Proteinase K (peqlab, Erlangen, Germany). The time of incubation and the concentration of the Proteinase K added

to the Proteinase K buffer were dependent on the age of the samples (P2: 1:3000 for 4 min; P5: 1:1300 for 7 min; P8: 1:1300 for 10 min). After washing with DEPC-PBS again, the sections were blocked with Dual endogenous enzyme block (DAKO Envision™ + Dual Link System-HRP (DAB+) kit, Carpinteria, CA, USA) and then washed with DEPC-PBS once more. 0.01% Glutaraldehyde solution (Sigma-Aldrich Chemie GmbH, Steinheim, Germany) diluted in 4% PFA (Carl Roth GmbH & Co. KG, 335.2, Karlsruhe, Germany) was put on the sections and incubated for 10 min. After another step of DEPC-PBS washing, the samples were pre-incubated with miRCURY LNA™ microRNA Detection Hybridization Buffer for 5 h at 54°C to be incubated with the miRCURY LNA™ Detection probe (miR-154*; probe sequence: 5'-AATAGGTCAACCGTGTATGATT-3') diluted in Hybridization Buffer (1:625) for 37 h at 54°C afterwards. To protect the samples from drying out during incubation the samples were covered with HybriWell Incubation chambers (Bio Cat, Heidelberg, Germany).

The samples were washed with a decreasing gradient of SSC (Sodium/Sodium citrate stock solution, 1054.1, Roth) at 52°C and incubated in a blocking solution (DIG Wash and Block Buffer Set, Roche Diagnostics GmbH, Mannheim, Germany) containing 72% DEPC water, 18% Maleic acid Buffer 10x and 10% blocking solution 10x at room temperature for 30 min. Anti-DIG-POD (Roche; ratio 1:400) and Sheep Serum (Normalserum (Schaf)-unkonj., Dianova, Hamburg, Germany; 1:250) were added to the blocking solution from the previous step. The sections were covered in this new mixture remaining for 4 h at room temperature. After another step of DEPC-PBS washing, TSA™-plus Fluorescein System (Perkin Elmer, Boston, MA, USA) was applied to the samples for 15 h.

Coverslips were mounted on the slides with Prolong® Gold antifade reagent with DAPI (ProLong™ Gold antifade reagent with DAPI, P36935, life technologies, Eugene, OR). Slides were stored at 4°C.

At least 3 histological samples and 5 areas of each sample were used for quantitative analysis. The number of *miR-154-3p* positive cells (*miR-154-3p* positive and DAPI positive) was counted and compared to the total number of cells (total DAPI positive) for both bronchiolar and alveolar epithelium. For each sample an average percentage of *miR-154-3p* positive cells was calculated (*miR-154-3p* positive and DAPI positive cells relative to total DAPI positive cells). Unpaired, two-tailed Student's T-test was performed to quantify whether the percentage of

miR-154-3p positive cells was significantly different between the comparing groups.

3.8 Immunofluorescence

Slides were deparaffinized with Xylol (3 x 10 min) and with descending concentrations of ethanol (100%, 95%, 70%, 50% and 30% for 2 min each). Washing steps were performed with PBST.

Slides were blocked with bovine serum albumin (BSA 3%; Triton-X 0.4%) in PBS at room temperature for 1 h.

Staining for Acta-2

Acta-2 was used as a marker for alveolar myofibroblasts (De Langhe et al., 2006). Monoclonal Anti-Actin, α-Smooth Muscle – Cy3TM (Sigma Life Science, C6198-.2ML, St. Louis, MO) diluted 1:100 in incubation buffer (see above) was used overnight at 4°C as a conjugated antibody.

Staining for Surfactant Protein C

Surfactant Protein C (Sftpc) was used as a marker for AECII cells (Hobi et al., 2016). Anti-Prosurfactant Protein C (proSP-C) Antibody (Merck Millipore, AB3786, Darmstadt, Germany) diluted 1:500 in incubation buffer was used overnight as the primary antibody. The slides were washed with PBST (3 x 5 min). Rabbit IgG (H+L) Secondary Antibody (ThermoFisher Scientific, A-31572, Dreieich, Germany) diluted 1:500 was left on the sections for 60 min at room temperature.

Staining for pSmad3

pSmad3 as a Tgf-β downstream effector was used to demonstrate and measure Tgf-β signaling activity (Derynck and Zhang, 2003). After lung harvest, lung fixation and slicing sections from the paraffin block, the pSmad3 staining was kindly performed by Volker Zimmermann.

After washing the slides with PBST and PBS (see above) samples were covered with DAPI. Slides were stored at 4°C. Leica DM5500 B fluorescence microscope and Leica Advanced Fluorescence software (2.6.0.7266) were used to capture images of the stainings.

3.9 Alveolar Morphometry

Mean linear intercept (MLI; in µm), mean air space (in %) and mean septal wall thickness (in µm) measurement was performed using hematoxylin and eosin (HE; see above) stained lung sections of 5 µm. A Leica DM6000B microscope with an automated stage according to the procedure previously described (McGrath-Morrow et al., 2004; Woyda et al., 2009), which was implemented into the Qwin V3 software (Leica, Wetzlar, Germany), was used for scanning the left lobe. Horizontal lines of 40 µm were positioned across the lung sections. The number of times the lines cross alveolar walls was calculated by multiplying the length of the horizontal lines and the number of lines per section then dividing by the number of intercepts. Bronchi and vessels were excluded before the measurement started in order to exclusively measure alveoli. The air space was determined as the nonparenchymatous nonstained area. The septal wall thickness was measured as the length of the line perpendicularly crossing a septum. Mean values were calculated from each measurement.

3.10 Genetic Expression Measurements

3.10.1 Reverse Transcription and quantitative PCR (RT-qPCR)

RNA samples were kept in -80°C. After thawing, *RNA* was extracted and diluted to the required *RNA* concentration. QuantiTect Reverse Transcription Kit (QIAGEN GmbH, 151046697, Hilden, Germany) was used for genomic *DNA* elimination and reverse transcription, Platinum SYBR Green qPCR SuperMix-UDG (invitrogen/life technologies, 1655057, Carlsbad, CA) was used for qPCR. For genomic *DNA* elimination gDNA wipeout buffer was added to the *RNA* and incubated for 2 min at 42°C. For reverse transcription RT, RT buffer and RT primer mix (QuantiTect Reverse Transcription Kit) were added to the *RNA* and incubated for 50 min at 42°C and for 3 min at 95°C. The *cDNA* resulting out of this procedure can be stored at -20°C.

Before qPCR starts *cDNA* was diluted to at least 4 ng/µl. A 96-well plate was used for qPCR. 2 µl of *cDNA* and 18 µl of Mastermix (containing 10 µl Mastermix SybrGreen, 7.2 µl RNase free water, 0.4 µl forward and reverse 10 µM primer respectively) were added to each well. For qPCR the LightCycler 480 Instrument II (Roche) was used with the following setting:

- Pre-incubation: 55°C for 2 min, 95°C for 5 min.
- Amplification: 95°C for 5 sec, 60°C for 10 sec, 72°C for 10 sec (45 cycles).
- Melting curve: 95°C for 15 sec, 65°C for 1 min, increasing temperature for 0.57°C/s until 97°C.
- Cooling: 40°C for 10 sec.

Gene	**Forward primer**	**Reverse primer**
Acta2	5'-act ctc ttc cag cca tct ttc a-3'	5'-ata ggt ggt ttc gtg gat gc-3'
Aqp5	5'-taa cct ggc cgt caa tgc-3'	5'-gcc agc tgg aaa gtc aag at-3'
Bmp4	5'-gag gag ttt cca tca cga aga-3'	5'- gct ctg ccg agg aga tca-3'
CC10 (scgb1a1)	5'-gat cgc cat cac aat cac tg-3'	5'-cag atg tcc gaa gaa gct ga-3'
Elastin	5'-cca cct ctt tgt gtt tcg ct-3'	5'-cca aag agc aca cca aca atc a-3'
Epcam	5'-tgt cat ttg ctc caa act gg-3'	5'-gtt ctg gat cgc ccc ttc-3'
Etv4	5'-cag act tcg cct acg act ca-3'	5'-gcc ata acc cat cac tcc at-3'
Etv5	5'-gca gtt tgt ccc aga ttt tca-3'	5'-gca gct ccc gtt tga tct t-3'
Fgf9	5'-tgc agg act gga ttt cat tta g-3'	5'-cca ggc cca ctg cta tac tg-3'
Fgf10	5'-atg act gtt gac atc aga ctc ctt-3'	5'cac tgt tca gcc ttt tga gga-3'
Fgfr1b	5'-tgg gtc ggt gcg gag atc gt-3'	5'-acg gac aac aac aaa cca aac cct-'3
Fgfr2b	5'-cct acc tca agg tcc tga agc-3'	5'-cat cca tct ccg tca cat tg-3'
Fgfr4	5'-gga agg tgg tca gtg gga ag-3'	5'-ctc ttg ctg ctc cag gat tg-3'
Hprt	5'-cca cag gac tag aac acc tgc taa-3'	5'-cct aag atg agc gca agt tga a-3'
Il-1b	5'-tgt aat gaa aga cgg cac acc-3'	5'-tct tct ttg ggt att gct tgg-3'
Nkx2.1 (*Ttf1*)	5'-aaa act gcg ggg atc tga g-3'	5'-tgc ttt gga ctc atc gac at-3'
Nmyc	5'-cct ccg gag agg ata cct tg-3'	5'-tct cta cgg tga cca cat cg-3'
Pai-1	5'-agg ata gga tcg agg taa acg aga gc-3'	5'-gcg ggc tga gat gac aaa-3'
p63	5'-aga cct cag tga ccc cat gt-3'	5'-ctg ctg gtc cat gct gtt c-3'
Pdgfa	5'-tga ggt tag agg aac acc tg-3'	5'-tct cac ctc aca tct gtc tc-3'
Pdgfra	5'-tgc aaa ttg aca tag aag gag aag-3'	5'-gcc ctg tga gga gac agc-3'
Smad3	5'-tgg tgc tcc atc tcc tac ta-3'	5'-tac agt tgg gag act gga ca-3'
Smad7	5'-aag tgt tca ggt ggc cgg atc tca g-3'	5'-aca gca tct gga cag cct gca gtt g-3'
SPB	5'-aac ccc aca cct ctg aga ac-3'	5'-gtg cag gct gag gct tgt-3'
SPC	5'-ggt cct gat gga gag tcc ac-3'	5'-gat gag aag gcg ttt gag gt-3'
Shh	5'-gac atc ata ttt aag gat gag gaa aac-3'	5'-tta act tgt ctt tgc acc tct ga-3'
Spry2	5'-gag agg ggt tgg tgc aaa g-3'	5'-ctc cat cag gtc ttg gca gt-3'
Spry4	5'-gca tgc aaa aag cta tcg tg-3'	5'-aaa acc cac cca cac aac a-3'
Tgf-β1	5'- tgg agc aac atg tgg aac tc-3'	5'-cag cag ccg gtt acc aag-3'
Tgf-β3	5'-gca gac aca acc cat agc ac-3'	5'-ggg ttc tgc cca cat agt aca-3'

Tab 8: Mouse primer list

For statistical analysis Unpaired, two-tailed Student's T-test was performed in order to determine significant changes in genetic expression.

For *miRNA* detection previously isolated *RNA* samples were kept in -80°C. After thawing, *RNA* was diluted to 15 ng/µl and 2 µl were used for Reverse

Transcription. TaqMan® MicroRNA Reverse Transcription Kit (Applied Biosystems, 4366596, Foster City, CA, USA) was used for Reverse Transcription. 1 µl of *cDNA* was used for qPCR. TaqMan® MicroRNA Assays (Applied Biosystems, P00987946, Foster City, CA, USA) was used for qPCR with a LightCycler 480 Instrument II (Roche). Unpaired, two-tailed Student's T-test was used to analyze the change of expression of *miR-154-3p* and *miR-154-5p* between the comparing groups.

3.10.2 Gene Array Analysis

After isolation of the AECII cells, the Gene Array was kindly performed by Dr. Jochen Wilhelm. Furthermore he provided the graphical depiction of the data (see Figure 10).

4. Results

4.1 *miR-154-3p* is differentially expressed in murine lungs after hyperoxic lung injury

4.1.1 *miR-154-3p* expression is localized in proximal and distal airway epithelium. Hyperoxia increases the *miRNA* expression level of *miR-154-3p* positive cells

In order to localize the *miR-154-3p* expressing cells in the murine lung and to show how hyperoxia alters *miR-154-3p* expression, we exposed mice to 85% O_2 after birth until the lungs were harvested. For this examination we used three different time points (Postnatal day 2 (P2), P5 and P8) and used mice without exposure to hyperoxia (room air; 21% O_2) as controls. The lung samples were prepared for histologic examination and FISH staining for *miR-154-3p* was performed as previously described (see Material and Methods, section 3.3.2).

Under normoxic conditions high expression of *miR-154-3p* was found to be located in the airway epithelial cells of both, proximal and distal airways. Mesenchymal cells also expressed *miR-154-3p*, but in a lower extent. Notably, the expression level of *miR-154-3p* was highest at P2, followed by P5 and can be hardly seen at P8, indicating a continuous decrease of *miR-154-3p* expression in the first days after birth (see Figure 7.A).

After hyperoxic lung injury the signal for *miR-154-3p* increased compared to normoxia. Counting of the *miR-154-3p* positive cells revealed that at P2 and P5 the percentage of positive cells was not altered in alveolar (P2: p=0.9193; P5: p=0.8224), or in bronchiolar epithelium (P2: p=0.2437; P5: p=0.5095). Interestingly, at P8, a stage that barely showed any *miR-154-3p* expression in normoxia, the number of *miR-154-3p* expressing cells increased after hyperoxic lung injury in the alveolar (p=0.0049), as well as in the bronchiolar epithelium (p=0.0138) (see Figure 7.A).

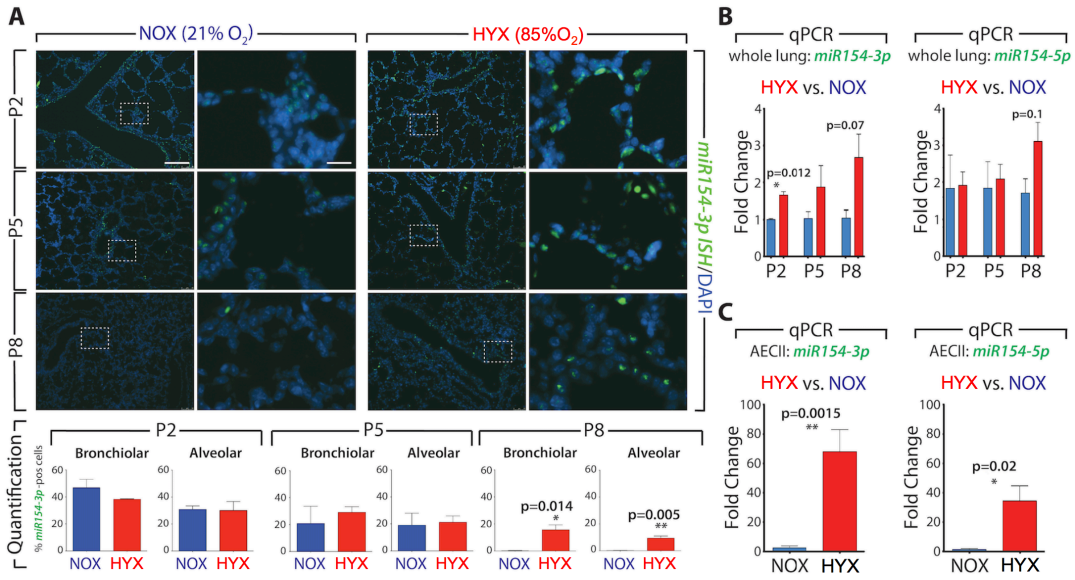

Figure 7: *miR-154-3p* and *miR-154-5p* expression levels after hyperoxic lung injury: A.: *miR-154-3p* expression in hyperoxic lung injury at P2, P5 and P8 by FISH and Quantification of *miR-154-3p* positive cells in bronchiolar and alveolar epithelium. **B.:** *miR-154-3p* and *miR-154-5p* expression in whole lung by RT-qPCR. **C.:** *miR-154-3p* and *miR-154-5p* expression in isolated AECII cells by RT-qPCR. **A.+B.:** P2: NOX n=2, HYX n=3; P5: NOX n=3, HYX n=4; P8: NOX n=3, HYX n=3; **C.:** P3: NOX n=6, HYX n=6.

4.1.2 Hyperoxic treatment induces the expression of both *isomiRNAs* in whole lung samples, especially in alveolar type II cells (AECII)

To demonstrate the responsiveness of *miR-154-3p* and *miR-154-5p* expression on hyperoxia we treated mice with hyperoxia as previously mentioned (see 3.1.1), harvested murine lungs, isolated *RNA* from whole lung samples and performed an RT-qPCR on *miR-154-3p* and *miR-154-5p*. Again we examined the same postnatal time points as we did in 4.1.1 (P2, P5 and P8). For the RT-qPCR of the *miRNAs* of interest *U6* was used as a reference gene. The expression is presented as fold change, meaning that values >1 depict an increase, whereas a value <1 shows a decrease of expression level.

At all time points (P2, P5 and P8) *miR-154-3p* expression appeared to be increased in whole lungs treated under hyperoxic conditions compared to normoxia. For P2 a

significant increase was seen (p=0.0121), for P5 a slight trend towards an increase can be shown (p=0.2862) and for P8 an increase close to significance (p=0.0711) was achieved after hyperoxic treatment (see Figure 7.B).

For *miR-154-5p* there was no striking increase of expression level after hyperoxic injury (P2: p=0.9270; P5: p=0.7588). Merely at P8 a trivial trend towards an increase can be seen (p=0.0950) (see Figure 7.B).

For the purpose of showing which of the lung cell types highly contributes to the previously shown increase of *miR-154-3p* and *miR-154-5p* expression in whole lung samples we performed an isolation of AECII cells after lung injury, isolated *RNA* from the remaining AECII cells and again performed a RT-qPCR for both *isomiRNAs*. At this juncture I'd like to give special thanks to Elisabeth Kappes for performing the AECII cell isolation for us. In this case we used P3 as the time point of lung harvest and examination. Hyperoxic lung injury was performed from birth until lung harvest as previously described. Control mice were exposed to normoxia. A significant increase of expression level was attained for both *miRNAs* (p=0.0015 for *miR-154-3p*; p=0.0183 for *miR-154-5p*) (see Figure 7.C).

In summary, these data possibly indicate that hyperoxia leads to the increase of *miR-154-3p* expression (in a certain manner *miR-154-5p* as well) in the lung epithelium, especially in AECII cells. But so far it is not clear yet how the increase of *miR-154-3p* expression can be integrated in the context of hyperoxic lung injury.

4.2 Hyperoxia affects alveolar formation and genetic expression profiles during postnatal lung development

To demonstrate the impact of hyperoxic injury on the lung structure we performed an Alveolar Morphometry on histological lung samples. Mice were exposed to hyperoxia (85% O_2) from P0 until P8 and kept under normoxic conditions (room air) from P9 until P16 for recovery (HYX; see Figure 8.A). Control mice were kept under normoxic conditions from P0 until P16 (NOX). The lungs were harvested at P16. The left lobe of the lung was prepared for histological examination and hematoxylin eosin (H.E.) staining was performed.

4.2.1 Alveolar Morphometry shows impaired alveologenesis in lungs treated with hyperoxia

Compared to mice kept in room air (NOX), the lung structure of mice exposed to hyperoxia showed simplified alveoli, indicating an interruption of alveologenesis after hyperoxic lung injury (Figure 8.B): the septal thickness appeared to be almost significantly altered (p=0.06), as well as the mean linear intercept, which was significantly increased (MLI; p=0.0029). No change was registered concerning percentage of airspace (p=0.8010).

4.2.2 RT-qPCR indicates differentially expressed genetic profiles in whole lungs after hyperoxic lung injury

After exposure to either hyperoxia (HYX) or normoxia (NOX), the right lung lobe was used for RNA isolation. RT-qPCR was performed for different sets of genes (see Figure 8.C). For the examination of epithelial cells' activity we have used different genes as markers, such as *Nkx2.1* as a lung epithelial marker in general and early lung epithelial cell marker (Hawkins et al., 2017), *Sftpb* and *Sftpc* for alveolar type 2 cells (AECII) (Fukumoto et al., 2016; Hobi et al., 2016), *CC10* (Singh and Katyal, 1997) (alternatively referred to as *CCSP* (Chen et al., 2001) or *Scgb1a1* (El Agha and Bellusci, 2014)) for club cells (formerly Clara cells (Fukumoto et al., 2016)), *Epcam* as a general marker for epithelial cells (Litvinov et al., 1994) and *Aqp5* as an AECI marker (El Agha and Bellusci, 2014; Rozycki, 2014). For further information about the genes found under Fgf signaling, Tgf-β signaling or alveolar MYF markers see 1.2.1.2, 1.4.1 and 1.4.2 from the section "Introduction".

The genetic expression of Fgf signaling genes was altered in hyperoxia compared to normoxia, showing a significant increase for *Fgfr2b* (p=0.0015), *Fgfr1b* (p=0.0022), *Etv4* (p=0.0048), *Nmyc* (p=0.0188) and *Spry2* (p=0.0478) on the *mRNA* level. Other genes were not significantly altered (*Bmp4*: p=0.1026; *Spry4*: p=0.1225; *Etv5*: p=0.1641; *Fgf10*: p=0.5440). Interestingly, the downstream components of Fgf10 signaling, but not the ligand itself appeared to be altered in expression. Furthermore the expression of some epithelial cell markers was altered such as *Aqp5* (p=0.0060), followed by *Sftpb* (p=0.0220) and *Epcam* (p=0.0461), but

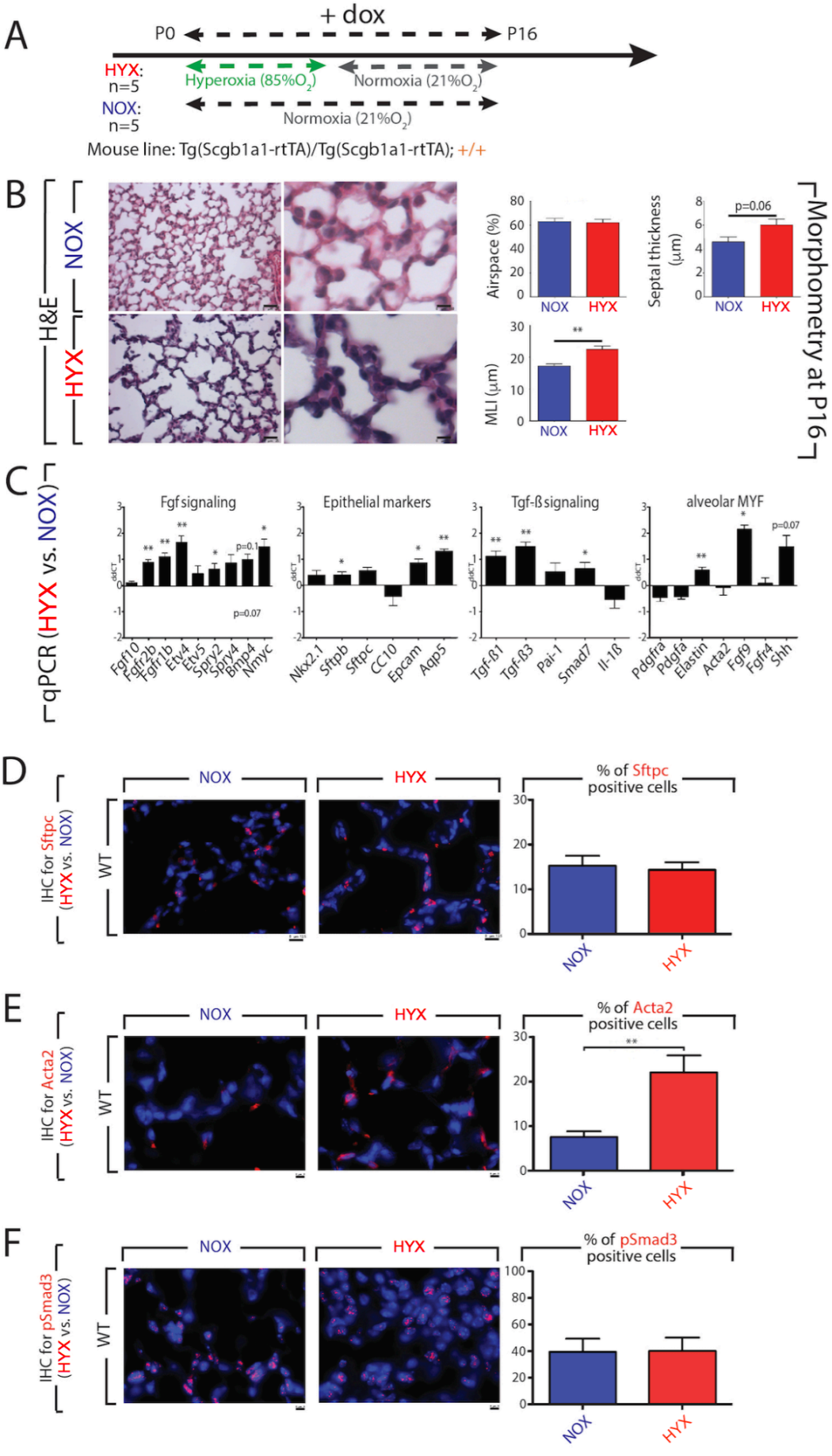
A
+ dox
P0
P16
HYX:
n=5
Hyperoxia (85%O2)
Normoxia (21%O2)
NOX:
n=5
Normoxia (21%O2)
Mouse line: Tg(Scgb1a1-rtTA)/Tg(Scgb1a1-rtTA); +/+
B
H&E
NOX
HYX
Airspace (%)
Septal thickness (µm)
p=0.06
MLI (µm)
Morphometry at P16
C
qPCR (HYX vs. NOX)
Fgf signaling
Epithelial markers
Tgf-ß signaling
alveolar MYF
Fgf10
Fgfr2b
Fgfr1b
Etv4
Etv5
Spry2
Spry4
Bmp4
Nmyc
Nkx2.1
Sftpb
Sftpc
CC10
Epcam
Aqp5
Tgf-ß1
Tgf-ß3
Pai-1
Smad7
Il-1ß
Pdgfra
Pdgfa
Elastin
Acta2
Fgf9
Fgfr4
Shh
D
IHC for Sftpc (HYX vs. NOX)
WT
% of Sftpc positive cells
E
IHC for Acta2 (HYX vs. NOX)
% of Acta2 positive cells
F
IHC for pSmad3 (HYX vs. NOX)
% of pSmad3 positive cells

Figure 8: Alveolar Morphometry and RT-qPCR data on whole lung comparing hyperoxic lung injury (HYX) to normoxic controls (NOX): A. Model of hyperoxic treatment. **B.** Alveolar Morphometry showed impaired alveolar development after postnatal hyperoxic lung injury indicated by increased MLI and septal thickness. **C.** RT-qPCR analysis revealed dynamically altered genetic expression profiles upon hyperoxic treatment. Fgf signaling, Tgf-β signaling, epithelial cell markers and genes linked to alveolar myofibroblasts appeared to be affected. **D.-F.** Immunohistochemical stainings for Surfactant Protein C (Sftpc; **D.**), Acta-2 (**E.**) and pSmad3 (**F.**) comparing changes in protein expression after hyperoxic injury to normoxic controls. For HYX n=5, for NOX n=5.

showing no significant increase for *Sftpc* (p=0.1057), *Nkx2.1* (p=0.1848) and *CC10* (p=0.3479), potentially indicating processes of repair on the level of alveolar epithelial cells. Tgf-β signaling also appeared to be increased with significant change for *Tgf-β3* (p=0.0018), *Tgf-β1* (p=0.0073) and *Smad7* (p=0.0439), but no change in *Pai-1* (p=0.2320) and *Il-1β* (p=0.3018) expression. Some of the genes, which are known to play a crucial role in alveologenesis (De Langhe et al., 2006) and which were found to be involved with alveolar myofibroblast formation and function, show an increased expression (*Elastin*: p=0.0063; *Fgf9*: p=0.0114; no change for *Shh*: p=0.0749; *Pdgfa*: p=0.1365; *Pdgfra*: p=0.2740; *Fgfr4*: p=0.8873 and *Acta2*: p=0.8880), demonstrating a potential effect of hyperoxia on the alveolar myofibroblast and consequently the deposition of Elastin and the process of secondary septation.

4.2.3 Increased number of Acta2 positive cells in lungs exposed to hyperoxia

For some of the genes we examined the expression on the protein level by immunohistological stainings. Interestingly, the number of Acta2 expressing cells was highly increased in the mesenchyme after hyperoxic lung injury (p=0.0064; Figure 8.E), although there was no difference seen on the *mRNA* expression level (see above). No change was found in Sftpc (p=0.7479; Figure 8.D) and pSmad3 (p=0.9604; Figure 8.F) expressing cells.

The data gathered so far show an impact of hyperoxia on the formation of alveoli, as indicated by increased MLI and septal thickness (Figure 8.B). The thinning of

the alveolar walls and the secondary septation are interrupted. Furthermore the change of expression levels of *Elastin*, *Fgf9* and *Shh* as representative genes for alveologenesis and secondary septation confirms the disruption of alveolar formation by hyperoxic treatment. The differential expression of genes of the Fgf and Tgf-β signaling pathways, as well as epithelial cell markers underline the interference of inhaling high oxygen concentrations on the postnatal lung development. Still it has to be kept in mind that this examination is mainly based on the *mRNA* levels and the protein expression for most of the genes is still unclear. An increased *mRNA* level of a particular gene does not necessarily mean that the level of the protein product is increased as well. It can be merely deduced that the translational machinery is more active.

4.3 Airway-specific *miR-154* overexpression partly mimics the phenotype and genetic expression profile of hyperoxic lung injury

The expression of *miR-154* appeared to be induced by exposure to hyperoxia (Figure 7). In order to deduce the function of *miR-154* in hyperoxic lung injury, a mouse line was created by our lab allowing overexpression of *miR-154-3p* and *miR-154-5p* in airway epithelial cells (*Tg(Scgb1a1-rtTA)/Tg(Scgb1a1-rtTA);Tg(miR-154)/*+) after doxycycline administration. Comparing this *miR-154* overexpressing mouse line to mice, which are not overexpressing the *miRNAs* of interest (*Tg(Scgb1a1-rtTA)/Tg(Scgb1a1-rtTA);*+/+), we have performed Alveolar Morphometry, RT-qPCR and immunohistological stainings for the same genes as we previously did in section 4.2.2 (see Figure 8.C) in order to examine the potential role of *miR-154* in the context of hyperoxic lung injury. The generation of the mouse line (*Tg(Scgb1a1-rtTA)/Tg(Scgb1a1-rtTA);Tg(miR-154)/*+) and the validation of the functioning of the mouse line have been previously described in section 3.1.4 and Figure 6 in the section “Material and Methods”.

4.3.1 Overexpression of *miR-154* leads to hypoalveologenesis indicated by increased mean linear intercept (MLI) of the alveoli

Alveolar Morphometry revealed that overexpression of *miR-154* in the airway epithelium leads to hypoalveologenesis characterized by a significant

increase of MLI (p=0.0022; see Figure 9.B). Unlike hyperoxic lung injury (see 4.2 and Figure 8.B) the septal thickness of the alveoli remained unaffected (p=0.9730). Again there was no significant change in percentage of airspace (p=0.2111).

4.3.2 Differential expression of genetic profiles upon *miR-154* overexpression is similar to hyperoxic lung injury in whole lung

Genes of the Fgf signaling pathway were altered in expression levels under *miR-154* overexpression similar to hyperoxia (see 4.2 and Figure 8): *Etv4* (p=0.0021), *Fgfr1b* (p=0.0028), *Spry2* (p=0.0197) and *Spry4* (p=0.0412) were significantly increased in expression levels, whereas *Fgfr2b* (p=0.0996), *Etv5* (p=0.1276), *Nmyc* (p=0.1599) *Bmp4* (p=0.2947) and *Fgf10* (p=0.4968) showed no significant increase. Interestingly, just like under hyperoxic conditions we found the expression of the ligand *Fgf10* to be unaffected upon *miRNA* induction, whereas the *mRNAs* of the downstream molecules are differentially expressed. Epithelial cell markers didn't show a significant change in expression levels (*Epcam*: p=0.2317; *Nkx2.1*: p=0.4167; *Sftpb*: p=0.6656; *Sftpc*: p=0.7354; *CC10*: p=0.9835). Merely the expression level of the AECI marker *Aqp5* was almost significantly increased upon *miRNA* overexpression (p=0.0685). Similar to hyperoxia *miR-154* overexpression displayed an increase in Tgf-β signaling: *Tgf-β3* (p=0.0113) and *Smad7* (p=0.0394) were significantly up-regulated, while *Pai-1* (p=0.0585) showed a trend towards an up-regulation. No difference was seen in the expression of *Tgf-β1* (p=0.1123) and *Il-1β* (p=0.7778). Unlike hyperoxia no mentionable change in expression levels was recorded for alveolar myofibroblast markers (*Elastin*: p=0.1711; *Shh*: p=0.1837; *Pdgfa*: p=0.1859; *Fgf9*: p=0.3385; *Pdgfra*: p=0.4394; *Fgfr4*: p=0.6130; *Acta2*: p=0.7829).

4.3.3 No significant difference for the expression of Sftpc, Acta2 and pSmad3 upon *miR-154* induction

Immunohistological stainings showed unaltered numbers of positive cells for Sftpc (p=0.2219; see Figure 9.D) or pSmad3 (p=0.4603; see Figure 9.F). Acta2 positive cells showed no increase in number upon *miR-154* overexpression either

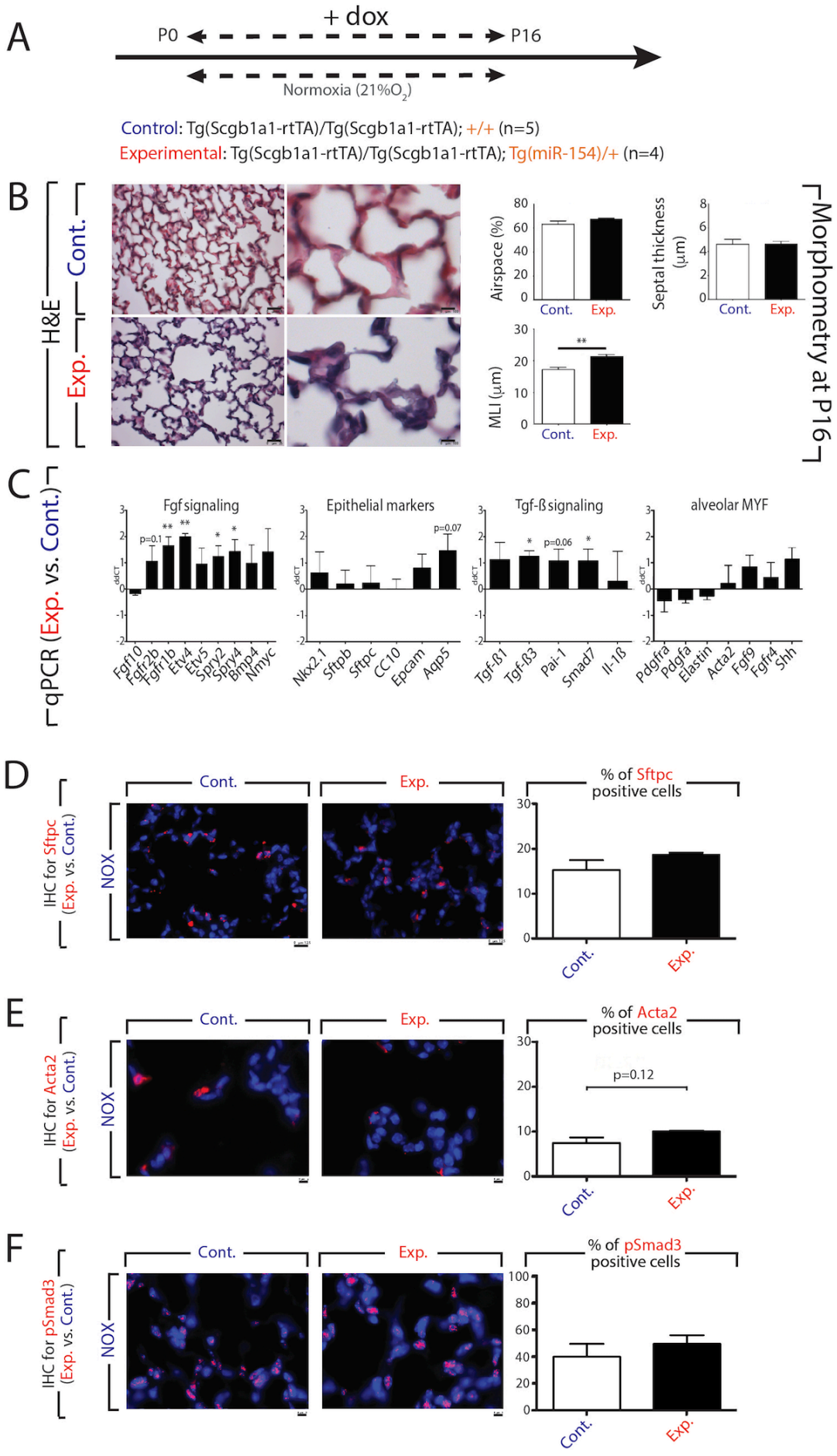
A
+ dox
P0
P16
Normoxia (21%O2)
Control: Tg(Scgb1a1-rtTA)/Tg(Scgb1a1-rtTA); +/+ (n=5)
Experimental: Tg(Scgb1a1-rtTA)/Tg(Scgb1a1-rtTA); Tg(miR-154)/+ (n=4)
B
H&E
Cont.
Exp.
Airspace (%)
Septal thickness (μm)
MLI (μm)
Cont.
Exp.
Morphometry at P16
C
qPCR (Exp. vs. Cont.)
Fgf signaling
Epithelial markers
Tgf-ß signaling
alveolar MYF
Fgf10
Fgfr2b
Fgfr1b
Etv4
Etv5
Spry2
Spry4
Bmp4
Nmyc
Nkx2.1
Sftpb
Sftpc
CC10
Epcam
Aqp5
Tgf-ß1
Tgf-ß3
Pai-1
Smad7
Il-1ß
Pdgfra
Pdgfa
Elastin
Acta2
Fgf9
Fgfr4
Shh
D
IHC for Sftpc (Exp. vs. Cont.)
NOX
% of Sftpc positive cells
E
IHC for Acta2 (Exp. vs. Cont.)
% of Acta2 positive cells
p=0.12
F
IHC for pSmad3 (Exp. vs. Cont.)
% of pSmad3 positive cells

Figure 9: Effect of *miR-154* overexpression on lung morphology and gene expression: **A.** Model of transgenic induction of *miR-154* expression by doxycycline (Dox) administration. **B.** Alveolar Morphometry shows impaired alveolar development after *miR-154* overexpression indicated by increased MLI. **C.** RT-qPCR analysis reveals dynamically altered genetic expression profiles upon *miRNA* overexpression. Fgf signaling, Tgf-β signaling and epithelial cell markers appear to be affected in a similar manner as under hyperoxic conditions (compare to Figure 8), although the same levels of significance are not reached concerning Tgf-β signaling and epithelial cell markers. Interestingly, unlike hyperoxia, genes linked to alveolar myofibroblasts do not show any significant alterations upon *miRNA* Induction. **D.-F.** Immunohistochemical stainings for Surfactant Protein C (Sftpc; **D.**), Acta-2 (**E.**) and pSmad3 (**F.**) comparing changes in protein expression after double transgenic *miRNA* Induction upon doxycyclin administration compared to single transgenic controls. For Experimental n=4, for Control n=5.

(p=0.1184; see Figure 9.E). In hyperoxia this increase was highly significant (p=0.0064; see 4.2.3 and Figure 8.E).

Comparing the data from this section, where we induced *miR-154* expression in epithelial cells (section 4.3) to the data we gathered from the hyperoxic lung injury experiments (section 4.2), we could find certain similarities: In both cases Alveolar Morphometry shows impaired alveologenesis with increased alveolar diameter (MLI). Under *miRNA* overexpression a thickening of the alveolar septal walls cannot be found as it is shown in hyperoxia (compare Figure 8.B to Figure 9.B). Furthermore the *mRNA* expression profiles for both, hyperoxia (section 4.2) and *miR-154* induction (section 4.3), share certain similarities. For Fgf signaling a similar expression profile was found upon *miRNA* induction compared to hyperoxia, here again increasing downstream receptors and pathway effectors, but not the ligand (compare Figure 8.C and Figure 9.C). Although differing in levels of significance, Tgf-β signaling components tend to an increase in expression level in *miR-154* overexpression similar to hyperoxic lung injury. Interestingly, although a significant increase in epithelial cell markers is missing under *miRNA* overexpression, *Aqp5* appears to be increased without reaching significance (p=0.0685). In hyperoxia it is the epithelial marker with the most significant

increase (p=0.0060; see Figure 8.C). This might indicate a regenerative effect on the AECI population under both conditions. Unlike hyperoxia the genes linked to alveolar myofibroblasts remain unaffected after *miRNA* induction.

Taken together, the data gathered up to this point, the fact that hyperoxia leads to an increase of *miR-154-3p* and *miR-154-5p* (section 4.1) and the fact that overexpression of the *miRNAs* of interest leads to a similar phenotype and a similar expression profile of genes, raises the hypothesis, that *miR-154-3p* or *miR-154-5p* or perhaps both may function as downstream mediators of hyperoxic lung injury and hypoalveologenesis. The induction of Fgf signaling and Tgf-β signaling in a similar fashion as under hyperoxic conditions emphasizes this. Interestingly, the dynamic alteration of *Aqp5* indicates an increased AECI activity similar to hyperoxia. *miR-154* induction obviously does not mediate an effect on the alveolar myofibroblasts, as the markers remain unaltered.

4.4 Overexpression of *miR-154* leads to a more AECI specific transcription signature in isolated AECII cells

The similarities concerning alveolar phenotype and genetic expression profile for many examined genes between hyperoxia and *miR-154* induction lead to the hypothesis that there might exist an undetected mutual molecular process in alveolar formation, which is affected by both conditions. When taking a closer look at the gathered RT-qPCR data we found another interesting circumstance: for both treatments, hyperoxia and *miRNA* overexpression, the AECI specific marker *Aqp5* was the most affected epithelial cell marker (compare Figure 8.C and Figure 9.C). Interestingly, Hou and colleagues found that after hyperoxic lung injury of rats AECII cells appear to express AECI markers, such as *Aqp5* and *T1α* (another expression for Podoplanin (Ugorski et al., 2016)), indicating that hyperoxia leads to the activation of the stem cell function of AECII cells and the AECII-to-AECI transdifferentiation of these cells in order to repopulate the AECI cell population, which is highly impacted upon hyperoxia (Hou et al., 2015). Furthermore, they described an increased number of cells positive for both proteins Aqp5 and Sftpc after hyperoxic treatment, indicating a state of transition between the two cell populations. Still they were not able to find a molecular factor mediating this

phenomenon of alveolar epithelial cell transdifferentiation. Since the expression of *Aqp5* was also increased upon *miR-154* overexpression in airway epithelial cells (see Figure 9) and both, *miR-154-3p* and *miR-154-5p*, are increased in expression after hyperoxic lung injury, we hypothesize that *miR-154* overexpression might lead to the same transdifferentiation of AECII-to-AECI cells as hyperoxia does, which may be shown by an increased expression of AECI specific markers among the AECII population. If that is the case, it is even imaginable, that our *miRNAs* of interest might be the missing link between hyperoxia and AECII-to-AECI transdifferentiation, described by Hou and colleagues (Hou et al., 2015). In order to examine this hypothesis, we have performed another isolation of AECII cells (again I'd like to give my special thanks to Elisabeth Kappes for performing the AECII isolation for us!): the experimental group was composed of mice overexpressing *miR-154* in the airway epithelium from birth (P0) until lung harvest (P16) and compared to control mice, which were not overexpressing the *miRNAs* of interest (same transgenic mouse line and controls and same procedure and time points as in Figure 9). We then yielded *RNA* from the isolated AECII cells and performed a Gene Array Analysis (see Figure 10.A). Here, I'd like to thank Dr. Jochen Wilhelm for performing the Gene Array Analysis and providing the graphical figure for us (Figure 10). The analysis of the results gathered by the Gene Array clearly shows that overexpression of *miR-154-3p* and *miR-154-5p* in the murine airway epithelium leads to a more AECI specific transcription signature in isolated AECII cells (see Figure 10.E-G). AECI specific markers such as *Cav1*, *Pdpn* and *Hopx* (Jung et al., 2012; Treutlein et al., 2014; Ugorski et al., 2016) are expressed in higher levels in isolated AECII cells after *miRNA* induction (Figure 10.E). Interestingly, *Cav1* and *Hopx* are among the putative target genes of *miR-154* (see section 2.1 "Aims of the Current Study" and Figure 10.D). As this phenomenon of AECII-to-AECI transition has been previously described and shown to be induced by hyperoxia (Hou et al., 2015), and as we have demonstrated that hyperoxia leads to a significantly increased expression of *miR-154-3p* and *miR-154-5p* in AECII cells (see Figure 7), we hereby found indicative data for our assumption that hyperoxia might induce *miR-154* expression in AECII cells, which consequently might lead to an increased AECII-to-AECI transdifferentiation. In order to confirm this idea further experiments have to be done. The results from this study and the consequent hypothesis are discussed in the sections further below.

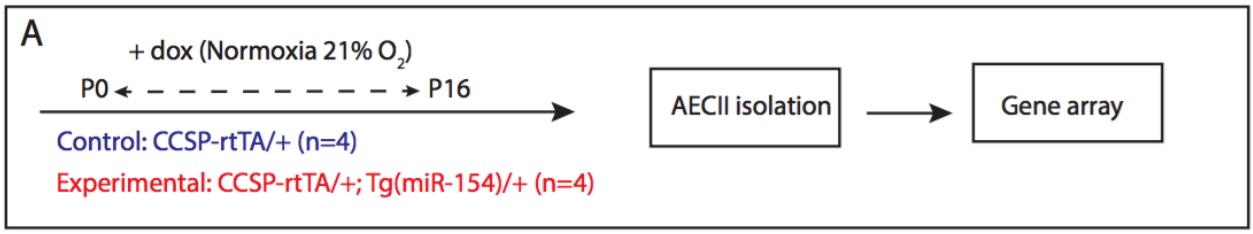

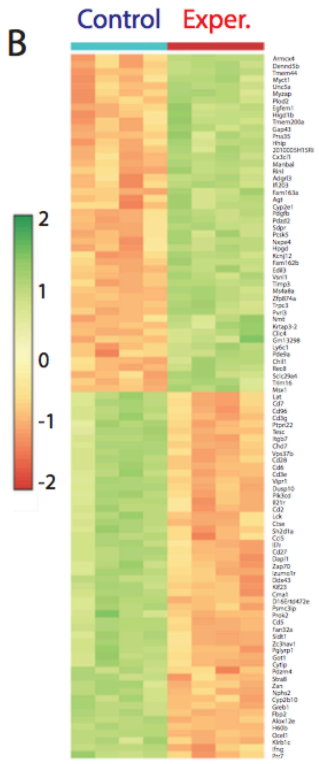

C

KEGG analysis

KEGG name	n Genes InSet	n expr. genes	-log(p value)
Focal adhesion	202	197	21.08
PI3K-Akt signa. path	338	345	18.53
ECM-recept. inter.	83	79	16.27
Pathways in cancer	392	376	11.77
Rap1 sign. path.	214	199	11.64
Cyt.-cyt. interaction	241	221	11.33
Proteoglycans in cancer	201	195	9.07
Hippo signa. path.	153	144	8.34

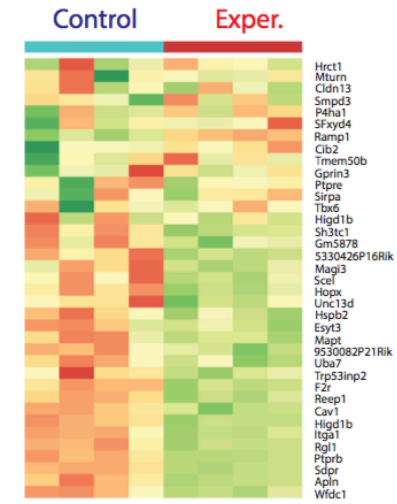

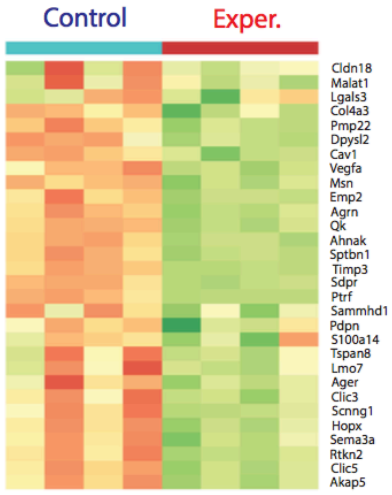

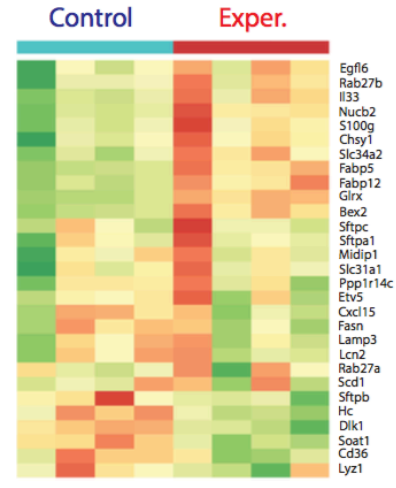

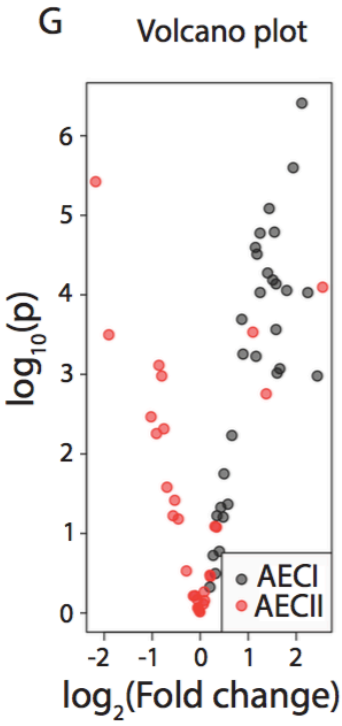

Figure 10: Gene Array Analysis performed on isolated AECII samples: A.: Model of *miR-154* induction by doxycycline administration. **B.:** Differentially expressed genes upon *miRNA* overexpression. **C.:** KEGG Analysis. **D.:** Putative *miR-154* target genes. **E.:** Differential regulation of AECI markers. AECI markers appear to be increased in expression levels upon *miR-154* overexpression (Exper.) compared to Control. **F.:** Differential regulation of AECII markers. AECII markers appear to be inconsistently altered in expression levels upon *miR-154* overexpression (Exper.) compared to Control. **G.:** Volcano plot demonstrating the increased AECI specific transcription signature in isolated AECII cells after *miRNA* induction compared to Control. (*Gene Array Analysis, KEGG analysis, heat maps and volcano plots depicted here were provided to us by Dr. Jochen Wilhelm*). For Control and Experimental n=4.

4.5 Additional hyperoxic lung injury on top of *miR-154* overexpression is not able to further worsen the alveolar phenotype or to alter the genetic expression profile of the genes of interest

As both, hyperoxia and *miR-154* overexpression, are able to individually interrupt alveologenesis and alter gene expression, we raised the question, whether combining both injurious stimuli may lead to a further worsening of alveolar formation and further alterations of genetic expression profiles in the lungs. To do so, we compared mice exposed to both, overexpression of the *miRNAs* of interest and hyperoxia (HYX; see Figure 11) to mice overexpressing the *miRNAs* of interest only, which were kept under room air (NOX) using the same transgenic mouse line as we previously did (see sections 4.2 and 4.3). To put it in other words: we compare double-injury (*miRNA* induction and hyperoxia) to single-injury (*miRNA* induction only). Again we used Alveolar Morphometry, RT-qPCR and Immunohistochemistry to examine this situation. The preparation of the samples was performed as previously described.

4.5.1 Double injury shows no further worsening of the alveolar structures compared to single injury by means of *miRNA* overexpression only

Neither the percentage of airspace (p=0.2605), nor the alveolar septal thickness (p=0.2690), nor the mean linear intercept (p=0.7414) was significantly altered comparing the previously described double to single injury (see Figure 11.B). As expected *miR-154* overexpression alone (NOX) leads to an increased MLI already (see Figure 9.B), which was not further increased by additional hyperoxic lung injury.

4.5.2 No change of expression levels of Fgf and Tgf-β signaling components and epithelial cell markers, but single genes involved with alveolar myofibroblast function were increased upon additional hyperoxia

Genes of the Fgf signaling pathway appeared to be mostly unaffected by double injury (hyperoxia and *miR-154* overexpression) compared to single injury (*miR-154* overexpression only) (*Spry2*: p=0.1106; *Spry4*: p=0.2387; *Etv5*: p=0.4157; *Bmp4*: p=04420; *Fgfr2b*: p=0.4640; *Etv4*: p=0.6678; *Fgf10*: p=0.7790; *Nmyc*: p=0.8647). Merely *Fgfr1b* showed a decrease close to significance (p=0.0633). The same is the case for epithelial cell markers (*CC10*: p=0.1061; *Nkx2.1*: p=0.3256; *Epcam*: p=0.6088; *Aqp5*: p=0.6813; *Sftpb*: p=0.7072; *Sftpc*: p=0.8853) and Tgf-β signaling genes (*Smad7*: p=0.1870; *Pai-1*: p=0.3482; *Tgf-β3*: p=0.4315; *Il-1β*: p=0.5435; *Tgf-β1*: p=0.7523). Some of the genes connected to the alveolar myofibroblasts are increased in expression after double injury relative to *miRNA* overexpression only, such as *Fgf9* (p=0.0101), *Shh* (p=0.0195) and *Elastin* (close to; p=0.0519). Intriguingly, these are the very same genes, which are increased upon hyperoxic lung injury compared to room air without overexpression of *miRNAs* (see 4.2.2 and Figure 8). This fact raises the assumption that *miR-154* does not interact with the alveolar myofibroblast formation or function, but the effect on the alveolar myofibroblasts seen here, as well as after hyperoxic injury only (see Figure 8), can solely be attributable to the effect of hyperoxia. The remaining genes in the context of alveolar myofibroblasts appeared to be unaffected (*Pdgfa*: p=0.0854; *Fgfr4*: p=0.2101; *Pdgfra*: p=0.3915; *Acta2*: p=0.7849).

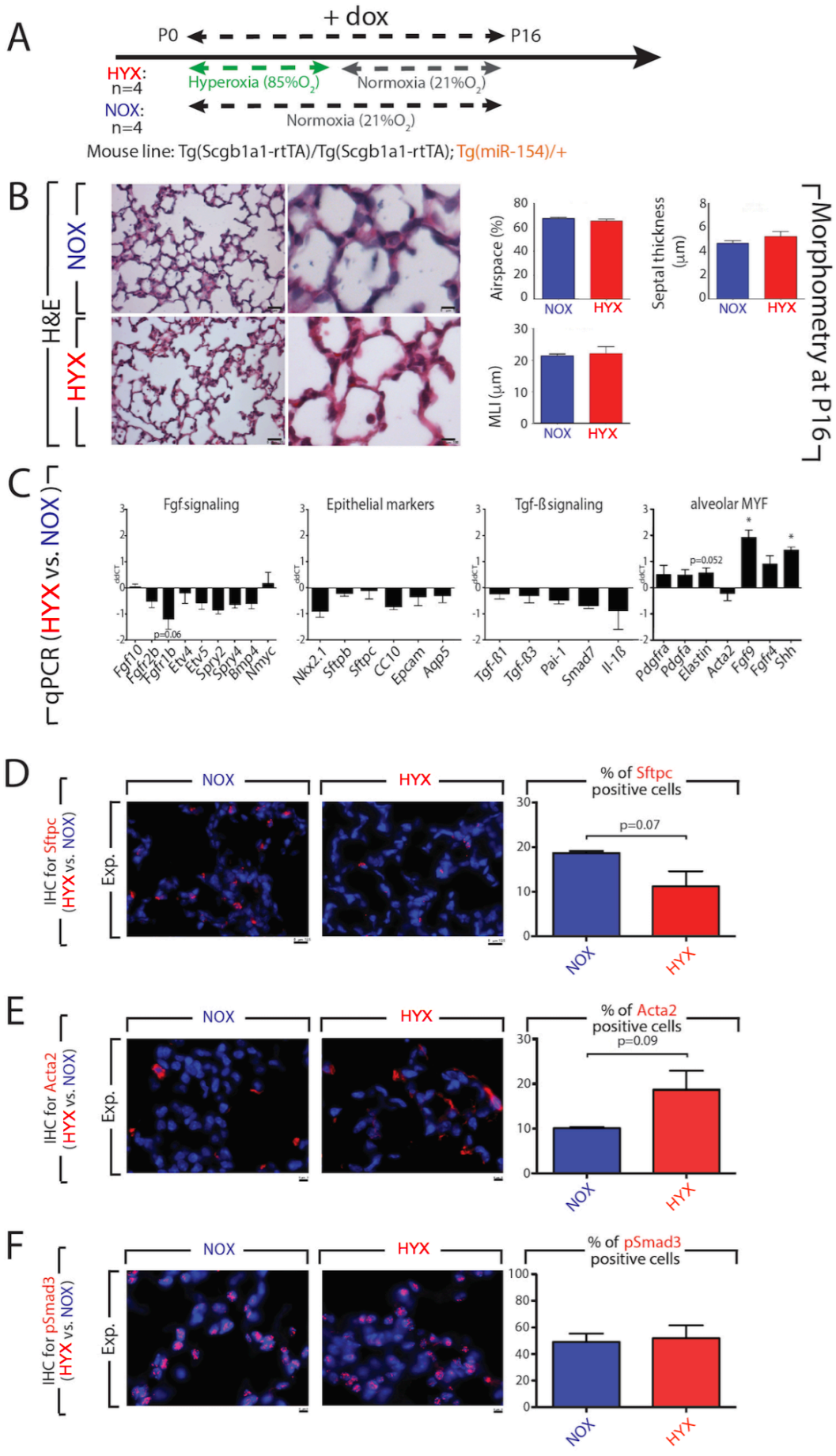
A
+ dox
P0
P16
HYX: n=4
Hyperoxia (85%O2)
Normoxia (21%O2)
NOX: n=4
Normoxia (21%O2)
Mouse line: Tg(Scgb1a1-rtTA)/Tg(Scgb1a1-rtTA); Tg(miR-154)/+
B
H&E
NOX
HYX
Airspace (%)
Septal thickness (μm)
MLI (μm)
NOX
HYX
Morphometry at P16
C
qPCR (HYX vs. NOX)
Fgf signaling
Epithelial markers
Tgf-ß signaling
alveolar MYF
p=0.06
p=0.052
Fgf10
Fgf2b
Fgfr1b
Etv4
Etv5
Spry2
Spry4
Bmp4
Nmyc
Nkx2.1
Sftpb
Sftpc
CC10
Epcam
Aqp5
Tgf-ß1
Tgf-ß3
Pai-1
Smad7
Il-1ß
Pdgfra
Pdgfa
Elastin
Acta2
Fgf9
Fgfr4
Shh
D
IHC for Sftpc (HYX vs. NOX)
Exp.
NOX
HYX
% of Sftpc positive cells
p=0.07
E
IHC for Acta2 (HYX vs. NOX)
% of Acta2 positive cells
p=0.09
F
IHC for pSmad3 (HYX vs. NOX)
% of pSmad3 positive cells

Figure 11: Hyperoxic lung injury on top of overexpression of *miR-154* (double injury) compared to *miRNA* overexpression only (single injury): A.: Model of hyperoxic treatment and doxycycline (Dox) administration in order to activate *miR-154* overexpression. **B.:** Alveolar Morphometry reveals no further effect of double injury (hyperoxia and *miRNA* overexpression) on alveolar parameters compared to single injury (*miRNA* overexpression only). **C.:** RT-qPCR data show no obvious effect of additional hyperoxic injury on top of *miR-154* overexpression for Fgf signaling, Tgf-β signaling and epithelial cell markers. Merely genes connected to alveolar myofibroblast formation and function seem to be affected by additional hyperoxic exposure. **D.-F.:** Immunohistochemical stainings for Sftpc (**D.**), Acta2 (**E.**) and pSmad3 (**F.**) comparing hyperoxia and *miRNA* overexpression to *miRNA* overexpression only. For HYX and NOX n=4.

4.5.3 No significant difference for the expression of Sftpc, Acta2 and pSmad3 under double damage compared to *miR-154* overexpression only

Immunohistological staining for Sftpc showed a non-significant decrease (p=0.0735) of Sftpc positive cells after double injury compared to single injury (*miRNA* overexpression only; see Figure 11.D). In the case of Acta2 a tendency towards an increase of Acta2 positive cells can be recorded (p=0.0916; see Figure 11.E). No change was seen for pSmad3 (p=0.8142; see Figure 11.F).

Taking together the herein gathered data, it can be shown that additional injury by treatment with hyperoxia on top of *miRNA* overexpression, does not lead to a further worsening of neither the alveolar morphometric phenotype, nor the general genetic gene expression compared to *miR-154* overexpression only. Merely some genes involved in alveolar myofibroblast formation (*Fgf9*, *Shh* and *Elastin*) were increased in expression, which is not surprising when compared to hyperoxic lung injury without *miRNA* overexpression (see 4.2 and Figure 8). Obviously *miR-154* overexpression simply has no effect on the alveolar myofibroblast formation. It can be assumed that hyperoxia impacts the alveolar myofibroblast without *miR-154* as a potential downstream regulator being required. Also immunohistological stainings showed some alterations of protein expressing cells, such as a non-significant decrease of Sftpc and a non-significant increase for Acta2. Taking together these

data and comparing them to 4.2 and Figure 8, it is tempting to ascribe the recorded changes to hyperoxia only, irrespective of *miR-154* overexpression, as the changes found here are similar to hyperoxic injury only (compare to section 4.2 and Figure 8). To keep it in other words: These effects are probably not attributable to an additional injurious stimulus combining overexpression of *miRNAs* and hyperoxic treatment, but attributable to hyperoxia only.

4.6 Additional overexpression of *miR-154* on top of hyperoxic lung injury is not able to worsen the phenotype of alveoli or to further alter the genetic expression profiles

In order to complete our data we have compared additional overexpression of the *miRNAs* of interest on top of hyperoxic lung injury (double injury) compared to hyperoxic treatment only (single injury) to see whether further worsening of the alveolar structure or further alterations of the genetic expression occur. Again we used Alveolar Morphometry, RT-qPCR and Immunohistochemistry for the examination of this issue.

4.6.1 No further worsening of the alveolar structures after double injury compared to single injury by hyperoxia only

Alveolar Morphometry showed no difference in any of the parameters (see Figure 12.B; percentage of airspace: p=0.3961; septal thickness: p=0.2739; mean linear intercept: p=0.8879). Single damage by hyperoxia leads to a thickening of the alveolar septal walls (see Figure 8.B) and an increase of the MLI already, which was not further increased by additional overexpression of *miRNA-154*.

4.6.2 Single epithelial cell markers and alveolar myofibroblast-associated genes were altered in expression upon additional *miRNA-154* overexpression

None of the genes of Fgf signaling and Tgf-β signaling are significantly altered under double injury compared to hyperoxia only (For Fgf signaling: *Fgfr1b*: p=0.1514; *Fgfr2b*: p=0.1982; *Spry2*: p=0.4354; *Etv4*: p=0.7668; *Etv5*: p=08123;

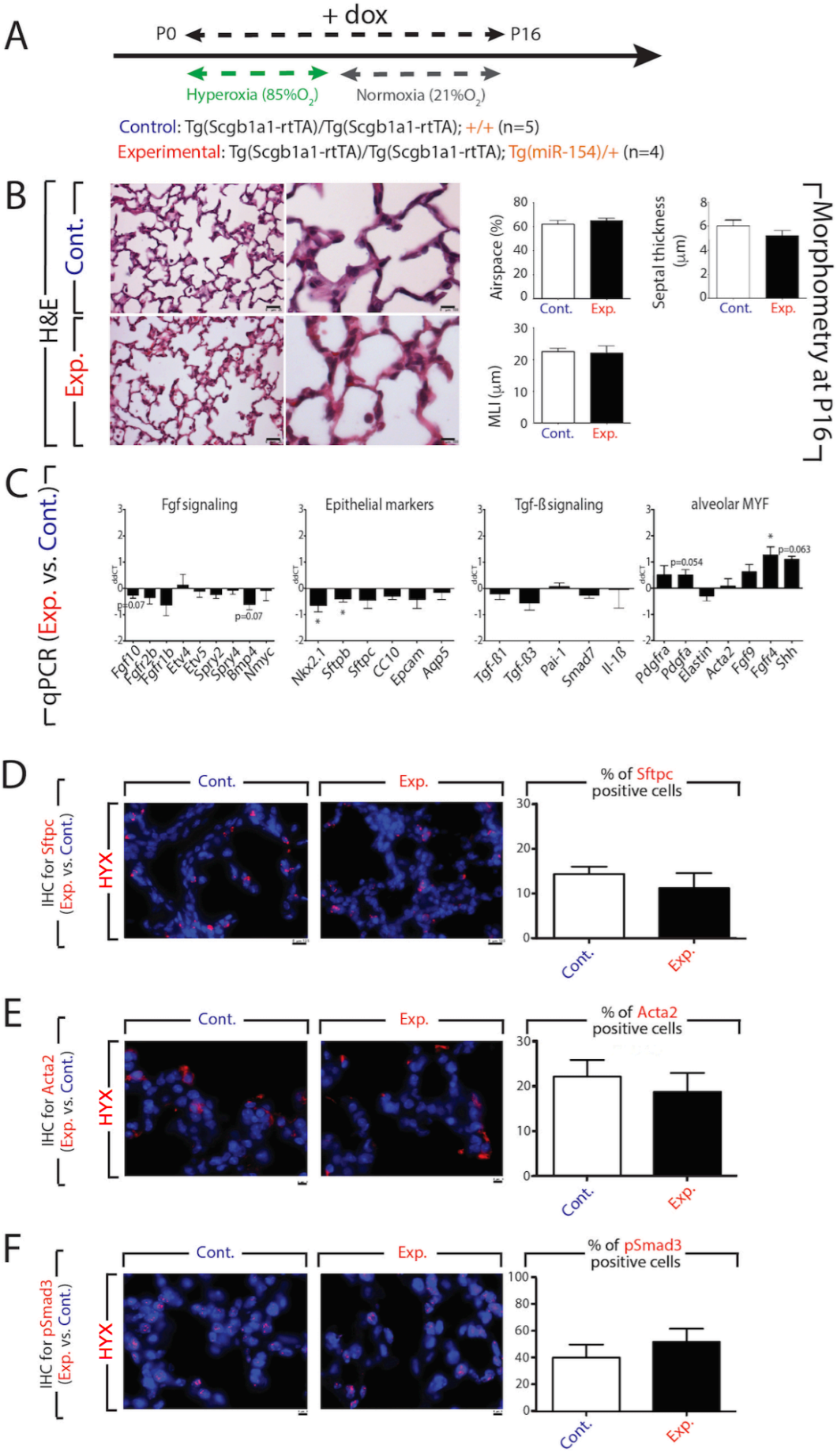
A
+ dox
P0
P16
Hyperoxia (85%O2)
Normoxia (21%O2)
Control: Tg(Scgb1a1-rtTA)/Tg(Scgb1a1-rtTA); +/+ (n=5)
Experimental: Tg(Scgb1a1-rtTA)/Tg(Scgb1a1-rtTA); Tg(miR-154)/+ (n=4)
B
H&E
Cont.
Exp.
Airspace (%)
Septal thickness (µm)
MLI (µm)
Cont.
Exp.
Morphometry at P16
C
qPCR (Exp. vs. Cont.)
Fgf signaling
Epithelial markers
Tgf-ß signaling
alveolar MYF
p=0.07
p=0.07
p=0.054
p=0.063
Fgf10
Fgfr2b
Fgfr1b
Etv4
Etv5
Spry2
Spry4
Bmp4
Nmyc
Nkx2.1
Sftpb
Sftpc
CC10
Epcam
Aqp5
Tgf-ß1
Tgf-ß3
Pai-1
Smad7
Il-1ß
Pdgfra
Pdgfa
Elastin
Acta2
Fgf9
Fgfr4
Shh
D
IHC for Sftpc (Exp. vs. Cont.)
HYX
Cont.
Exp.
% of Sftpc positive cells
E
IHC for Acta2 (Exp. vs. Cont.)
% of Acta2 positive cells
F
IHC for pSmad3 (Exp. vs. Cont.)
% of pSmad3 positive cells

Figure 12: Overexpression of *miR-154* on top of hyperoxic lung injury (double injury) compared to hyperoxic treatment only (single injury): A.: Model of hyperoxic treatment and doxycycline (Dox) administration in order to activate *miR-154* overexpression. **B.:** Alveolar Morphometry reveals no further effect of double injury (hyperoxia and *miRNA* overexpression) on alveolar parameters compared to single injury (hyperoxia only). **C.:** RT-qPCR data show no obvious effect of additional *miR-154* overexpression (double injury) on top of hyperoxic injury (single injury) for Fgf signaling, Tgf-β signaling and epithelial cell markers. Merely some genes connected to alveolar myofibroblasts seem to be affected by additional *miR-154* overexpression. In how far this can be interpreted in the context of this study remains unsolved for now. **D.-F.:** Immunohistochemical stainings for Sftpc (**D.**), Acta2 (**E.**) and pSmad3 (**F.**) comparing hyperoxia and *miRNA* overexpression to hyperoxia only. For Control n=5, for Experimental n=4.

Spry4= p=0.8584; *Nmyc*: p=0.8804; for Tgf-β signaling: *Tgf-β3*: p=0.1257; *Smad7*: p=0.3809; *Tgf-β1*: p=0.4980; *Pai-1*: p=0.8601; *Il-1β*: p=0.9635). Merely *Fgf10* (p=0.0702) and *Bmp4* (p=0.0706) tend to a decrease in expression level (see Figure 12.C). Among the epithelial cell markers *Nkx2.1* (p=0.0363) and *Sftpb* (p=0.0461) appeared to be significantly decreased. Other epithelial cell markers remained without significantly altered expression levels (*Sftpc*: p=0.2023; *Epcam*: p=0.2611; *CC10*: p=0.4943; *Aqp5*: p=0.5984). Amongst the alveolar myofibroblast associated genes *Fgfr4* was significantly increased (p=0.0102), whereas *Pdgfa* (p=0.0535), *Shh* (p=0.0629) and *Fgf9* (p=0.0776) showed a trend towards an increase.

4.6.3 Immunohistological staining shows no significant difference for the expression of Sftpc, Acta2 and pSmad3 under double damage compared to hyperoxia only

No difference in the number of expressing cells was shown for Sftpc (see Figure 12.D; p=0.4102), Acta2 (see Figure 12.E; p=0.5654) and pSmad3 (see Figure 12.F; p=0.4293).

Alveolar Morphometry revealed no further impairment of the alveolar structure

upon double injury by hyperoxia and *miRNA* overexpression compared to hyperoxia only. RT-qPCR showed no outstanding changes in Fgf and Tgf-β signaling. Single epithelial and alveolar myofibroblast associated genes were altered. The fact, that single alveolar myofibroblast factors tend to be elevated in expression upon double injury compared to hyperoxia only, is difficult to integrate into the whole context. It might actually depict an additional effect of double injury. Further investigation is necessary to examine this issue.

The fact that a combination of both injurious stimuli (hyperoxia and *miR-154* overexpression) was not able to worsen the impairment of alveologenesis leads to the assumption that the process of injury is saturated already by either of the injurious stimuli and that an addition of the other detrimental factor does not worsen the phenotypic situation or change the genetic expression profile (see sections 4.5 and 4.6). This raises the hypothesis that the injurious effect on the alveolar development in the context of hyperoxic lung injury might be mediated by *miR-154-3p*, as the expression of this *miRNA* is induced by hyperoxia (see Figure 7) and as this is the *microRNA*, which is more significantly increased upon hyperoxia compared to *miR-154-5p* (see section 4.1). In other words, both factors (hyperoxia and *miR-154* overexpression) use the same pathway to interrupt with the process of alveolarization and as *miR-154-3p* activity (and to a lesser extent *miR-154-5p*) is enhanced upon hyperoxic treatment, hyperoxia possibly is the upstream activator of *miR-154-3p*, which in turn leads to the idea that *miR-154-3p* might be regarded as a potential downstream effector of hyperoxic lung injury. Furthermore it is tempting to assume, that inhibiting the expression of *miR-154-3p* in the context of hyperoxia might be able to alleviate or even prevent the injurious effect of hyperoxia on the formation of alveoli, as *miR-154-3p* possibly promotes damage on the alveolar structure caused by hyperoxia. More experiments have to be done to further investigate and define the role of *miR-154-3p* in the context of hyperoxic lung injury in the murine animal model.

In summary, we have shown that overexpression of *miR-154* leads to a similar alveolar phenotype as hyperoxic lung injury does. Furthermore the dynamic expression profiles of genes belonging to Fgf signaling, Tgf-β signaling and epithelial cell markers share certain similarities between hyperoxia and *miRNA* overexpression, although upon *miRNA* overexpression significant alterations of

genetic expression were not always achieved in the same extent as under hyperoxic treatment, but trends towards alterations in the same direction were shown (compare 4.2 and 4.3). As *miR-154* overexpression leads to hypoalveologenesis in a similar fashion as upon hyperoxia (compare Figure 8 and Figure 9), and as it was previously described that hyperoxia interrupts the formation of alveolar myofibroblasts at the tips of emerging secondary septa in rats (Hou et al., 2015), it appeared likely, that the *miRNAs* of interest might also affect alveolar myofibroblast formation and function, and therefore lead to the same phenotype of impaired formation of alveoli. Contrary to our expectations RT-qPCR and immunohistochemical data revealed that the alveolar myofibroblasts are not noticeably affected upon *miR-154* (see Figure 9.C). We therefore hypothesized that there is another molecular process existing, which is activated by both hyperoxia and *miRNA* overexpression, leading to the same deleterious effect on alveologenesis. With the gathered data from the Gene Array Analysis and the previously summarized findings of other studies (see section 4.3) we assume that the mutually affected molecular process, which is shared by both, hyperoxia and *miR-154* overexpression, may be the transdifferentiation of AECII cells to AECI cells in the context of hyperoxia described by Hou and colleagues (Hou et al., 2015).

5. Discussion

BPD is the most common chronic lung disease of preterm babies (Baraldi and Filippone, 2007). Although it has been firstly described decades ago (Northway et al., 1967), a curative approach for this disease is lacking. Due to improved symptom-oriented care more BPD patients survive leading to an increased number of patients suffering from long-term limitations as a consequence of the lung injury associated with BPD implying a financial burden for the healthcare system (Baraldi and Filippone, 2007; Chao et al., 2015; Owen et al., 2017). In order to understand the underlying pathophysiological mechanisms of BPD it is necessary to apply animal models and examine the effect of injurious stimuli on the lung. New findings and the elaboration of processes, which are affected on the biochemical level, are essential to find potential targets and develop new therapeutical approaches in the future.

5.1 Hyperoxia increases the expression of *miR-154-3p* in murine lungs, especially in AECII cells

In order to demonstrate the effect of inhalation of high oxygen concentrations on *miR-154-3p* and *miR-154-5p* expression we have used the previously described BPD mouse model and exposed mice to oxygen concentrations of 85% from birth until lung harvest. We have examined the expression levels of both *isomiRNAs* in whole lung samples at three different time points (P2, P5 and P8) by RT-qPCR. While *miR-154-3p* expression appeared to be increased upon hyperoxic exposure, there was no significant increase of the *miR-154-5p* expression level after hyperoxia (see Figure 7.B). Therefore we assume that *miR-154-3p* potentially plays a more relevant role in the context of BPD than *miR-154-5p* does. To our knowledge, this is the first study to demonstrate that *miR-154-3p* is increased upon treatment with hyperoxia in whole lung samples (see Figure 7.A-B).

Comparison of results from different Publications using a BPD animal model is difficult a priori, as the procedures lack standardization. This issue has been reviewed by Nardiello and Morty (Nardiello and Morty, 2016) and Silva and

coworkers (Silva et al., 2015): there are many factors, which can differ between different studies, such as animal or "rodent species", "rodent strain" and the hyperoxic treatment itself, which can differ in duration, and applied oxygen concentration and also include or exclude a recovery phase after hyperoxic lung injury before lung harvest (Nardiello and Morty, 2016), hampering comparability between the published studies. Even the nomenclature can differ: for example P1 usually denotes the day of birth, but in some cases it denotes the first day after the day of birth (Silva et al., 2015).

An advantage of using mice for experiments with high oxygen application is that mice are normally born in the saccular phase, whereas the human lung normally develops a little further before birth and therefore humans are born in the alveolar phase. This means that mice are born at a stage of lung development, which corresponds to a stage of preterm born human babies. Silva and colleagues have reviewed this issue before (Silva et al., 2015). With the BPD mouse model we simulate the effect of high oxygen concentrations on murine lungs, which are equivalently developed like lungs of preterm born human babies. Still it has to be kept in mind, that this stage is the physiological stage of birth for mice.

In order to explore which lung cell type highly contributes to the increased *miRNA* expression levels shown in whole lung samples, we have used isolated AECII cells (kindly provided to us by Elisabeth Kappes) and performed another RT-qPCR determining the relative expression levels of *miR-154-3p* and *miR-154-5p* in AECII cells with and without application of hyperoxia. Interestingly, for both, *miR-154-3p* and *miR-154-5p*, a significant increase in expression was seen in AECII cells after hyperoxic treatment (see Figure 7.C). As the increase was much stronger for *miR-154-3p* we kept the assumption that this is the *miRNA* that needs to be further examined in the context of BPD. Of course the increased *miR-154-5p* expression level in AECII cells after exposure to hyperoxia can also imply that this *miRNA* plays a role in BPD as well. In turn there are some other potential explanations for this phenomenon. On the one hand *miR-154-5p* baseline levels can be higher than *miR-154-3p* under normoxic conditions already and the increase after hyperoxia simply appears to be less substantial compared to normoxic conditions, although its increased expression upon hyperoxia is functional. At the end of the day the results still describe relative changes of expression levels. On the other hand we have to

keep in mind, that both mature *miRNAs* share a mutual pathway of biogenesis as they originate from the same precursor *miRNAs* (Krol et al., 2010), which can mean, that an increase of expression of one of the mature *miRNAs* at least partly leads to an increase of the counterpart *miRNA* (see section 1.1.2). On the other hand, it is commonly believed that the counterpart *miRNA* is degraded while the actual *miRNA* remains stable and functional. The connection of the two related *miRNAs*, especially in the context of hyperoxic injury, still remains unclear. We have decided to further investigate *miR-154-3p* in the following steps, as its change of expression level was more evident.

Next, we have performed a Fluorescence In Situ-Hybridization (FISH) staining comparing *miR-154-3p* expression after hyperoxic lung injury to normoxia (see Figure 7.A). Under normoxic conditions we can see, that the *miR-154-3p* expression is predominantly located in the epithelial cells of distal and proximal airways (see Figure 7.A). *miR-154-3p* positive cells seem to pattern the epithelial layer of the airways. Although in a lesser extent, there are *miR-154-3p* positive cells also found in the mesenchymal areas. All in all, it is noticeable that *miR-154-3p* expression is mainly located in the proximal and distal airway epithelial cells. To our knowledge we are the first group to describe the allocation of *miR-154-3p* expression in the postnatal murine lung with this study. After treatment with hyperoxia the intensity of the *miR-154-3p* signal increases compared to normoxia. Counting *miR-154-3p* positive cells reveals, that not the number of *miR-154-3p* expressing cells, but the expression level, changes (see Figure 7.A). This may possibly indicate that hyperoxia leads to an increased expression of *miR-154-3p* in cells, which already express *miR-154-3p* at lower levels in normoxia, instead of recruiting further *miR-154-3p* positive cells.

In summary, this is the first study to deduce that hyperoxia is able to induce an increased expression of *miR-154-3p* in the lung, especially in the lung epithelium, where AECII cells highly contribute to this increase. It still remains unclear, how other lung cell types react to that injurious stimulus. Perhaps not only AECII cells contribute to the change of *miR-154-3p* expression, as the different lung cell types are highly interwoven in interaction amongst each other and cannot be contemplated as functionally isolated cell units. Perhaps other cell types, which normally express *miR-154-3p* even have a decreased expression level of *miR-154-*

3p after hyperoxic injury or cells, which are not expressing *miR-154-3p* in normoxia, induce *miR-154-3p* expression after hyperoxia. A more detailed examination of which cells express *miR-154-3p* and their dynamic change of expression level after hyperoxic lung injury has to be undertaken to fulfill this issue. Furthermore BPD has various different causative factors beside inhalation of high oxygen concentrations, such as ventilation with high pressures leading to volutrauma and barotrauma, going along with increased susceptibility for infection and inflammatory processes (Silva et al., 2015). With the BPD mouse model as we use it we can only examine the effect of high oxygen concentrations on the lung, leaving out ventilation with high pressures, and hence not considering volutrauma and barotrauma. Therefore, the present BPD mouse model only depicts the effect of a single factor (high oxygen concentration) of a complex disease, which has a multifactorial cause. Approaches examining the effect of ventilation and associated mechanical stress on the lung could add further information to the BPD research and complete the whole issue (Silva et al., 2015). It has been shown already that mechanical ventilation with room air leads to a BPD like phenotype with impaired alveolarization in C57BL/6 mice (Ratner et al., 2013). Again this shows that beside hyperoxia mechanical ventilation is another factor damaging the lung structure causing BPD. Alternatively, examining single causative factors can be regarded as advantageous, as the gathered data can be unmistakably attributed to the effect of the solely examined condition.

After gathering the demonstrated data so far we were able to demonstrate that there is an increased expression of both, *miR-154-3p* and *miR-154-5p*, in the AECII cells upon hyperoxic exposure without knowing the role of the *miRNAs* of interest in the context of BPD yet. Potentially they have a protective function in the context of hyperoxia, but they might also have a detrimental effect, for example functioning as a mediator of hyperoxic damage. Whether *miR-154-3p* plays a role in the pathomechanism of BPD at all remains to be further investigated, as a change of expression doesn't automatically lead to the conclusion of involvement. To this point the demonstration of action is still lacking (Nardiello and Morty, 2016).

5.2 Hyperoxic lung injury during postnatal lung development leads to hypoalveolarization with simplified alveoli

With the next step we examined the impact of inhaling high oxygen concentrations on the histologic lung structure and the genetic expression profile (see Figure 8). For this objective we exposed mice to high oxygen concentrations (85% O_2) from birth (P0) until P8, harvested the lungs after a recovery period of 8 days at P16 and compared these mice to normoxic conditions (see Figure 8.A). As expected we found the alveolar structures to be interrupted in development showing an increased diameter (MLI; mean linear intercept) and thickened alveolar walls (see Figure 8.B). These findings indicate impaired alveolarization, which among others is a typical characteristic of lungs suffering from BPD (Coalson et al., 1995; Voynow, 2017). Our results are consistent with findings from other studies using a BPD animal model, which also found increased MLI and thickened alveolar walls in lungs after exposure to hyperoxia compared to control animals (Alejandre-Alcazar et al., 2007; Madurga et al., 2014; Martin et al., 2014; Niedermaier and Hilgendorff, 2015; Porzionato et al., 2016). It has been discussed that MLI and septal thickness are parameters, which might be affected during lung harvest and histological preparation and hence possibly adulterated (Porzionato et al., 2016). Indeed, the preparative procedure may affect parameters of lung architecture of individual samples, because the preparations were manually performed, meaning that a variation of handling between the individual subjects may occur. In order to eliminate this factor, we masked the mice while doing the preparation, not knowing which mouse belongs to which group of treatment. Therefore, mice belonging to different experimental groups are equally exposed to potential disturbing factors. There was no possibility to manipulate the lungs in our favor.

As expected and described by others, our findings demonstrate that hyperoxia during the first 8 days after birth leads to an interruption of lung development and alveolar formation in mice, showing enlarged alveoli and thickened septal walls. As proper gas exchange requires a preferably large alveolar surface and short distance for diffusion between the alveolar and the capillary lumen, it is easily conceivable that mice showing the depicted alveolar phenotype after hyperoxic treatment have a less sufficient gas exchange in the lung than their littermates, which were kept in room air.

5.3 Hyperoxic treatment during postnatal lung development affects the genetic expression activity of Fgf and Tgf-β signaling, epithelial cell markers and alveolar myofibroblast-specific genes

Next, we checked the effect on genetic expression profiles after hyperoxic lung injury by RT-qPCR (see Figure 8.C). We found genes involved in the Fgf signaling to be increased in expression after hyperoxia compared to normoxic controls. The ligand's transcription product *Fgf10* was not altered in expression, but the corresponding receptors and downstream targets were, showing increased *mRNA* levels. It seems like upon recovery after hyperoxia the organism induces a protecting mechanism, which increases Fgf10 signaling: the level of the ligand remains unaltered, whereas the availability of its receptor increases, as apparently Fgf10 has a protective function in the context of hyperoxia (Chao et al., 2017), meaning that the same level of Fgf10 protein may potentially have a stronger induction of its downstream signaling cascade. Our lab already examined the role of Fgf10 in the context of hyperoxic lung injury showing a decreased *Fgf10* expression at P5 and P8 after hyperoxic treatment without recovery (Chao et al., 2017). Apparently hyperoxia decreases the formation of *Fgf10*. This does not necessarily stand in contrast to our result of an unaltered *Fgf10* level, as many factors hamper the comparability between the two studies: Firstly, Chao and coworkers examined earlier time points (P2, P5 and P8 vs. P16 in our case). Secondly, they used mice of a different background (C57BL/6 vs. CD1). And thirdly and probably most importantly, they did not include a recovery phase between hyperoxic treatment and lung harvest. Perhaps the recovery phase, which is included in our model, is the key difference, giving time for the Fgf signaling axis to recuperate, leading to a normalized *Fgf10* expression level. Chao and colleagues have shown that Fgf10 itself can be considered as a protective factor in the BPD model, as *Fgf10*-deficient mice died upon hyperoxic lung injury. Probably the activated downstream pathway of Fgf10 induces processes in the cell, leading to the expression of genes in the nucleus required for protection against ROS (reactive oxygen species), indicated by increased mortality in mice with decreased *Fgf10* expression (Chao et al., 2017). A possible mechanism of protection in a recovery phase after detrimental hyperoxia might be an up-regulation of the Fgf10 signaling cascade by enhancing the expression of Fgf10 targets. The fact that the downstream

Fgf10 targets are increased in *mRNA* expression levels in our model, whereas *Fgf10* is not, may show a common mechanism for recovery: when the ligand is limited, an up-regulation of the receptor can preserve the level of signaling activity: The system is more or less "striving" for more Fgf10 signaling activity. When considering the lungs' histology (Figure 8.B), this potential effort for recovery fails, as the phenotype remains impaired. In the end, an up-regulation of *mRNA* levels doesn't necessarily imply that the emergence of the protein product is increased in equal measures.

Several cell markers were altered in expression levels after hyperoxic lung injury compared to normoxia (see Figure 8.C). *Epcam* as a general epithelial cell marker (Litvinov et al., 1994) was significantly increased in expression, indicating an effect of hyperoxia on the epithelial compartment. It appears that the distal lung epithelium (*Sftpb*, *Aqp5*) is more affected, than the proximal (e.g. *CC10*): *Sftpb*, a marker for AECII cells, appears to be increased in expression after hyperoxic treatment, whereas the more specific AECII marker *Sftpc* only shows a slight trend towards an increase (Fukumoto et al., 2016; Hobi et al., 2016; Singh and Katyal, 1997). Even on the protein level the immunohistological staining for Sftpc could not reveal any change of number of AECII cells. Roper and coworkers described the AECII cells' morphology and viability as not affected upon hyperoxia, but they found DNA strand breaks in the AECII cells (Roper et al., 2004). AECII cells appear to be more resistant to hyperoxia and, although their DNA seems to be damaged upon ROS injury, they are able to maintain the populations' cell number. Still the study has only limited utilization for confirming our results, as Roper and colleagues used mice with a C57BL/6 background, older mice (8-12 weeks), higher O_2 concentrations (100%) and no recovery period in their study's approach. Lee and coworkers examined the AECII cells' DNA damage and proliferation after 24h, 48h and 72h of recovery after exposure to hyperoxia (Lee et al., 2006), which due to the recovery phase comes closer to the experimental model of the current study. During the period of recovery DNA damage was repaired, whereas proliferation still remained increased after 72h. But here again, a comparison with our study is difficult, as the mice had a C57BL/6 background and were aged between 6 and 8 weeks, which is far away from our P16 mice. Furthermore, Lee and colleagues used higher O_2 concentrations of 95%. But most importantly, they examined a recovery

phase of only 72h, whereas the recovery phase in our study consists of 8 days. Perhaps we have simply missed the action of recovery on the level of AECII cells, as 8 days of recovery seem to be enough for the AECII cells to completely revive and attain a state of equilibrium again. The increased *Sftpb* might simply be a remnant of previous AECII recovery activity. Yee and coworkers found AECII cells to be increased in number during exposure to hyperoxia, but decreased after a recovery period (Yee et al., 2014). Our findings show no change of *Sftpc* expression and no change of Sftpc expressing cell numbers.

Again, the comparability of BPD model studies is clearly aggravated, when not using standardized procedures, as previously mentioned (Nardiello and Morty, 2016; Silva et al., 2015), even though the mentioned studies show results, which are not necessarily contradicting to our findings. Presumably our study model with 8 days of recovery is unsuitable in the context of AECII behavior after lung injury. An approach with either a much shorter period of recovery, or without a recovery phase could possibly yield more useful information about the AECII reaction after hyperoxic lung injury.

It was commonly believed, that upon hyperoxia AECI cells perish, but AECII survive (Roper et al., 2004). It has been even described that SPC-positive AECII cells increase in number after hyperoxia (Hou et al., 2015). But in the current study we find the AECI marker *Aqp5* to be significantly increased, whereas the AECII marker *Sftpc* more or less remains stable. How can this be connected? The increased *Aqp5* expression is consistent with results from Yee and colleagues (Yee et al., 2014). They found not only *Aqp5*, but also *T1α* (also known as Podoplanin (Ugorski et al., 2016)), another AECI specific marker, to be increased after hyperoxia. Chao and colleagues found an increased AECI specific expression signature upon hyperoxic treatment in isolated AECII cells, indicated by Gene Array Analysis (Chao et al., 2017). This apparent higher AECI activity might depict the state of issue, that during hyperoxia AECI cells are affected much more than AECII cells, and that during recovery AECI cells require a higher extent of recreation than AECII cells. The increased *Aqp5* expression might represent processes of repair within the AECI population with increased gene expression. As AECII cells are believed to function as AECI progenitors after hyperoxic lung injury, in recovery they might differentiate into and repopulate the AECI population

and hence the AECI expression signature predominates, which has been examined and described by Hou and coworkers (Hou et al., 2015): They found a much more pronounced expression of AECI specific markers in isolated AECII cells after hyperoxic treatment. Furthermore, they described a more abundant appearance of AECII cells transdifferentiating to AECI cells, which were detected by a positive immunohistological double staining for both, AECII specific Sftpc and AECI specific Aqp5. This is the most interesting and the most obvious aspect explaining the increased expression of *Aqp5* after hyperoxic lung injury in our study: More AECII cells exert their function as AECI progenitors under hyperoxia in order to repopulate the damaged AECI population. Why AECII cells are more resistant to the same injurious stimulus than AECI cells remains unclear (Roper et al., 2004). A potential idea was discussed, saying that AECI cells simply cover most of the alveolar surface (Hou et al., 2015), and are therefore more easily exposed to hyperoxia (Rozycki, 2014). Perhaps AECII cells have a different set of protection factors or protective mechanisms, which the AECI cells simply do not have.

But is the action of AECI cells in BPD simply described as perishing and then regenerating? Recently Rozycki reviewed the role of AECI cells in the context of hyperoxic lung injury (Rozycki, 2014). He listed several studies questioning the fact that AECI cells are terminally differentiated and that they originate exclusively from the AECII population. Furthermore, he depicted the behavior of AECI cells in hyperoxic lung injury as potentially species-dependent and less passive than previously described. For example the set of receptors on the AECI cell's surface may indicate an involvement in inflammatory processes (TLR-4 and RAGE). In this case special attention has been paid on RAGE as a potential promoter of inflammatory cytokines in hyperoxic lung injury. Of course, the topic about AECI cells opens another chapter in BPD that would go far beyond the scope of this study. But the fact, that we find *Aqp5* to be up-regulated in hyperoxia (see Figure 8.C), taken together with Rozycki's review (Rozycki, 2014) raises the question whether AECI cells may play a far more important role in the BPD mouse model than previously believed. As already discussed by Yee and coworkers, the increased AECI activity can either mean an increased number of AECI cells or increased AECI gene expression activity upon hyperoxic treatment (Yee et al., 2014). In this case the best match to our findings is the study from Hou and colleagues (Hou et al., 2015): A stronger transdifferentiation of AECII-to-AECI

cells can very well explain the increased *Aqp5* activity seen in our results after hyperoxic treatment (see Figure 8.C). This circumstance was further examined by experiments, which are discussed in the sections further below.

Tgf-β signaling appears to be activated in murine lungs exposed to hyperoxia (see Figure 8.C), indicated by increased expression of ligands (*Tgf-β1* and *Tgf-β3*) and downstream targets (*Smad7*). Surprisingly, this was not confirmed by immunohistological pSmad3 staining, which revealed no change of Tgf-β activity (see Figure 8.F). Increased *Tgf-β* activity was previously found in other studies in the context of BPD animal models (Alejandre-Alcazar et al., 2007; Nakanishi et al., 2007). Interestingly, when inhibiting Tgf-β signaling in *Tgfβr2* knockout mice and exhibiting them to hyperoxia, the mice exhibit less impairment of alveolarization compared to control mice (Sureshbabu et al., 2015). The authors even speak of "equivalency to room air controls" regarding alveolar development. This indicates that hyperoxia possibly mediates its injurious effect on alveolar development at least in part via Tgf-β signaling. Overexpression of *Tgf-β1* in murine lung airway epithelium under the control of the *CC10* promoter without application of hyperoxia can mimic a BPD-like alveolar phenotype, leading to impaired alveolar formation indicated by enlarged alveolar units and thickened alveolar septa (Vicencio et al., 2004), whereas knockout of the receptor *Tgfβr2* was able to ameliorate this effect (Sureshbabu et al., 2015). These examples demonstrate that hyperoxic lung injury in mice is at least partly mediated via Tgf-β signaling, as inhibition of Tgf-β signaling is able to protect the lung from injury. Therefore, it is not very surprising that upon exposure to hyperoxia we find Tgf-β signaling components to be up-regulated in expression levels compared to normoxia (control) in the current study as well.

As Tgf-β signaling is important for lung development at various stages (Chen et al., 2010; Chen et al., 2005; Nakanishi et al., 2007), but overexpression leads to impairment of alveolar formation (Vicencio et al., 2004), it is obviously important to fine-tune and balance the level of Tgf-β signaling in the lung in order to properly develop (Alejandre-Alcazar et al., 2007). Here, we demonstrate that hyperoxia influences signaling pathways, which are involved in lung development (Fgf signaling, Tgf-β signaling), and hence disturbs alveolar development in the murine lung.

Different factors and signaling pathways are involved in the process of secondary septation and alveolarization of the lung (already described in Introduction) (Bostrom et al., 1996; De Langhe et al., 2006; Kugler et al., 2017; Perl and Gale, 2009; Popova et al., 2014; Weinstein et al., 1998). We determined the change of expression levels of a set of genes, which are involved with secondary septation, in order to show an effect of hyperoxic treatment on the most important cell type involved in alveolarization: the alveolar myofibroblasts (see Figure 8.C). Indeed, some markers were affected upon hyperoxia compared to normoxic controls. The *Elastin mRNA* level appears to be increased. An immunohistological staining for Elastin protein localization would be a very helpful method to examine, whether alveolar myofibroblasts in murine lungs affected by hyperoxia actually fail to deposit Elastin at the positions of new emerging septa for alveolar septation, which is one of the main events in alveolarization (De Langhe et al., 2006). In the current study, we can merely say that this process is affected upon hyperoxia, but we cannot say in how far. Whether alveolar myofibroblasts are formed upon hyperoxia or not can be shown by *Acta2 mRNA* levels in RT-qPCR and Acta2 immunohistological staining. RT-qPCR reveals no change in *Acta2* expression levels after hyperoxia. But Acta2 immunohistological staining shows increased numbers of Acta2 positive cells. How can this be explained? When taking a closer look at the histological staining we first examined the alveolar myofibroblasts. Typically they are situated at the tip of an emerging secondary septum (Morrisey and Hogan, 2010; Popova et al., 2014). For both groups, hyperoxia and normoxic controls, there were Acta2 positive cells present depicting the alveolar myofibroblasts, found at the tips of emerging secondary septa, indicating that alveolar myofibroblast formation does not fail upon hyperoxia (*data not shown*). This finding is in contrast to previous examinations in rats, where hyperoxia leads to a decreased number of alveolar myofibroblast on the emerging tips of the secondary septa, indicated by a decreased number of α-SMA (Acta2) positive cells (Hou et al., 2015). Perhaps the eight-day recovery phase after hyperoxia, which was implemented in the current study, is the crucial difference, which enables alveolar myofibroblast recovery. The question remains in our case, whether these obviously present alveolar myofibroblasts are functioning. As previously mentioned *mRNA* levels of *Elastin* are affected upon hyperoxia and therefore an immunohistological staining for Elastin might be enlightening in order to answer this question, as an

absence or reduction of Elastin protein, which is deposited by the alveolar myofibroblasts, would give proof that upon hyperoxia the present alveolar myofibroblasts are dysfunctional. Acta2 is a molecule known in the context of fibrosis (Vittal et al., 2013). The increased level of Acta2 in Immunohistochemistry (Figure 8.E) might be the result of fibrotic processes, which is typical for BPD experiments (Baraldi and Filippone, 2007; Chao et al., 2015; Voynow, 2017), and alterations in the consistence of the ECM by increased smooth muscle cell activity. This finding however harmonizes with the results from Hou and colleagues (Hou et al., 2015). All in all the immunohistologic appearance of more Acta2 protein might be the remnant of the 8 days of hyperoxic treatment, whereas the following 8 days of recovery were long enough for the *mRNA* levels to return to baseline values. *Fgf9* expression appears to be up-regulated upon hyperoxia. It has been previously shown that increased Fgf9 activity can lead to impaired formation of the alveolar myofibroblasts via Fgfr2c and hereby disturb secondary septation (De Langhe et al., 2006). Finally, *Shh* shows a trend towards an increase. It has been already shown that Shh signaling is required for alveolar development by regulating myofibroblast function (Kugler et al., 2017). Here, we have found several candidates with altered expression levels after hyperoxic lung injury, indicating a disruption of alveolar formation.

All in all, our findings clearly show a disruption of the formation of alveoli after hyperoxia shown in the morphometric analysis. The signaling pathways and lung cells examined here, which are known to be involved in alveolarization, are affected by inhaling air with high oxygen concentrations. Our results are mostly compatible with findings of previously published studies. In how far *miR-154-3p* or *miR-154-5p* are involved in any of the described processes, which are obviously affected by hyperoxia, was examined in the current study by further approaches, which are discussed in the following sections.

5.4 Airway epithelium-specific overexpression of *miR-154* shows similar alveolar phenotype and genetic expression profile compared to hyperoxia

In order to examine the role of *miR-154* in the context of BPD we have generated a mouse line, which overexpresses *miR-154-3p* and *miR-154-5p* in the

murine airway epithelium. This has been elaborately described and validated in "Material and Methods" (see section 3.1.4 and Figure 6). Briefly worded, upon doxycycline administration both *isomiRNAs* are overexpressed in the airway epithelium of experimental mice. The levels of the *miRNAs* of interest remain unaltered in control mice. The subjects received doxycycline food from E18 (day before birth) until lung harvest (P16), which means that for this period experimental mice overexpress both *isomiRNAs* in the airway epithelium. It has previously been described that the *CCSP-rTTA* (or *Scgb1a1-rtTA*) driver line may affect alveolar formation leading to impaired alveolarization and therefore increased MLI ab initio even without doxycycline administration (Perl et al., 2002; Perl et al., 2009). Wu and colleagues have resolved this issue by showing no effect of the *CCSP-rtTA* driver line on the MLI (Wu et al., 2010).

In *miR-154* overexpressing murine lungs Alveolar Morphometry revealed an increased MLI indicating impaired alveolarization, whereas percentage of airspace and septal thickness remained unaffected. Here, the changes in MLI are similarly pronounced as in hyperoxia (compare Figure 8.B to Figure 9.B). Interestingly, the septal thickness was altered under hyperoxic treatment (not significantly, but close to significance), but not when the *miRNAs* were overexpressed (no change at all). Given the fact that *miR-154* really is a downstream effector of hyperoxia, it is possibly imaginable that overexpression of *miR-154* only depicts a part of the hyperoxic impact on alveolar structure, as hyperoxia probably activates several other signaling pathways, which are not dependent on *miR-154*. With the overexpression of *miR-154-3p* (and *miR-154-5p*) we might have only activated one (or only few) of these hypothetical pathways, which therefore only leads to an attenuated alteration of phenotype, meaning an increased MLI, but unaltered septal thickness. Regarding these findings, *miR-154-3p* and *miR-154-5p*, which are both up-regulated upon hyperoxia (see Figure 7), appear to be potential downstream effectors of hyperoxic injury, mediating damage on the developing alveoli, indicated by increased MLI levels upon *miRNA* up-regulation.

The same concept is applicable concerning alterations of genetic expression: when having a look at and comparing the bars demonstrating alterations of genetic expression after hyperoxia and after *miR-154* overexpression, both share certain similarities (compare Figure 8.C and Figure 9.C). Concerning Fgf signaling *miR-*

154 overexpression even reaches the same levels of significance as seen under hyperoxia. For Tgf-β signaling *miRNA* overexpression doesn't achieve the same levels of significant changes compared to control mice as seen after hyperoxia, but the bars tend to the same direction, indicating trends towards increased Tgf-β signaling after *miR-154* overexpression, although not as effective as upon hyperoxic treatment. The fact that *miR-154* overexpression alters signaling axes in a similar manner as hyperoxia gives a hint towards *miR-154-3p* (and possibly *miR-154-5p*) actually having a potential role in the BPD mouse model and potentially being a downstream effector of hyperoxic lung injury.

When looking at the genes involved with alveolar myofibroblasts, overexpression of the *miRNAs* of interest does not show any alterations in the examined genes, unlike hyperoxia, which affected the activity of *Elastin*, *Fgf9* and to a lesser extent *Shh* (compare Figure 8.C and Figure 9.C). Here, we have to presume that *miR-154* apparently does not affect the alveolar myofibroblasts as far as our findings are concerned. Although at first glance alveolar myofibroblasts appeared to be the most probable target when considering the alveolar phenotype with impaired alveolarization when applying hyperoxia and when overexpressing *miR-154* as well, another mutual targeting mechanism has to be present affecting the proper formation of the alveoli. Perhaps another cell type, which is involved in the process of alveolar development and maturation, is affected by *miR-154* overexpression as well as by hyperoxia.

Furthermore, we also performed the same immunohistological stainings for the examination of *miR-154* overexpression compared to control mice as we did for hyperoxia, but herein we found no changes for Sftpc, Acta2 and pSmad3 (see Figure 9.D-F).

Interestingly, when looking at epithelial markers, *miR-154* overexpression doesn't attain as significant alterations in genetic expression compared to hyperoxia. But the alteration of expression level of one epithelial marker is noticeable: *Aqp5*. *miR-154* overexpression leads to an almost significantly increased expression of *Aqp5*, which is somewhat similar to the finding in hyperoxic lung injury. Among the epithelial markers it is even the one with the strongest alteration of expression level in both, hyperoxic lung treatment and *miRNA* overexpression, which again

demonstrates certain similarities between the compared conditions concerning alterations of genetic expression (compare Figure 8 and Figure 9). At this point an interesting idea came up, when considering the findings from Hou and Colleagues (Hou et al., 2015). The transdifferentiation of AECII cells to AECI cells under hyperoxic treatment described by Hou and coworkers might advance via an up-regulation of *miR-154-3p* (or *miR-154-5p*). Hou and colleagues were able to describe the process of alveolar epithelial cell transdifferentiation without actually naming factors, which are involved in this process. With our findings we hypothesize that hyperoxia leads to an increased AECII-to-AECI transdifferentiation by inducing increased expression of *miR-154-3p*, as we have shown that *miR-154-3p* is highly overexpressed in AECII cells under hyperoxic conditions (see Figure 7.C), and as both, hyperoxic lung treatment and *miR-154* overexpression, lead to an increased activity of the AECI marker *Aqp5* and share a similar alveolar phenotype. If this is the case, an induced expression of *miR-154-3p* should lead to the same findings of an increased AECI specific transcription signature within the AECII population, as previously described and published (Hou et al., 2015). This is further discussed in the sections below.

AECI cells form a substantial part of the air-blood barrier, which is also formed by the endothelial cells of the alveolar capillaries and a basal membrane in between and they play an important role in gas exchange (Hou et al., 2015; Makanya et al., 2013). Alveolar maturation means optimization of gas exchange, which is on the one hand achieved by an increase of the number of alveoli and a decrease of alveolar size, leading to a larger area for gas exchange, and on the other hand by thinning of the appendices of the AECI cells, which are forming the alveolar wall, and consequently leading to a decreased alveolar-to-capillary distance and easing of gas diffusion (Wang et al., 2016b). It is imaginable that AECI cells, as they form the inner alveolar layer, are highly involved in the process of alveolar maturation. The elongation and thinning of their cellular bodies is one of the underlying mechanical processes in alveolar maturation (Makanya et al., 2013; Wang et al., 2016b). If this process is disrupted by either hyperoxia or *miR-154-3p* overexpression it is easily imaginable, that we see a phenotype with impaired alveolarization. In the context of BPD animal model in rats, Hou and colleagues have examined the transdifferentiation of AECII cells to AECI cells (Hou et al.,

2015). Injurious stimuli may for example alter the morphology of AECI cells from an elongated thin cell to a broader cell, which could explain the increased septal thickness seen in Alveolar Morphometry under hyperoxic conditions (see Figure 8.B). Another possibility is that we simply find an overpopulation of AECI cells after hyperoxia or *miRNA* induction. In this case too many AECI cells might be packed in a limited area: the AECI cells more or less stand in each other's way leading to an uncoordinated alveolar formation. Of course, these ideas are purely hypothetical. But the results we have gathered point in the direction of AECI cells. Beside an increased AECII-to-AECI transdifferentation Hou and colleagues also found increased levels of Aqp5 protein expression, marking AECI cells and showing a disordered collocation of AECI cells (Hou et al., 2015). Furthermore they found a disruption of the typical three-layer formation of the air-blood barrier and morphological changes of AECI cells. This is in accordance with the idea of disturbance of AECI cells and air-blood barrier by hyperoxia. Ultimately, they found cells being positive for both Sftpc and Aqp5 protein, representing AECII cells transdifferentiating into AECI cells. We therefore decided to perform a Gene Array Analysis in order to further examine this hypothesis of *miR-154-3p* being a key molecule in the context of hyperoxia-induced AECII-to-AECI transdifferentiation: again we isolated AECII cells of mice, which are overexpressing *miR-154-3p* and *miR-154-5p* in the airway epithelium (experimental group) and control mice, which are not overexpressing the *miRNAs* of interest, isolated *RNA* from the obtained AECII cells and performed a Gene Array Analysis in order to determine, whether we find an altered AECI-specific expression signature in the AECII population when overexpressing the *miRNAs* of interest.

5.5 Overexpression of *miR-154* in the murine airway epithelium leads to a more AECI-specific transcription signature in AECII cells

The Gene Array Analysis of isolated AECII cells showed that upon overexpression of *miR-154* in the airway epithelium a stronger expression of AECI marker *mRNAs* such as *Cav1*, *Pdpn* and *Hopx* (Jung et al., 2012; Treutlein et al., 2014; Ugorski et al., 2016) was seen (see Figure 10). This is strongly indicative for an actually happening transdifferentiation of AECII cells to AECI cells in the

context of *miR-154* overexpression, which has similarly been described by Hou and colleagues when exposing rats to hyperoxia (Hou et al., 2015). In order to confirm our results and to proof our hypothesis that *miR-154-3p* is the key regulator of AECII-to-AECI transdifferentiation in the context of hyperoxia, which was described by Hou and colleagues, further experimental procedures are meaningful: A revision of the *miR-154* overexpressing mouse model, similar to the one we have already performed in this study (see Figure 9), and the acquisition of further lung sections embedded in paraffin in order to double-stain the sections for Sftpc as an AECII marker and Aqp5 as an AECI marker is standing to reason. Hou and colleagues have performed this experimental approach in the context of hyperoxia and found an increased number of cells positive for both markers after hyperoxic treatment of rats, which in turn demonstrates an intermediary stage during AECII-to-AECI transdifferentiation. If *miR-154* overexpression in the murine airway epithelium leads to the appearance of an increased number of equally double-stained cells, it would be a very strong finding to proof our hypothesis. Additionally, a knockdown approach might be the final step, for instance by using a *miR-154-3p* antagonizing in vivo system. For this purpose the creation of a new transgenic mouse line, which is down-regulating *miR-154-3p*, or the application of a *miR-154-3p* antagonist (e.g. by inhalation) would be required. Another possibility is culturing isolated AECII cells and using a morpholino approach. Either way, these ideas are very complex. But let us keep this thought up for a moment: we expose mice to hyperoxia in an experimental approach ones more and apply a *miR-154-3p*-antagonizing approach in the experimental group and compare it to a control group without *miR-154-3p*-antagonism. If we find an absence of AECII-to-AECI transdifferentiation under administration of the antagonist, indicated by the equalization of the previous findings in Gene Array Analysis and Sftpc/Aqp5 immunohistochemical double-staining, which still occur in the control groups, we would undoubtedly proof that *miR-154-3p* indeed is the key regulator of AECII-to-AECI transdifferentiation in the context of hyperoxia.

5.6 Double injury, namely overexpression of *miR-154* on top of hyperoxia, does not further alter alveolar morphology or genetic expression compared to single injury

In the previous experiments we have found both hyperoxia and *miR-154* overexpression to be injurious stimuli on the postnatally developing lung, especially when considering alveolarization. Another question to be answered is whether the addition of one injurious stimulus on top of the other one (double injury) would lead to an even worse alveolar phenotype, namely worse alveolar simplification indicated by a further increase of MLI, or whether it further alters genetic expression profiles. Therefore we have performed the same experiments as described in the previous sections, comparing mice exposed to both, hyperoxia and *miR-154* overexpression (double injury), to mice exposed to *miRNA* overexpression only (single injury). Later we also proceeded in much the same manner comparing mice exposed to both, hyperoxia and *miR-154* overexpression, to mice exposed to hyperoxia only.

Indeed Alveolar Morphometry and RT-qPCR mostly revealed no significant changes comparing double injury to *miR-154* overexpression only (see Figure 11). Alveolar parameters show similar values and none of the genes of Fgf and Tgf-β signaling and epithelial cell markers showed any significant changes. Merely *Fgfr1b* was insignificantly decreased in expression. But when looking at genes linked to alveolar myofibroblasts we see several genes, which are increased upon additional hyperoxia, namely *Elastin*, *Fgf9* and *Shh*. These are the very same genes, which are altered in the same fashion upon hyperoxia in mice without *miRNA* overexpression (compare Figure 11 and Figure 8). Therefore we can conclude that potential effects on alveolar myofibroblasts seen here are clearly attributable to hyperoxia. In a way this underscores our findings of hyperoxia affecting alveolar myofibroblasts, which was described and discussed in the current study. We have previously not found any clear impact of *miR-154* overexpression on the level of alveolar myofibroblast associated genes (at least not for the genes that we have examined; see Figure 9). Immunohistochemical stainings revealed insignificant changes for Sftpc and Acta2, but not pSmad3. As hyperoxia is the variable in this case, once more it is clear, that hyperoxia is responsible for these changes. A trend towards a decrease of Sftpc positive AECII cells is in contrast to our previous

findings and to literature (compare to sections above). It has previously been reported, that AECII cells remain stable upon hyperoxic lung injury (Roper et al., 2004). Why AECII cells are more susceptible for hyperoxic injury when overexpressing *miR-154* remains questionable. A possible explanation is that either *miR-154-3p* or *miR-154-5p* is able to deactivate protective programs in AECII cells, which are usually keeping the AECII cells from perishing upon hyperoxia (Roper et al., 2004). Furthermore Acta2 appeared to be insignificantly increased after double injury. This harmonizes with our previous finding that hyperoxia may lead to a stronger profibrotic phenotype (thickened septal walls, increased Acta2 presence in the lung). Unaltered pSmad3 levels indicate that Tgf-β activity is not further enhanced. As expected the effects of double injury on the postnatal murine alveolar development does not further worsen the phenotype or the genetic expression profile than *miRNA* overexpression in the murine airway epithelium does without additional hyperoxia. Again, this supports our idea of hyperoxia at least partly exerting its detrimental effects on alveolar development via *miR-154-3p*, as the damage exerted by either of the injurious stimuli appears to be saturated and not further increasable upon double injury.

In order to complete the data gathered so far, we have compared the double injury of murine lungs (namely hyperoxia and *miR-154* overexpression in the airway epithelium) to hyperoxia only (single injury), similar to the procedure discussed in this section, where we compared double injury to *miR-154* overexpression only. Figure 12 shows the results we gathered when comparing mice exposed to double injury to mice exposed to hyperoxia only. The parameters of Alveolar Morphometry remained unaltered. Therefore we concluded that additional *miRNA* overexpression on top of hyperoxic lung injury is not able to further worsen alveolarization. This harmonizes with our hypothesis that hyperoxia exerts its effects via its putative downstream effector *miR-154-3p*, as both injurious stimuli obviously do not function independently: in hyperoxia *miR-154-3p* is activated and up-regulated already. A further induction of *miR-154-3p* does not show a further effect, as the process is saturated a priori, because the (hypothetical) "*miR-154-3p* signaling axis" is activated upon hyperoxia already. We therefore assume that increasing the input of *miR-154-3p* does not lead to any further changes concerning alveolar phenotype (see Figure 12.B). The same applies to genetic expression. In

Fgf signaling none of the examined genes is altered in expression level. Merely *Fgf10* and *Bmp4* are insignificantly decreased. But this effect is inverse to the results in *miR-154* overexpression under normoxic conditions (compare Figure 12 to Figure 9). An explanation for these adverse effects of *miRNA* overexpression under hyperoxic compared to normoxic conditions is hardly found and, as the changes are not significant, probably not even required. We see similar findings in the context of epithelial call markers. Among the unaltered genes *Nkx2.1* and *Sftpb* appear to be down-regulated upon *miR-154* overexpression on top of hyperoxia. Under normoxic conditions *miRNA* overexpression did not show an effect on either of the two genes. Why a decrease of expression is seen in hyperoxia remains obscure. Interestingly, the AECI marker *Aqp5* was not further affected upon double injury. This strengthens the idea that the effect of hyperoxia on the AECI population, namely by promoting AECII-to-AECI transdifferentiation (Hou et al., 2015), might actually be mediated via *miR-154-3p* (or *miR-154-5p*). Tgf-β signaling was not altered after double injury. Stainings for Sftpc and pSmad3 indicate the same as RT-qPCR results (see Figure 12.D-F). Interestingly, concerning genes linked to alveolar myofibroblast formation some genes are increased in expression, namely *Fgfr4*, *Pdgfa* and *Shh*. Why these genes are altered when overexpressing *miR-154* on top of hyperoxic exposure, but not in normoxia (compare Figure 12 to Figure 9) remains to be enlightened and does not really fit into the whole story of the current study.

All in all, *miR-154* induction on top of hyperoxia is not able to lead to an appreciable amplification of injury. Still, some genes are altered due to *miRNA* overexpression. These alterations are attributable to *miR-154-3p* and *miR-154-5p* activity, as this is the variable between the two examined conditions (in this case hyperoxia applies for both groups; see Figure 12.A). Why we have differing findings compared to *miRNA* overexpression in normoxia remains unclear. We must keep in mind that here we examined whole lung samples, which do not enable an isolated examination of particular cell types and compartments. Furthermore certain genes are present in different locations of the lung, which is not considered in our approach when using whole lung samples for RT-qPCR. For example Acta2 (also known as smooth muscle actin; α-SMA) is found in pulmonary vessel walls, namely in vascular smooth muscle cells (Cushing et al., 2015), alveolar

myofibroblast (Chao et al., 2015), interstitial myofibroblasts (Perl and Gale, 2009), but is also known to be a factor, which is connected to lung matrix and fibrosis (Vittal et al., 2013). This example shows how both examination and interpretation of results is aggravated, as it is not clearly deducible, which compartment is affected, when considering whole lung samples. Furthermore, we have to keep in mind that *miRNA* functioning is very complex, when considering that a single *miRNA* can have different functions as it can have different targets, as it can potentially act differently at different expression levels and as it can exert different functions in different locations (Bartel, 2004; Friedman et al., 2009; Krol et al., 2010; Sessa and Hata, 2013). When overexpressing *miR-154*, these increased *miRNA* levels are found in the epithelium of the airways. But in the current study hyperoxia was shown to induce *miR-154-3p* and *miR-154-5p* expression in AECII cells (see Figure 7.C), keeping in mind, that we haven't isolated and examined other cell types. Thus, it is not excluded that there are even other cell types with increased *miR-154-3p* and *miR-154-5p* levels in the context of hyperoxia. Nevertheless, we can conclude that concerning alveolarization an overexpression of *miR-154* on top of hyperoxic lung injury does not further impair alveolarization in the postnatally developing lung. A possible explanation is that induction of *miR-154* occurs in hyperoxia already and further reinforcement of an ongoing saturated process brings no additional effect.

5.7 Limitations of this study

Compared to the impact of hyperoxia on the developing postnatal lung, we see similar findings in the *miR-154* overexpressing lung. But in how far are the results of these two approaches comparable?

First of all, when examining hyperoxia, we have exposed mice to 85% O_2 for only 8 days (P0 until P8) with a subsequent period of recovery (P9 until P16) (see Figure 8.A), whereas, when examining *miR-154* overexpression (Figure 9.A), the mice exhibited increased *miRNA* expression in the airway epithelium for 16 days (P0 until P16). A comparison between these two groups, although showing similar findings, is difficult, as the period of exposure to either of the obviously injurious stimuli (hyperoxia or increased *miR-154-3p* and *miR-154-5p* levels lead to

hypoalveologenesis) is substantial. Still the similarities of the morphometric analysis and RT-qPCR are obvious. Taken into account that hyperoxia leads to increased *miR-154-3p* (and to a lesser extent *miR-154-5p*) levels and induction of both, hyperoxia and *miR-154*, leads to a similar alveolar phenotype, namely impaired alveolar development, and genetic expression profile alterations, *miR-154-3p* and possibly *miR-154-5p* have to be considered as potential mediators of the injurious effects of hyperoxia on the lung. A meaningful approach would be a revision of the experiments with adjusted periods of exposure to either of the factors hyperoxia and *miRNA* overexpression. If the same findings can still be seen, the comparability of the two conditions is mended.

According to our findings increased *miR-154-3p* and *miR-154-5p* expression is located in the alveolar epithelium in hyperoxic injury, namely the AECII cells (see Figure 7), whereas in the *miRNA* overexpressing mouse line *miR-154-3p* and *miR-154-5p* expression is induced in the airway epithelium (in club cells under the control of *Scgb1a1*). The differing location of increased *miR-154-3p* and *miR-154-5p* expression under the two conditions (hyperoxia vs. *miRNA* overexpression) weakens the comparability. As we did not isolate other cell types, we do not know about the *miR-154-3p* and *miR-154-5p* expression levels in other cell types apart from AECII cells. Perhaps an approach with the *SPC-rtTA* (AECII specific) driver line instead of the *Scgb1a1-rtTA* driver line (airway specific) is a better simulation of hyperoxic lung injury when overexpressing *miR-154*. In this case the induction of *miR-154-3p* and *miR-154-5p* would occur in the AECII cells instead, just like it is the case in hyperoxia.

Another noteworthy issue is the fact that in our transgenic mouse model we overexpress two *miRNAs*, namely *miR-154-3p* and *miR-154-5p* (see Figure 6). Now the question still remains, which alterations of alveolar phenotype and genetic expression profile in the *miRNA* overexpressing murine lungs are attributable to which *miRNA*? In hyperoxia we do actually see an increase of expression levels for both *miRNAs*, indicating that our approach does approximately simulate the situation of hyperoxia. But still in this case an important question remains unanswered: which of the two *miRNAs* is the crucial player in this issue? Perhaps they both have a share, as they are both induced in AECII cells upon hyperoxia. Perhaps one of the *miRNAs* is only a byproduct of the strongly activated biogenesis

of the other one in the context of hyperoxia. We can only suggest that *miR-154-3p* may be the *miRNA* to look for, as its expression levels underwent a more augmented increase, both in hyperoxia (see Figure 7.C) and induced *miRNA* expression (see Figure 6). Perhaps none of them are relevant and their change of expression level doesn't have an effect in BPD at all. In the end an approach is required, which proves causality and definitely clears those doubts about which of the seen effects are attributable to which *miRNA*. For example, another mouse line, which only overexpresses one of the *miRNAs* would clearly attribute the observed effects to the particular *miRNA*. An even better approach would be a *miR-154-3p* knockdown mouse line. Hereby it is possible to see, whether the effects of hyperoxia on the lung are reversible upon *miR-154-3p* knockdown, giving a clear result about whether *miR-154-3p* actually is a downstream effector of hyperoxia, whether knocking down *miR-154-3p* is able to attenuate the phenotypic and genetic alterations induced by hyperoxia and whether the observed findings are actually attributable to *miR-154-3p*. The same approach is applicable for *miR-154-5p* as well.

Moreover, the alterations in both Alveolar Morphometry and RT-qPCR data in *miRNA* overexpression do not reach the extent of the alterations caused by hyperoxia (indicated by less significant p-values), although the period of exposure to hyperoxia is much shorter and even includes a recovery phase (compare Figure 8.A to Figure 9.A). Under the premise that *miR-154-3p* actually is a downstream mediator of hyperoxia, how can this be explained? One possibility is that hyperoxia induces a complex reaction in the exposed cells leading to the activation of several different parallel signaling cascades. If *miR-154-3p* is part of one of them, but is paralleled by other pathways, it is possible that *miR-154-3p* and *miR-154-5p* overexpression only partly depicts the "full strength" of hyperoxia and its impact on the developing lung. Of course this scenario is only hypothetical.

The most interesting finding in the current study is a possibly increased transdifferentiation of AECII cells to AECI cells in *miR-154* overexpressing lungs, indicated by an increased *Aqp5* level after *miRNA* overexpression (although only nearly significant) and hyperoxia (see Figure 8.C and Figure 9.C) and a more AECI specific transcription signature in isolated AECII cells after *miR-154-3p* and *miR-154-5p* overexpression, revealed by Gene Array Analysis (see Figure 10). Indeed,

the similarities between this circumstance and the results from other studies showing strong evidence for AECII-to-AECI transdifferentiation upon hyperoxia (Hou et al., 2015) are tempting to attribute the function of inducing alveolar epithelial transdifferentiation to *miR-154-3p* (and in a sense *miR-154-5p*). From the current point of view it is reasonable to hypothesize that hyperoxic lung injury leads to an increased AECII-to-AECI transdifferentiation by activating *miR-154-3p*, as our findings are indicative for potentially augmented AEC transdifferentiation. Still there are further experiments required for final proof. Using an immunohistological staining, the demonstration of a more abundant appearance of Sftpc/Aqp5 double-positive cells as an intermediary stage between AECII and AECI cells in the context of *miR-154* overexpression, just like in the context of hyperoxia as previously discussed, would be an easily practicable approach and substantiate our hypothesis. But the strongest approach would be a model, in which the knockdown of *miR-154-3p* would possibly hamper AECII-to-AECI transdifferentiation in the context of hyperoxic exposure. Hereby it would be clearly shown, that *miR-154-3p* is an indispensable factor for the induction of AECII-to-AECI transdifferentiation in the context of hyperoxic lung injury. For instance culturing AECII cells on a plate and exposing them to hyperoxia should expectably lead to an augmented AECII-to-AECI transdifferentiation, again demonstrated by Sftpc/Aqp5 immunohistological double-staining showing increased numbers of double-positive cells. If one group of cells receives an antagonistic stimulus against *miR-154-3p* and thereupon does not show these double-stained cells after hyperoxic treatment anymore, we would be able to show reversibility of hyperoxia-induced AECII-to-AECI transdifferentiation after *miR-154-3p* inhibition. This would reveal *miR-154-3p* as the key mediator of hyperoxia-induced alveolar epithelial cell transdifferentiation. As it is still within the realms of possibility that *miR-154-5p* might be involved in this process too, the same approach should be performed for *miR-154-5p* as well.

All in all, we have found alterations of alveolar structure and genetic expression profiles in hyperoxic lung injury and *miR-154* overexpression, which are conspicuously similar (compare Figures 8 and 9). Although the comparability of the conditions under which the sets of experiments were performed is aggravated as previously mentioned (e.g. duration of exposure), the idea of *miR-154-3p* as a

potential mediator of hyperoxic lung damage and AECII-to-AECI transdifferentiation does not appear to be unimaginable. Further experiments are required in order to examine and comprehend the potential link between hyperoxia and *miR-154* overexpression.

6. Conclusion

Before we started with the study, we had only few hints indicating a potential role of *miR-154-3p* in the BPD mouse model and postnatal lung development: Metabolomics data indicated that *miR-154-3p* and *miR-154-5p* (the approach was not able to examine a *miRNA* in particular) might affect the redox homeostasis, synthesis of phospholipids and extracellular matrix components (*data not shown*). Furthermore, we found some potential targets of *miR-154*, which are connected to Fgf and Tgf-β signaling (see sections above; 2.1). Taking together these findings and previously published literature we assumed that *miR-154-3p* might have an important role in the BPD mouse model, as we found its expression to be regulated more significantly than *miR-154-5p* upon hyperoxic treatment. But as these hints were not very indicatory, we launched a widespread approach by examining quite some signaling pathways and processes in the cell, which are known to be involved in alveolarization and postnatal lung development and might be affected upon hyperoxia. Although at first glance the approach of the current study rather resembles an imprecise shotgun than a precise sniper rifle, we have gathered interesting findings, which are worthwhile to be further examined.

In the current study we find *miR-154-3p* to be highly increased upon hyperoxia in the murine lung, especially in the AECII cells. Furthermore, we find *miR-154-3p* to be a potential mediator of hyperoxic lung damage in the BPD mouse model. Still the present study lacks proof of causality (Nardiello and Morty, 2016): the circumstance that a *miRNA* is altered in expression level in a certain context is not evidencing for a direct involvement. In search of a potential target for *miR-154-3p* we found potential indices for increased AECII-to-AECI transdifferentiation upon *miR-154-3p* (and *miR-154-5p*) overexpression in the current study, which was similarly described in the context of hyperoxia (Hou et al., 2015). Although further experiments are required in order to proof the coherence of our findings and previously published studies (discussed in previous sections), from the contemporary point of view we hypothesize, that hyperoxic treatment of murine lungs leads to an induction of alveolar epithelial cell transdifferentiation from AECII to AECI cells by increasing *miR-154-3p* activity. To our knowledge, this is the first study describing the behavior and potential role of *miR-154-3p* in the context of the BPD mouse model.

The most undisputable approach for showing causality is finding the target *mRNA* of the *miRNA* of interest and demonstrating direct interaction between both. If this *mRNA* encodes a protein, which is clearly involved in the examined context and if a model of action can be unambiguously concluded out of the gathered results, causality is proven. Several studies have used luciferase assays in order to unravel target genes of *miRNAs* (Chen and Shen, 2013; Cheng et al., 2015; Liu et al., 2016; Packer et al., 2008; Polytarchou et al., 2015; Rebane et al., 2014; Zhang et al., 2011), where a luciferase reporter with the corresponding *3'-UTR* of the *mRNA* of interest is transferred. Induction of the *miRNA* of interest therefore (if the potential target gene actually is targeted by the examined *miRNA*) leads to a decrease of luciferase activity by inhibiting translation, proving direct interaction. Softwares, such as TargetScan are used in order to find potential target genes of the *miRNA* of interest (Ceribelli et al., 2011). These are computational processes checking for complementarity of sequences of the *miRNA* of interest and potential target *mRNAs*. Next, the dynamic expression of the previously found potential target genes is examined in an experiment, in which the *miRNA* of interest is overexpressed. In this case target genes of the *miRNA* of interest are down-regulated, according to the function of *miRNAs* as negative regulators of their target *mRNAs*. Subsequently, the down-regulated genes are checked for a potential involvement in the context of the cellular process and signaling cascades of interest (in our case BPD, Fgf signaling, Tgf-β signaling, lung development…). So far, potential target genes of *miR-154* have been indicated by a pulldown approach using MLE-12 cells and an *in-vivo* approach using a *miR-154* overexpressing mouse line, under the control of the ubiquitous *Rosa26* driver line and have been already mentioned and related to either Tgf-β or Fgf signaling, such as *Cav1*, *Gprin3*, *Hopx* and *Apln* (see section "Aims of the Study", 2.1; *data not shown*; *data not published*). Two further steps are missing in our case: Firstly, we still have to find the crucial gene, connecting *miR-154-3p* or *miR-154-5p* to the critical pathways involved in BPD. *Cav1*, *Gprin3*, *Hopx* and *Apln* are promising for further examination, as they are found to be involved in Fgf and Tgf-β signaling. Interestingly, *Cav1* and *Hopx* have been described as being expressed by AECI cells (Jung et al., 2012; Treutlein et al., 2014). Secondly, Luciferase assay would clearly show whether there is a direct interaction between the *miRNA* and the potential target *mRNA* indicated by decreased luciferase activity. A mutation of either the *3'-UTR* binding site of the

mRNA (Rebane et al., 2014), or the seed region of the *miRNA* of interest (Chen and Shen, 2013) could be used to show reversibility of luciferase activity decrease and validate the examined binding site. Finally, a model of action can be deduced showing the molecular mechanism. If this context can be transferred to the human lung of BPD patients, a potential therapeutic approach can possibly be developed, which one-day might be used for treatment of hyperoxic lung injury in preterm babies and long-term consequences. But this is a long way to go from here.

An approach of indirect proof of involvement would be the construction of a *miR-154-3p* knockdown experiment. If *miR-154-3p* knockdown hinders or at least alleviates the injurious effects of hyperoxic lung injury on the lung, it is demonstrated, that *miR-154-3p* actually mediates hyperoxic lung damage. Target genes or a model of action remain unexposed. Still further approaches can be undertaken in order to further examine *miR-154-3p* as a potential therapeutic target. In our case, it would be reasonable to examine whether a knockdown model of *miR-154-3p* would reverse the effects mediated by hyperoxia, which are alveolar impairment and AECII-to-AECI transdifferentiation.

The findings of the current study demonstrate a potential role of *miR-154-3p* (and/or *miR-154-5p*) in the context of BPD mouse model. Further experimental approaches, as discussed in the sections above, have to be undertaken in the future. From the current point of view *miR-154-3p* remains to be far away from a potential therapeutic target in the treatment of sequelae of application of high oxygen concentrations. Presently, *miR-154-3p* remains a potential mediator of the impact of hyperoxia on the murine lung, which seems to affect the process of AECII cells transdifferentiating to AECI cells in the context of hyperoxic treatment. From our current point of view, for finding a targeted cellular process of *miR-154-3p* this is the mechanism that should be further investigated.

Previous data from experiments generated by our lab indicate a potential involvement of *miR-154-3p* and *miR-154-5p* in the context of lung development, or more precisely in the Fgf and Tgf-β signaling cascades, which are known to be important for both, prenatal and postnatal lung development. It has been shown that both *miRNAs* are rather expressed in the embryonic lung than in the postnatal lung. We have decided to examine the role of *miR-154-3p* and *miR-154-5p* in the context of postnatal lung development and BPD. For these purposes we applied high oxygen concentrations using a BPD mouse model and used an inducible transgenic mouse line overexpressing both *isomiRNAs* in the murine airway epithelium, in order **1.** to examine the temporo-spatial expression pattern of *miR-154-3p* and *miR-154-5p* in the model of hyperoxic lung injury, **2.** to show the impact of airway epithelial-specific *miR-154-3p* (and *miR-154-5p*) overexpression on lung histology and gene expression in mutants compared to wildtype and under hyperoxia compared to normoxia, and **3.** to describe the potential role of *miR-154-3p* in the BPD mouse model as a potentially protective factor.
1. *miR-154-3p* appeared to be expressed in the proximal and distal airway epithelial cells. Applying hyperoxia to the murine lungs after birth enhanced *miR-154-3p* (and to a lesser extent *miR-154-5p*) expression in the distal airway epithelium, especially in AECII cells. **2.** A deterioration of alveolar formation was found after hyperoxic lung injury, indicated by increased MLI (mean linear intercept of the alveoli) and septal wall thickness, beside a dynamic change of genetic expression levels for *mRNAs*, which are involved in Fgf and Tgf-β signaling. Also AECI cells and alveolar myofibroblasts appeared to be affected. Overexpression of *miR-154-3p* and *miR-154-5p* leads to a similar alveolar phenotype and similar alterations of the genetic expression profile as previously seen after hyperoxia. **3.** In isolated AECII cells, a more AECI specific transcription profile was found after *miR-154-3p* and *miR-154-5p* overexpression compared to controls, potentially indicating a transition from AECII to AECI cells upon *miR-154-3p* and *miR-154-5p* induction. Interestingly, this AECII-to-AECI transition has already been described in the context of hyperoxia in rats.

As seen in the results of the current study hyperoxia is able to enhance *miR-154-3p* expression in the AECII cells and both, hyperoxia and *miRNA* overexpression, lead to similar injurious effects in the murine lung, it appears to be plausible that *miR-154-3p* might be a mediator of hyperoxic lung injury. In literature we were able to find that AECII-to-AECI transdifferentiation is activated upon hyperoxia. Our findings are possibly indicative for the initiation of the very same process after *miR-154-3p* and *miR-154-5p* overexpression.
Thus, we hypothesize, that hyperoxia may induce an augmented AECII-to-AECI transdifferentiation in the murine lung epithelium by activating *miR-154-3p*.

Zusammenfassung auf Deutsch

Von unserem Labor zuvor generierte Daten deuteten auf eine mögliche Verwicklung von *miR-154-3p* und *miR-154-5p* mit der Lungenentwicklung, beziehungsweise mit den Fgf und Tgf-β Signalkaskaden, welche bekannt für ihre wichtigen Rollen in Bezug auf prä- und postnatale Lungenentwicklung sind. Es wurde bereits gezeigt, dass beide *miRNAs* eher in der embryonalen und weniger in der postnatalen Lunge exprimiert werden. Wir haben uns entschieden die Rolle von *miR-154-3p* und *miR-154-5p* im Zusammenhang mit postnataler Lungenentwicklung und BPD genauer zu untersuchen. Zu diesem Zweck haben wir im BPD Maus Modell die Tiere hohen Sauerstoffkonzentrationen ausgesetzt und durch eine induzierbare transgene Mauslinie beide *isomiRNAs* im murinen Atemwegsepithel hochreguliert, **1.** um das zeitliche und räumliche Expressionsmuster von *miR-154-3p* und *miR-154-5p* im Zusammenhang mit Applikation hoher Sauerstoffkonzentrationen zu untersuchen, **2.** um den Effekt der atemwegsspezifischen Überexpression von *miR-154-3p* (und *miR-154-5p*) auf die Lungenhistologie und das genetische Expressionsprofil darzustellen, und **3.** um die potenzielle Rolle von *miR-154-3p* als möglicherweise protektiver Faktor im BPD Mausmodel zu beschreiben.
1. *miR-154-3p* wird vor allem in den Epithelzellen der proximalen und distalen Atemwege exprimiert. Nach der Applikation von Hyperoxie kommt es zu einer erhöhten Expression von *miR-154-3p* (in geringerem Maße auch *miR-154-5p*) im Epithel der distalen Atemwege vor allem in den AECII Zellen. **2.** Eine gestörte Formierung der Alveolen lag nach Exposition mit hohen Sauerstoffkonzentrationen vor, was an einem erhöhten alveolären Diameter und einer Verdickung der septalen Wände neben einer dynamischen Änderung der *mRNA*-Expression von Genen, die zu den Fgf und Tgf-β Signalwegen zugehörig sind, zu erkennen war. Die Überexprimierung von *miR-154-3p* und *miR-154-5p* führte zu einem ähnlichen alveolären Phänotyp und einem ähnlichen genetischen Expressionsprofil wie es im zuvor durchgeführten Hyperoxie-Experiment der Fall war. **3.** In isolierten AECII Zellen lag ein eher AECI-typisches genetisches Expressionsprofil vor, wenn man *miR-154-3p* und *miR-154-5p* überexprimierende Mäuse mit Kontrolltieren verglich, was möglicherweise mit einer vermehrten, durch die Hochregulierung von *miR-154-3p* und *miR-154-5p* induzierten, Transition von AECII zu AECI Zellen vereinbar ist. Ein derartiges Phänomen der AECII-zu-AECI Transdifferenzierung ist im Zusammenhang mit Hyperoxie bereits in Ratten beschrieben worden.

Wie den Ergebnissen der aktuellen Arbeit zu entnehmen ist, führt Hyperoxie zu einer Hochregulierung von *miR-154-3p* in den AECII Zellen und beide Faktoren, Hyperoxie und *miRNA* Hochregulierung, führen zu ähnlichen schädigenden Effekten im Bezug auf die murine Lunge. Es erscheint naheliegend, dass *miR-154-3p* wie ein Mediator hyperoxie-bedingter Lungenschädigung fungiert. In der Literatur ist eine vermehrte AECI-zu-AECII Zelltransdifferenzierung in Ratten bereits beschrieben. Unsere Ergebnisse sprechen womöglich dafür, dass eine Überexpression von *miR-154-3p* und *miR-154-5p* zu einer Einleitung des gleichen Prozesses führen könnte.
Daher formulieren wir die Hypothese, dass Hyperoxie eine vermehrte AECII-zu-AECI Zelltransdifferenzierung im murinen Lungenepithel über eine Aktivierung von *miR-154-3p* hervorruft.

References

Akhavantabasi, S., Sapmaz, A., Tuna, S., Erson-Bensan, A.E., 2012. miR-125b targets ARID3B in breast cancer cells. Cell Struct Funct 37, 27-38.

Al Alam, D., Danopoulos, S., Schall, K., Sala, F.G., Almohazey, D., Fernandez, G.E., Georgia, S., Frey, M.R., Ford, H.R., Grikscheit, T., Bellusci, S., 2015. Fibroblast growth factor 10 alters the balance between goblet and Paneth cells in the adult mouse small intestine. Am J Physiol Gastrointest Liver Physiol 308, G678-690.

Alejandre-Alcazar, M.A., Kwapiszewska, G., Reiss, I., Amarie, O.V., Marsh, L.M., Sevilla-Perez, J., Wygrecka, M., Eul, B., Kobrich, S., Hesse, M., Schermuly, R.T., Seeger, W., Eickelberg, O., Morty, R.E., 2007. Hyperoxia modulates TGF-beta/BMP signaling in a mouse model of bronchopulmonary dysplasia. Am J Physiol Lung Cell Mol Physiol 292, L537-549.

Ambros, V., Bartel, B., Bartel, D.P., Burge, C.B., Carrington, J.C., Chen, X., Dreyfuss, G., Eddy, S.R., Griffiths-Jones, S., Marshall, M., Matzke, M., Ruvkun, G., Tuschl, T., 2003. A uniform system for microRNA annotation. RNA 9, 277-279.

Baraldi, E., Filippone, M., 2007. Chronic lung disease after premature birth. N Engl J Med 357, 1946-1955.

Bartel, D.P., 2004. MicroRNAs: Genomics, Biogenesis, Mechanisms, and Function. Cell 116, 281-297.

Bellusci, S., Grindley, J., Emoto, H., Itoh, N., Hogan, B.L., 1997. Fibroblast growth factor 10 (FGF10) and branching morphogenesis in the embryonic mouse lung. Development 124, 4867-4878.

Benetatos, L., Hatzimichael, E., Londin, E., Vartholomatos, G., Loher, P., Rigoutsos, I., Briasoulis, E., 2013. The microRNAs within the DLK1-DIO3 genomic region: involvement in disease pathogenesis. Cell Mol Life Sci 70, 795-814.

Benjamin, J.T., Smith, R.J., Halloran, B.A., Day, T.J., Kelly, D.R., Prince, L.S., 2007. FGF-10 is decreased in bronchopulmonary dysplasia and suppressed by Toll-like receptor activation. Am J Physiol Lung Cell Mol Physiol 292, L550-558.

Berezikov, E., Chung, W.J., Willis, J., Cuppen, E., Lai, E.C., 2007. Mammalian mirtron genes. Mol Cell 28, 328-336.

Bernardo, B.C., Nguyen, S.S., Gao, X.M., Tham, Y.K., Ooi, J.Y., Patterson, N.L., Kiriazis, H., Su, Y., Thomas, C.J., Lin, R.C., Du, X.J., McMullen, J.R., 2016. Inhibition of miR-154 Protects Against Cardiac Dysfunction and Fibrosis in a Mouse Model of Pressure Overload. Sci Rep 6, 22442.

Borchert, G.M., Lanier, W., Davidson, B.L., 2006. RNA polymerase III transcribes human microRNAs. Nat Struct Mol Biol 13, 1097-1101.

Bostrom, H., Willetts, K., Pekny, M., Leveen, P., Lindahl, P., Hedstrand, H., Pekna, M., Hellstrom, M., Gebre-Medhin, S., Schalling, M., Nilsson, M., Kurland, S., Tornell, J., Heath, J.K., Betsholtz, C., 1996. PDGF-A signaling is a critical event in lung alveolar myofibroblast development and alveogenesis. Cell 85, 863-873.

Burri, P.H., 2006. Structural aspects of postnatal lung development - alveolar formation and growth. Biol Neonate 89, 313-322.

Cao, Y., Zhang, D., Moon, H.G., Lee, H., Haspel, J.A., Hu, K., Xie, L., Jin, Y., 2016. MiR-15a/16 Regulates Apoptosis of Lung Epithelial Cells after Oxidative Stress. Mol Med 22.

Cardoso, W.V., Itoh, A., Nogawa, H., Mason, I., Brody, J.S., 1997. FGF-1 and FGF-7 induce distinct patterns of growth and differentiation in embryonic lung epithelium. Dev Dyn 208, 398-405.
Ceribelli, A., Nahid, M.A., Satoh, M., Chan, E.K., 2011. MicroRNAs in rheumatoid arthritis. FEBS Lett 585, 3667-3674.
Chao, C.M., El Agha, E., Tiozzo, C., Minoo, P., Bellusci, S., 2015. A breath of fresh air on the mesenchyme: impact of impaired mesenchymal development on the pathogenesis of bronchopulmonary dysplasia. Front Med (Lausanne) 2, 27.
Chao, C.M., Moiseenko, A., Zimmer, K.P., Bellusci, S., 2016. Alveologenesis: key cellular players and fibroblast growth factor 10 signaling. Mol Cell Pediatr 3, 17.
Chao, C.M., Yahya, F., Moiseenko, A., Tiozzo, C., Shrestha, A., Ahmadvand, N., El Agha, E., Quantius, J., Dilai, S., Kheirollahi, V., Jones, M., Wilhem, J., Carraro, G., Ehrhardt, H., Zimmer, K.P., Barreto, G., Ahlbrecht, K., Morty, R.E., Herold, S., Abellar, R.G., Seeger, W., Schermuly, R., Zhang, J.S., Minoo, P., Bellusci, S., 2017. Fgf10 deficiency is causative for lethality in a mouse model of bronchopulmonary dysplasia. J Pathol 241, 91-103.
Chen, F., Cao, Y., Qian, J., Shao, F., Niederreither, K., Cardoso, W.V., 2010. A retinoic acid-dependent network in the foregut controls formation of the mouse lung primordium. J Clin Invest 120, 2040-2048.
Chen, F., Desai, T.J., Qian, J., Niederreither, K., Lu, J., Cardoso, W.V., 2007. Inhibition of Tgf beta signaling by endogenous retinoic acid is essential for primary lung bud induction. Development 134, 2969-2979.
Chen, F., Zhao, X., Peng, J., Bo, L., Fan, B., Ma, D., 2014. Integrated microRNA-mRNA analysis of coronary artery disease. Mol Biol Rep 41, 5505-5511.
Chen, H., Sun, J., Buckley, S., Chen, C., Warburton, D., Wang, X.F., Shi, W., 2005. Abnormal mouse lung alveolarization caused by Smad3 deficiency is a developmental antecedent of centrilobular emphysema. Am J Physiol Lung Cell Mol Physiol 288, L683-691.
Chen, L.C., Zhang, Z., Myers, A.C., Huang, S.K., 2001. Cutting Edge: Altered Pulmonary Eosinophilic Inflammation in Mice Deficient for Clara Cell Secretory 10-kDa Protein. The Journal of Immunology 167, 3025-3028.
Chen, Y.L., Shen, C.K., 2013. Modulation of mGluR-dependent MAP1B translation and AMPA receptor endocytosis by microRNA miR-146a-5p. J Neurosci 33, 9013-9020.
Cheng, X., Zhang, X., Su, J., Zhang, Y., Zhou, W., Zhou, J., Wang, C., Liang, H., Chen, X., Shi, R., Zen, K., Zhang, C.Y., Zhang, H., 2015. miR-19b downregulates intestinal SOCS3 to reduce intestinal inflammation in Crohn's disease. Sci Rep 5, 10397.
Coalson, J.J., Winter, V., deLemos, R.A., 1995. Decreased alveolarization in baboon survivors with bronchopulmonary dysplasia. Am J Respir Crit Care Med 152, 640-646.
Coates, D., 2003. The angiotensin converting enzyme (ACE). The International Journal of Biochemistry & Cell Biology 35, 769-773.
Cushing, L., Costinean, S., Xu, W., Jiang, Z., Madden, L., Kuang, P., Huang, J., Weisman, A., Hata, A., Croce, C.M., Lu, J., 2015. Disruption of miR-29 Leads to Aberrant Differentiation of Smooth Muscle Cells Selectively Associated with Distal Lung Vasculature. PLoS Genet 11, e1005238.

De Langhe, S.P., Carraro, G., Warburton, D., Hajihosseini, M.K., Bellusci, S., 2006. Levels of mesenchymal FGFR2 signaling modulate smooth muscle progenitor cell commitment in the lung. Dev Biol 299, 52-62.
Derynck, R., Zhang, Y.E., 2003. Smad-dependent and Smad-independent pathways in TGF-beta family signalling. Nature 425, 577-584.
Desai, T.J., Brownfield, D.G., Krasnow, M.A., 2014. Alveolar progenitor and stem cells in lung development, renewal and cancer. Nature 507, 190-194.
Desvignes, T., Batzel, P., Berezikov, E., Eilbeck, K., Eppig, J.T., McAndrews, M.S., Singer, A., Postlethwait, J.H., 2015. miRNA Nomenclature: A View Incorporating Genetic Origins, Biosynthetic Pathways, and Sequence Variants. Trends Genet 31, 613-626.
Dixon-McIver, A., East, P., Mein, C.A., Cazier, J.B., Molloy, G., Chaplin, T., Andrew Lister, T., Young, B.D., Debernardi, S., 2008. Distinctive patterns of microRNA expression associated with karyotype in acute myeloid leukaemia. PLoS One 3, e2141.
El Agha, E., Bellusci, S., 2014. Walking along the Fibroblast Growth Factor 10 Route: A Key Pathway to Understand the Control and Regulation of Epithelial and Mesenchymal Cell-Lineage Formation during Lung Development and Repair after Injury. Scientifica (Cairo) 2014, 538379.
Entesarian, M., Dahlqvist, J., Shashi, V., Stanley, C.S., Falahat, B., Reardon, W., Dahl, N., 2007. FGF10 missense mutations in aplasia of lacrimal and salivary glands (ALSG). Eur J Hum Genet 15, 379-382.
Eswarakumar, V.P., Lax, I., Schlessinger, J., 2005. Cellular signaling by fibroblast growth factor receptors. Cytokine Growth Factor Rev 16, 139-149.
Fiore, R., Khudayberdiev, S., Christensen, M., Siegel, G., Flavell, S.W., Kim, T.K., Greenberg, M.E., Schratt, G., 2009. Mef2-mediated transcription of the miR379-410 cluster regulates activity-dependent dendritogenesis by fine-tuning Pumilio2 protein levels. EMBO J 28, 697-710.
Friedman, R.C., Farh, K.K., Burge, C.B., Bartel, D.P., 2009. Most mammalian mRNAs are conserved targets of microRNAs. Genome Res 19, 92-105.
Fukumoto, J., Soundararajan, R., Leung, J., Cox, R., Mahendrasah, S., Muthavarapu, N., Herrin, T., Czachor, A., Tan, L.C., Hosseinian, N., Patel, P., Gone, J., Breitzig, M.T., Cho, Y., Cooke, A.J., Galam, L., Narala, V.R., Pathak, Y., Lockey, R.F., Kolliputi, N., 2016. The role of club cell phenoconversion and migration in idiopathic pulmonary fibrosis. Aging (Albany NY) 8, 3091-3109.
Gardiner, E., Beveridge, N.J., Wu, J.Q., Carr, V., Scott, R.J., Tooney, P.A., Cairns, M.J., 2012. Imprinted DLK1-DIO3 region of 14q32 defines a schizophrenia-associated miRNA signature in peripheral blood mononuclear cells. Mol Psychiatry 17, 827-840.
Gioia, U., Di Carlo, V., Caramanica, P., Toselli, C., Cinquino, A., Marchioni, M., Laneve, P., Biagioni, S., Bozzoni, I., Cacci, E., Caffarelli, E., 2014. Mir-23a and mir-125b regulate neural stem/progenitor cell proliferation by targeting Musashi1. RNA Biol 11, 1105-1112.
Griffiths-Jones, S., 2004. The microRNA Registry. Nucleic Acids Res 32, D109-111.
Griffiths-Jones, S., Grocock, R.J., van Dongen, S., Bateman, A., Enright, A.J., 2006. miRBase: microRNA sequences, targets and gene nomenclature. Nucleic Acids Res 34, D140-144.

Gururajan, M., Josson, S., Chu, G.C., Lu, C.L., Lu, Y.T., Haga, C.L., Zhau, H.E., Liu, C., Lichterman, J., Duan, P., Posadas, E.M., Chung, L.W., 2014. miR-154* and miR-379 in the DLK1-DIO3 microRNA mega-cluster regulate epithelial to mesenchymal transition and bone metastasis of prostate cancer. Clin Cancer Res 20, 6559-6569.
Hamm, L.L., Nakhoul, N., Hering-Smith, K.S., 2015. Acid-Base Homeostasis. Clin J Am Soc Nephrol 10, 2232-2242.
Hawkins, F., Kramer, P., Jacob, A., Driver, I., Thomas, D.C., McCauley, K.B., Skvir, N., Crane, A.M., Kurmann, A.A., Hollenberg, A.N., Nguyen, S., Wong, B.G., Khalil, A.S., Huang, S.X., Guttentag, S., Rock, J.R., Shannon, J.M., Davis, B.R., Kotton, D.N., 2017. Prospective isolation of NKX2-1-expressing human lung progenitors derived from pluripotent stem cells. J Clin Invest 127, 2277-2294.
Herriges, J.C., Verheyden, J.M., Zhang, Z., Sui, P., Zhang, Y., Anderson, M.J., Swing, D.A., Zhang, Y., Lewandoski, M., Sun, X., 2015. FGF-Regulated ETV Transcription Factors Control FGF-SHH Feedback Loop in Lung Branching. Dev Cell 35, 322-332.
Hibino, N., Best, C.A., Engle, A., Ghimbovschi, S., Knoblach, S., Nath, D.S., Ishibashi, N., Jonas, R.A., 2016. Novel Association of miR-451 with the Incidence of TEVG Stenosis in a Murine Model. Tissue Eng Part A 22, 75-82.
Hobi, N., Giolai, M., Olmeda, B., Miklavc, P., Felder, E., Walther, P., Dietl, P., Frick, M., Perez-Gil, J., Haller, T., 2016. A small key unlocks a heavy door: The essential function of the small hydrophobic proteins SP-B and SP-C to trigger adsorption of pulmonary surfactant lamellar bodies. Biochim Biophys Acta 1863, 2124-2134.
Hou, A., Fu, J., Yang, H., Zhu, Y., Pan, Y., Xu, S., Xue, X., 2015. Hyperoxia stimulates the transdifferentiation of type II alveolar epithelial cells in newborn rats. Am J Physiol Lung Cell Mol Physiol 308, L861-872.
Hsi, E., Chen, K.C., Chang, W.S., Yu, M.L., Liang, C.L., Juo, S.H., 2013. A functional polymorphism at the FGF10 gene is associated with extreme myopia. Invest Ophthalmol Vis Sci 54, 3265-3271.
http://www.mirbase.org/.
Huang, S., Feng, C., Zhai, Y.Z., Zhou, X., Li, B., Wang, L.L., Chen, W., Lv, F.Q., Li, T.S., 2017. Identification of miRNA biomarkers of pneumonia using RNA-sequencing and bioinformatics analysis. Exp Ther Med 13, 1235-1244.
Itoh, N., Ornitz, D.M., 2011. Fibroblast growth factors: from molecular evolution to roles in development, metabolism and disease. J Biochem 149, 121-130.
Jain, S., Kapetanaki, M.G., Raghavachari, N., Woodhouse, K., Yu, G., Barge, S., Coronnello, C., Benos, P.V., Kato, G.J., Kaminski, N., Gladwin, M.T., 2013. Expression of regulatory platelet microRNAs in patients with sickle cell disease. PLoS One 8, e60932.
Jung, K., Schlenz, H., Krasteva, G., Muhlfeld, C., 2012. Alveolar epithelial type II cells and their microenvironment in the caveolin-1-deficient mouse. Anat Rec (Hoboken) 295, 196-200.
Kagami, M., O'Sullivan, M.J., Green, A.J., Watabe, Y., Arisaka, O., Masawa, N., Matsuoka, K., Fukami, M., Matsubara, K., Kato, F., Ferguson-Smith, A.C., Ogata, T., 2010. The IG-DMR and the MEG3-DMR at human chromosome 14q32.2: hierarchical interaction and distinct functional properties as imprinting control centers. PLoS Genet 6, e1000992.

Kim, J., Kang, Y., Kojima, Y., Lighthouse, J.K., Hu, X., Aldred, M.A., McLean, D.L., Park, H., Comhair, S.A., Greif, D.M., Erzurum, S.C., Chun, H.J., 2013. An endothelial apelin-FGF link mediated by miR-424 and miR-503 is disrupted in pulmonary arterial hypertension. Nat Med 19, 74-82.
Kiszalkiewicz, J., Piotrowski, W.J., Pastuszak-Lewandoska, D., Gorski, P., Antczak, A., Gorski, W., Domanska-Senderowska, D., Migdalska-Sek, M., Czarnecka, K.H., Nawrot, E., Brzezianska-Lasota, E., 2016. Altered miRNA expression in pulmonary sarcoidosis. BMC Med Genet 17, 2.
Krag, S., Danielsen, C.C., Carmeliet, P., Nyengaard, J., Wogensen, L., 2005. Plasminogen activator inhibitor-1 gene deficiency attenuates TGF-beta1-induced kidney disease. Kidney Int 68, 2651-2666.
Krol, J., Loedige, I., Filipowicz, W., 2010. The widespread regulation of microRNA biogenesis, function and decay. Nat Rev Genet 11, 597-610.
Kugler, M.C., Loomis, C.A., Zhao, Z., Cushman, J.C., Liu, L., Munger, J.S., 2017. Sonic Hedgehog Signaling Regulates Myofibroblast Function during Alveolar Septum Formation in Murine Postnatal Lung. Am J Respir Cell Mol Biol 57, 280-293.
Lagos-Quintana, M., Rauhut, R., Lendeckel, W., Tuschl, T., 2001. Identification of Novel Genes Coding for Small Expressed RNAs. Science 294, 853-858.

Lau, N.C., Lim, L.P., Weinstein, E.G., Bartel, D.P., 2001. An Abundant Class of Tiny RNAs with Probable Regulatory Roles in Caenorhabditis elegans. Science 294, 658-662.

Lebeche, D., Malpel, S., Cardoso, W.V., 1999. Fibroblast growth factor interactions in the developing lung. Mech Dev 86, 125-136.
Lee, C.R., Ambros, V., 2001. An Extensive Class of Small RNAs in Caenorhabditis elegans. Science 294, 862-864.

Lee, C.R., Feinbaum, R.L., Ambros, V., 1993. The C. elegans Heterochronic Gene lin-4 Encodes Small RNAs with Antisense Complementarity to lin-14. Cell 75, 843-854.

Lee, H.W., Park, S.H., 2017. Elevated microRNA-135a is associated with pulmonary arterial hypertension in experimental mouse model. Oncotarget.
Lee, J., Reddy, R., Barsky, L., Weinberg, K., Driscoll, B., 2006. Contribution of proliferation and DNA damage repair to alveolar epithelial type 2 cell recovery from hyperoxia. Am J Physiol Lung Cell Mol Physiol 290, L685-L694.
Li, C., Lyu, J., Meng, Q.H., 2017a. MiR-93 Promotes Tumorigenesis and Metastasis of Non-Small Cell Lung Cancer Cells by Activating the PI3K/Akt Pathway via Inhibition of LKB1/PTEN/CDKN1A. J Cancer 8, 870-879.
Li, S., Meng, H., Zhou, F., Zhai, L., Zhang, L., Gu, F., Fan, Y., Lang, R., Fu, L., Gu, L., Qi, L., 2013. MicroRNA-132 is frequently down-regulated in ductal carcinoma in situ (DCIS) of breast and acts as a tumor suppressor by inhibiting cell proliferation. Pathol Res Pract 209, 179-183.
Li, S.H., Chen, L., Pang, X.M., Su, S.Y., Zhou, X., Chen, C.Y., Huang, L.G., Li, J.P., Liu, J.L., 2017b. Decreased miR-146a expression in acute ischemic stroke directly targets the Fbxl10 mRNA and is involved in modulating apoptosis. Neurochem Int.

Lin, S.P., Youngson, N., Takada, S., Seitz, H., Reik, W., Paulsen, M., Cavaille, J., Ferguson-Smith, A.C., 2003. Asymmetric regulation of imprinting on the maternal and paternal chromosomes at the Dlk1-Gtl2 imprinted cluster on mouse chromosome 12. Nat Genet 35, 97-102.
Lin, X., Yang, Z., Zhang, P., Shao, G., 2015. miR-154 suppresses non-small cell lung cancer growth in vitro and in vivo. Oncol Rep 33, 3053-3060.
Litvinov, S.V., Velders, M.P., Bakker, H.A., Fleuren, G.J., Warnaar, S.O., 1994. Ep-CAM: a human epithelial antigen is a homophilic cell-cell adhesion molecule. J Cell Biol 125, 437-446.
Liu, F., Chen, N., Xiao, R., Wang, W., Pan, Z., 2016. miR-144-3p serves as a tumor suppressor for renal cell carcinoma and inhibits its invasion and metastasis by targeting MAP3K8. Biochem Biophys Res Commun 480, 87-93.
Madurga, A., Mizikova, I., Ruiz-Camp, J., Vadasz, I., Herold, S., Mayer, K., Fehrenbach, H., Seeger, W., Morty, R.E., 2014. Systemic hydrogen sulfide administration partially restores normal alveolarization in an experimental animal model of bronchopulmonary dysplasia. Am J Physiol Lung Cell Mol Physiol 306, L684-697.
Makanya, A., Anagnostopoulou, A., Djonov, V., 2013. Development and remodeling of the vertebrate blood-gas barrier. Biomed Res Int 2013, 101597.
Martin, C.R., Zaman, M.M., Gilkey, C., Salguero, M.V., Hasturk, H., Kantarci, A., Van Dyke, T.E., Freedman, S.D., 2014. Resolvin D1 and lipoxin A4 improve alveolarization and normalize septal wall thickness in a neonatal murine model of hyperoxia-induced lung injury. PLoS One 9, e98773.
McGrath-Morrow, S.A., Cho, C., Soutiere, S., Mitzner, W., Tuder, R., 2004. The effect of neonatal hyperoxia on the lung of p21Waf1/Cip1/Sdi1-deficient mice. Am J Respir Cell Mol Biol 30, 635-640.
Mian, C., Pennelli, G., Fassan, M., Balistreri, M., Barollo, S., Cavedon, E., Galuppini, F., Pizzi, M., Vianello, F., Pelizzo, M.R., Girelli, M.E., Rugge, M., Opocher, G., 2012. MicroRNA profiles in familial and sporadic medullary thyroid carcinoma: preliminary relationships with RET status and outcome. Thyroid 22, 890-896.
Milenkovic, J., Milojkovic, M., Jevtovic Stoimenov, T., Djindjic, B., Miljkovic, E., 2017. Mechanisms of plasminogen activator inhibitor 1 action in stromal remodeling and related diseases. Biomed Pap Med Fac Univ Palacky Olomouc Czech Repub 161, 339-347.
Milosevic, J., Pandit, K., Magister, M., Rabinovich, E., Ellwanger, D.C., Yu, G., Vuga, L.J., Weksler, B., Benos, P.V., Gibson, K.F., McMillan, M., Kahn, M., Kaminski, N., 2012. Profibrotic role of miR-154 in pulmonary fibrosis. Am J Respir Cell Mol Biol 47, 879-887.
Morrisey, E.E., Hogan, B.L., 2010. Preparing for the first breath: genetic and cellular mechanisms in lung development. Dev Cell 18, 8-23.
Nakanishi, H., Sugiura, T., Streisand, J.B., Lonning, S.M., Roberts, J.D., Jr., 2007. TGF-beta-neutralizing antibodies improve pulmonary alveologenesis and vasculogenesis in the injured newborn lung. Am J Physiol Lung Cell Mol Physiol 293, L151-161.
Nardiello, C., Morty, R.E., 2016. MicroRNA in late lung development and bronchopulmonary dysplasia: the need to demonstrate causality. Mol Cell Pediatr 3, 19.

Nickel, J., Ten Dijke, P., Mueller, T.D., 2017. TGF-beta family co-receptor function and signaling. Acta Biochim Biophys Sin (Shanghai).
Niedermaier, S., Hilgendorff, A., 2015. Bronchopulmonary dysplasia - an overview about pathophysiologic concepts. Mol Cell Pediatr 2, 2.
Northway, W.H., Jr., Rosan, R.C., Porter, D.Y., 1967. Pulmonary disease following respirator therapy of hyaline-membrane disease. Bronchopulmonary dysplasia. N Engl J Med 276, 357-368.
Oglesby, I.K., Agrawal, R., Mall, M.A., McElvaney, N.G., Greene, C.M., 2015. miRNA-221 is elevated in cystic fibrosis airway epithelial cells and regulates expression of ATF6. Mol Cell Pediatr 2, 1.
Ornitz, D.M., Itoh, N., 2015. The Fibroblast Growth Factor signaling pathway. Wiley Interdiscip Rev Dev Biol 4, 215-266.
Owen, L.S., Manley, B.J., Davis, P.G., Doyle, L.W., 2017. The evolution of modern respiratory care for preterm infants. The Lancet 389, 1649-1659.
Packer, A.N., Xing, Y., Harper, S.Q., Jones, L., Davidson, B.L., 2008. The bifunctional microRNA miR-9/miR-9* regulates REST and CoREST and is downregulated in Huntington's disease. J Neurosci 28, 14341-14346.
Pang, X., Huang, K., Zhang, Q., Zhang, Y., Niu, J., 2015. miR-154 targeting ZEB2 in hepatocellular carcinoma functions as a potential tumor suppressor. Oncol Rep. 34, 3272-3279.
Pasquinelli, A.E., Reinhart, B.J., Slack, F., Martindale, M.Q., Kuroda, M.I., Maller, B., Hayward, D.C., Ball, E.E., Degnan, B., Muller, P., Spring, J., Srinivasan, A., Fishman, M., Finnerty, J., Corbo, J., Levine, M., Leahy, P., Davidson, E., Ruvkun, G., 2000. Conservation of the sequence and temporal expression of let-7 heterochronic regulatory RNA. Nature 408, 86-89.
Perl, A.-K.T., Tichelaar, J.W., Whitsett, J.A., 2002. Conditional gene expression in the respiratory epithelium of the mouse. Transgenic Research 11, 21-29.
Perl, A.-K.T., Zhang, L., Whitsett, J.A., 2009. Conditional Expression of Genes in the Respiratory Epithelium in Transgenic Mice - Cautionary Notes and Toward Building a Better Mouse Trap. Am J Respir Cell Mol Biol 40, 1-3.
Perl, A.K., Gale, E., 2009. FGF signaling is required for myofibroblast differentiation during alveolar regeneration. Am J Physiol Lung Cell Mol Physiol 297, L299-308.
Polytarchou, C., Hommes, D.W., Palumbo, T., Hatziapostolou, M., Koutsioumpa, M., Koukos, G., van der Meulen-de Jong, A.E., Oikonomopoulos, A., van Deen, W.K., Vorvis, C., Serebrennikova, O.B., Birli, E., Choi, J., Chang, L., Anton, P.A., Tsichlis, P.N., Pothoulakis, C., Verspaget, H.W., Iliopoulos, D., 2015. MicroRNA214 Is Associated With Progression of Ulcerative Colitis, and Inhibition Reduces Development of Colitis and Colitis-Associated Cancer in Mice. Gastroenterology 149, 981-992 e911.
Popova, A.P., Bentley, J.K., Cui, T.X., Richardson, M.N., Linn, M.J., Lei, J., Chen, Q., Goldsmith, A.M., Pryhuber, G.S., Hershenson, M.B., 2014. Reduced platelet-derived growth factor receptor expression is a primary feature of human bronchopulmonary dysplasia. Am J Physiol Lung Cell Mol Physiol 307, L231-239.
Porzionato, A., Guidolin, D., Macchi, V., Sarasin, G., Grisafi, D., Tortorella, C., Dedja, A., Zaramella, P., De Caro, R., 2016. Fractal analysis of alveolarization in hyperoxia-induced rat models of bronchopulmonary dysplasia. Am J Physiol Lung Cell Mol Physiol 310, L680-688.

Ramasamy, S.K., Mailleux, A.A., Gupte, V.V., Mata, F., Sala, F.G., Veltmaat, J.M., Del Moral, P.M., De Langhe, S., Parsa, S., Kelly, L.K., Kelly, R., Shia, W., Keshet, E., Minoo, P., Warburton, D., Bellusci, S., 2007. Fgf10 dosage is critical for the amplification of epithelial cell progenitors and for the formation of multiple mesenchymal lineages during lung development. Dev Biol 307, 237-247.
Ratner, V., Sosunov, S.A., Niatsetskaya, Z.V., Utkina-Sosunova, I.V., Ten, V.S., 2013. Mechanical ventilation causes pulmonary mitochondrial dysfunction and delayed alveolarization in neonatal mice. Am J Respir Cell Mol Biol 49, 943-950.
Rebane, A., Runnel, T., Aab, A., Maslovskaja, J., Ruckert, B., Zimmermann, M., Plaas, M., Karner, J., Treis, A., Pihlap, M., Haljasorg, U., Hermann, H., Nagy, N., Kemeny, L., Erm, T., Kingo, K., Li, M., Boldin, M.P., Akdis, C.A., 2014. MicroRNA-146a alleviates chronic skin inflammation in atopic dermatitis through suppression of innate immune responses in keratinocytes. J Allergy Clin Immunol 134, 836-847 e811.
Reinhart, B.J., Slack, F.J., Basson, M., Pasquinelli, A.E., Bettinger, J.C., Rougvie, A.E., Horvitz, H.R., Ruvkun, G., 2000. The 21-nucleotide let-7 RNA regulates developmental timing in Caenorhabditis elegans. Nature 403, 901-906.
Ro, S., Park, C., Young, D., Sanders, K.M., Yan, W., 2007. Tissue-dependent paired expression of miRNAs. Nucleic Acids Res 35, 5944-5953.
Rohmann, E., Brunner, H.G., Kayserili, H., Uyguner, O., Nurnberg, G., Lew, E.D., Dobbie, A., Eswarakumar, V.P., Uzumcu, A., Ulubil-Emeroglu, M., Leroy, J.G., Li, Y., Becker, C., Lehnerdt, K., Cremers, C.W., Yuksel-Apak, M., Nurnberg, P., Kubisch, C., Schlessinger, J., van Bokhoven, H., Wollnik, B., 2006. Mutations in different components of FGF signaling in LADD syndrome. Nat Genet 38, 414-417.
Roper, J.M., Mazzatti, D.J., Watkins, R.H., Maniscalco, W.M., Keng, P.C., O'Reilly, M.A., 2004. In vivo exposure to hyperoxia induces DNA damage in a population of alveolar type II epithelial cells. Am J Physiol Lung Cell Mol Physiol 286, L1045-1054.
Rozycki, H.J., 2014. Potential contribution of type I alveolar epithelial cells to chronic neonatal lung disease. Front Pediatr 2, 45.
Sanders, Y.Y., Cui, Z., Le Saux, C.J., Horowitz, J.C., Rangarajan, S., Kurundkar, A., Antony, V.B., Thannickal, V.J., 2015. SMAD-independent down-regulation of caveolin-1 by TGF-beta: effects on proliferation and survival of myofibroblasts. PLoS One 10, e0116995.
Seitz, H., Royo, H., Bortolin, M.L., Lin, S.P., Ferguson-Smith, A.C., Cavaille, J., 2004. A large imprinted microRNA gene cluster at the mouse Dlk1-Gtl2 domain. Genome Res 14, 1741-1748.
Sekine, K., Ohuchi, H., Fujiwara, M., Yamasaki, M., Yoshizawa, T., Sato, T., Yagishita, N., Matsui, D., Koga, Y., Itoh, N., Kato, S., 1999. Fgf10 is essential for limb and lung formation. Nat Genet 21, 138-141.
Serra, R., Pelton, R.W., Moses, H.L., 1994. TGF beta 1 inhibits branching morphogenesis and N-myc expression in lung bud organ cultures. Development 120, 2153-2161.
Sessa, R., Hata, A., 2013. Role of microRNAs in lung development and pulmonary diseases. Pulm Circ 3, 315-328.

Shen, W., Liu, J., Zhao, G., Fan, M., Song, G., Zhang, Y., Weng, Z., Zhang, Y., 2017. Repression of Toll-like receptor-4 by microRNA-149-3p is associated with smoking-related COPD. Int J Chron Obstruct Pulmon Dis 12, 705-715.
Shi, Y., Massagué, J., 2003. Mechanisms of TGF-β Signaling from Cell Membrane to the Nucleus. Cell 113, 685-700.
Shu, W., Guttentag, S., Wang, Z., Andl, T., Ballard, P., Lu, M.M., Piccolo, S., Birchmeier, W., Whitsett, J.A., Millar, S.E., Morrisey, E.E., 2005. Wnt/beta-catenin signaling acts upstream of N-myc, BMP4, and FGF signaling to regulate proximal-distal patterning in the lung. Dev Biol 283, 226-239.
Silva, D.M., Nardiello, C., Pozarska, A., Morty, R.E., 2015. Recent advances in the mechanisms of lung alveolarization and the pathogenesis of bronchopulmonary dysplasia. Am J Physiol Lung Cell Mol Physiol 309, L1239-1272.
Singh, G., Katyal, S.L., 1997. Clara cells and Clara cell 10 kD protein (CC10). Am J Respir Cell Mol Biol 17, 141-143.
Sureshbabu, A., Syed, M.A., Boddupalli, C.S., Dhodapkar, M.V., Homer, R.J., Minoo, P., Bhandari, V., 2015. Conditional overexpression of TGFbeta1 promotes pulmonary inflammation, apoptosis and mortality via TGFbetaR2 in the developing mouse lung. Respir Res 16, 4.
Tian, M., Schiemann, W.P., 2009. The TGF-beta paradox in human cancer: an update. Future Oncol 5, 259-271.
Tomari, Y., Zamore, P.D., 2005. MicroRNA biogenesis: drosha can't cut it without a partner. Curr Biol 15, R61-64.
Treutlein, B., Brownfield, D.G., Wu, A.R., Neff, N.F., Mantalas, G.L., Espinoza, F.H., Desai, T.J., Krasnow, M.A., Quake, S.R., 2014. Reconstructing lineage hierarchies of the distal lung epithelium using single-cell RNA-seq. Nature 509, 371-375.
Ugorski, M., Dziegiel, P., Suchanski, J., 2016. Podoplanin - a small glycoprotein with many faces. Am J Cancer Res 6, 370-386.
Vicencio, A.G., Lee, C.G., Cho, S.J., Eickelberg, O., Chuu, Y., Haddad, G.G., Elias, J.A., 2004. Conditional overexpression of bioactive transforming growth factor-beta1 in neonatal mouse lung: a new model for bronchopulmonary dysplasia? Am J Respir Cell Mol Biol 31, 650-656.
Vittal, R., Mickler, E.A., Fisher, A.J., Zhang, C., Rothhaar, K., Gu, H., Brown, K.M., Emtiazdjoo, A., Lott, J.M., Frye, S.B., Smith, G.N., Sandusky, G.E., Cummings, O.W., Wilkes, D.S., 2013. Type V collagen induced tolerance suppresses collagen deposition, TGF-beta and associated transcripts in pulmonary fibrosis. PLoS One 8, e76451.
Voynow, J.A., 2017. "New" bronchopulmonary dysplasia and chronic lung disease. Paediatr Respir Rev 24, 17-18.
Wang, S., He, W., Wang, C., 2016a. MiR-23a Regulates the Vasculogenesis of Coronary Artery Disease by Targeting Epidermal Growth Factor Receptor. Cardiovasc Ther 34, 199-208.
Wang, Y., Frank, D.B., Morley, M.P., Zhou, S., Wang, X., Lu, M.M., Lazar, M.A., Morrisey, E.E., 2016b. HDAC3-Dependent Epigenetic Pathway Controls Lung Alveolar Epithelial Cell Remodeling and Spreading via miR-17-92 and TGF-beta Signaling Regulation. Dev Cell 36, 303-315.
Warburton, D., Schwarz, M., Tefft, D., Flores-Delgado, G., Anderson, K.D., Cardoso, W.V., 2000. The molecular basis of lung morphogenesis. Mech Dev 92, 55-81.

Wei, T., Zhu, W., Fang, S., Zeng, X., Huang, J., Yang, J., Zhang, J., Guo, L., 2017a. miR-495 promotes the chemoresistance of SCLC through the epithelial-mesenchymal transition via Etk/BMX. Am J Cancer Res 7, 628-646.
Wei, Y., Kim, T.J., Peng, D.H., Duan, D., Gibbons, D.L., Yamauchi, M., Jackson, J.R., Le Saux, C.J., Calhoun, C., Peters, J., Derynck, R., Backes, B.J., Chapman, H.A., 2017b. Fibroblast-specific inhibition of TGF-beta1 signaling attenuates lung and tumor fibrosis. J Clin Invest 127, 3675-3688.
Weinstein, M., Xu, X., Ohyama, K., Deng, C.X., 1998. FGFR-3 and FGFR-4 function cooperatively to direct alveogenesis in the murine lung. Development 125, 3615-3623.
Wightman, B., Ha, I., Ruvkun, G., 1993. Posttranscriptional Regulation of the Heterochronic Gene lin-14 by lin-4 Mediates Temporal Pattern Formation in C. elegans. Cell 75, 855-862.
Williams, A.E., Moschos, S.A., Perry, M.M., Barnes, P.J., Lindsay, M.A., 2007. Maternally imprinted microRNAs are differentially expressed during mouse and human lung development. Dev Dyn 236, 572-580.
Woyda, K., Koebrich, S., Reiss, I., Rudloff, S., Pullamsetti, S.S., Ruhlmann, A., Weissmann, N., Ghofrani, H.A., Gunther, A., Seeger, W., Grimminger, F., Morty, R.E., Schermuly, R.T., 2009. Inhibition of phosphodiesterase 4 enhances lung alveolarisation in neonatal mice exposed to hyperoxia. Eur Respir J 33, 861-870.
Wu, S., Platteau, A., Chen, S., McNamara, G., Whitsett, J., Bancalari, E., 2010. Conditional overexpression of connective tissue growth factor disrupts postnatal lung development. Am J Respir Cell Mol Biol 42, 552-563.
Xiang, Y., Cheng, J., Wang, D., Hu, X., Xie, Y., Stitham, J., Atteya, G., Du, J., Tang, W.H., Lee, S.H., Leslie, K., Spollett, G., Liu, Z., Herzog, E., Herzog, R.I., Lu, J., Martin, K.A., Hwa, J., 2015. Hyperglycemia repression of miR-24 coordinately upregulates endothelial cell expression and secretion of von Willebrand factor. Blood 125, 3377-3387.
Xin, C., Zhang, H., Liu, Z., 2014. miR-154 suppresses colorectal cancer cell growth and motility by targeting TLR2. Mol Cell Biochem 387, 271-277.
Xing, Y., Fu, J., Yang, H., Yao, L., Qiao, L., Du, Y., Xue, X., 2015. MicroRNA expression profiles and target prediction in neonatal Wistar rat lungs during the development of bronchopulmonary dysplasia. Int J Mol Med 36, 1253-1263.
Xu, H., Fei, D., Zong, S., Fan, Z., 2016. MicroRNA-154 inhibits growth and invasion of breast cancer cells through targeting E2F5. Am J Transl Res 8, 2620-2630.
Xu, N., Meisgen, F., Butler, L.M., Han, G., Wang, X.J., Soderberg-Naucler, C., Stahle, M., Pivarcsi, A., Sonkoly, E., 2013. MicroRNA-31 is overexpressed in psoriasis and modulates inflammatory cytokine and chemokine production in keratinocytes via targeting serine/threonine kinase 40. J Immunol 190, 678-688.
Yee, M., Buczynski, B.W., O'Reilly, M.A., 2014. Neonatal hyperoxia stimulates the expansion of alveolar epithelial type II cells. Am J Respir Cell Mol Biol 50, 757-766.
Zhang, J., Tu, Q., Bonewald, L.F., He, X., Stein, G., Lian, J., Chen, J., 2011. Effects of miR-335-5p in modulating osteogenic differentiation by specifically downregulating Wnt antagonist DKK1. J Bone Miner Res 26, 1953-1963.

Zhang, Y., Sun, E., Li, X., Zhang, M., Tang, Z., He, L., Lv, K., 2017. miR-155 contributes to Df1-induced asthma by increasing the proliferative response of Th cells via CTLA-4 downregulation. Cell Immunol 314, 1-9.
Zhao, D., Wang, R., Fang, J., Ji, X., Li, J., Chen, X., Sun, G., Wang, Z., Liu, W., Wang, Y., Cheng, G., Zhen, H., Sun, C., Fei, Z., 2017a. MiR-154 Functions as a Tumor Suppressor in Glioblastoma by Targeting Wnt5a. Mol Neurobiol 54, 2823-2830.
Zhao, Y., Ma, J., Fan, Y., Wang, Z., Tian, R., Ji, W., Zhang, F., Niu, R., 2017b. TGF-beta transactivates EGFR and facilitates breast cancer migration and invasion through canonical Smad3 and ERK/Sp1 signaling pathway. Mol Oncol.
Zheng, Y., Zhu, C., Ma, L., Shao, P., Qin, C., Li, P., Cao, Q., Ju, X., Cheng, G., Zhu, Q., Gu, X., Hua, L., 2017. miRNA-154-5p Inhibits Proliferation, Migration and Invasion by Targeting E2F5 in Prostate Cancer Cell Lines. Urol Int 98, 102-110.
Zhou, X., Wen, W., Shan, X., Qian, J., Li, H., Jiang, T., Wang, W., Cheng, W., Wang, F., Qi, L., Ding, Y., Liu, P., Zhu, W., Chen, Y., 2016. MiR-28-3p as a potential plasma marker in diagnosis of pulmonary embolism. Thromb Res 138, 91-95.

Acknowledgements

First of all, I would like to thank Prof. Dr. Saverio Bellusci for giving me the opportunity to work on my doctoral thesis as a medical student in Bellusci laboratory and for being a dedicated mentor. While I was working in the laboratory he has always helped me with excellent new ideas how to further proceed whenever I asked for good advice. I am very thankful for his patience and understanding, especially when considering that I had no laboratory experience when I started my work.
This laboratory has provided valuable materials, which I have required in order to continue with experiments. I really appreciate it. While some of my colleagues from university had difficulties with their laboratory work for their dissertations I am aware that Bellusci laboratory has provided facilities and material of high quality facilitating comfortable working conditions.

Secondly, I would like to thank Dr. Cho-Ming Chao, who has introduced me into the "*miR-154*-project" and taught me the methods required for this work. He was always patient with me and spent quite some time and effort in instructing me. He was always available whenever I had questions, although he was strongly bound to clinic. Cho is one of the most reliable persons I know. I am very thankful for the time he took for advising me when we met in the lab or when I gave him a phone call.

Thirdly, I would like to thank every single member of the Bellusci laboratory:

I would like to thank our laboratory manager Kerstin Goth, who takes care about correct procedures and works very hard. I am very thankful for her expertise as well, because she always had some time whenever I asked her for help.

Jana Rostkovius, who has helped me with the FISH staining. I am absolutely certain that without her help I would still be desperately trying to make those cells fluoresce.

Heike Habermann for patiently helping me with the paperwork, which was quite confusing sometimes.

Matthew Jones for the genotyping. I am sorry for complaining when the mice didn't have the genotype I was hoping for.

Thank you to Dr. Amit Shrestha, who has helped a lot, especially with FISH stainings, as he has performed the same staining for another *microRNA*.

Dr. Alyona Moiseenko, who has patiently helped me whenever I had questions and gave me constructive feedback regarding my data.

Vahid Kheirollahi, who has taught me the molecular essentials of the methods I have used, which was quite helpful in order to find out why experiments didn't work.

Dr. Elie El Agha for helping me whenever I had questions and giving me constructive feedback.

Thomas Sontag, who has given me helpful advice with software. Unfortunately I have not a clue concerning this kind of things. But with your help it didn't seem so complicated.

Jamschid Sedighi and Faady Yahya: Thank you for the support and help. As medical students they were in the same situation as I was. They did a great job with their projects and helped me a lot with mine.

Thank you Johannes Kolck and Volker Zimmermann, also known as the "*miR-154* boys"! The three of us were working on the "*miR-154*-project" together. It was my pleasure to collaborate with you gentlemen!

I am also thankful to Elisabeth Kappes for performing the isolation of AECII cells and Dr. Jochen Wilhelm for performing the gene array analysis. This was very important to generate vital data for the project.

I would also like to thank the animal caretakers Christian Eng, Martin Stellwagen and Sabrina Schick for their work in the animal facilities and for taking care of the animals, which I have required for the experiments.
Without the Excellence Cluster Cardio-Pulmonary System (ECCPS) this doctoral thesis would not have been possible. I am very thankful to Prof. Dr. Werner Seeger, who is leading the ECCPS and who is my chief physician in clinic now. I remember him motivating medical students for doing their doctoral thesis in the ECCPS while I still had lectures.

Furthermore I am very thankful to my parents Silvana and Ilija, to my sister Lucija and her boyfriend Johannes, to my brother Ivan and his wife Julia and to my nephew Lukas for giving me the emotional and financial support throughout my student days. I am very proud to be your son, brother, brother-in-law and uncle. Ivan and Lucija have always been role models for me.
Thank you for being there for me and knowing that you have my back when things don't turn out the way it was planned. Fortunately, everything went well so far.
I would like to thank my girlfriend Lena for the great support. And for her dissertation I will support her as well.
I would like to thank my family in Germany, Croatia, Ireland and Australia. You are too many to name every single one of you. And also I would like to thank my friends from Bielefeld and Giessen. Again there are too many of you to mention every single one of you.

15.10.2015	Poster-Präsentation: "Effect of *miR-154* overexpression during embryonic development on the metabolic profile of the developing mouse lung" ECCPS Minisymposium on Metabolomics Universitätsklinik Frankfurt a.M.
07.07.2016	Poster-Präsentation: "The role of *miR-154-3p* in postnatal lung development and hyperoxic lung injury" ECCPS Retreat 2016 Bad Nauheim